Stable Finite Element Algorithms for Analysing the Vertebral Artery

A Thesis

Submitted to the College of Graduate Studies and Research

in Partial Fulfillment of the Requirements

for the Degree of

Doctor of Philosophy

in the

Department of Mechanical Engineering

University of Saskatchewan

Saskatoon

by

Lisa M. Coley

Permission to Use

In presenting this dissertation in partial fulfillment of the requirements for a Postgraduate degree from the University of Saskatchewan, I agree that the Libraries of this University may make it freely available for inspection. I further agree that permission for copying of this dissertation in any manner, in whole or in part, for scholarly purposes may be granted by the professor who supervised my dissertation work or in his absence, by the Head of the Department or the Dean of the College in which my dissertation work was done. It is understood that any copying, publication or use of this dissertation, or parts thereof, for financial gain shall not be allowed without my written permission. It is also understood that due recognition shall be given to me and to the University of Saskatchewan in any scholarly use which may be made of any material in my dissertation.

Disclaimer

Reference in this dissertation to any specific commercial products, process, or service by trade name, trademark, manufacturer, or otherwise, does not constitute or imply its endorsement, recommendation, or favouring by the University of Saskatchewan. The views and opinions of the author expressed herein do not state or reflect those of the University of Saskatchewan, and shall not be used for advertising or product endorsement purposes.

Requests for permission to copy or to make other uses of materials in this dissertation in whole or in part should be addressed to:

Head of the Department of Mechanical Engineering
57 Campus Drive, University of Saskatchewan
Saskatoon, Saskatchewan
Canada, S7N 5A9

OR

Dean
College of Graduate Studies and Research
University of Saskatchewan
105 Administration Place
Saskatoon, Saskatchewan
Canada, S7N 5A2

Abstract

The research described in this thesis began with a single long-term objective: modelling of the vertebral artery during chiropractic manipulation of the cervical spine. Although chiropractic treatment has become prevalent, the possible correlation between neck manipulation and subsequent stroke in patients has been the subject of debate without resolution. Past research has been qualitative or statistical, whereas resolution demands a fundamental understanding of the associated mechanics.

Analysis in the thesis begins with a study of the anatomy and properties pertinent to the chiropractic problem. This indicates that the complexity of the problem will necessitate a long-term multidisciplinary effort including a nonlinear finite element formulation effective in analysing image data for soft tissue modelled as nearly incompressible. This leads to an assessment of existing finite element methods and the conclusion that new equation solving techniques are needed to ensure numerical stability.

Three techniques for effectively eliminating the source of numerical instability are developed and demonstrated with the aid of original finite element codes. Two of the methods are derived as modifications of matrix decomposition algorithms, while the third method constitutes a new finite element formulation. In addition, the understanding gained in developing these methods is used to produce a theorem for assessing a different but related problem: deformation of a nearly incompressible material subjected to a single concentrated force. Throughout the thesis, an interdisciplinary path from chiropractic problem to numerical algorithms is outlined, and results are in the form of mathematical proofs and derivations of both existing and new methods.

Acknowledgements

I would like to thank my supervisor, Professor A. Dolovich, for his guidance and encouragement throughout the course of my research and the writing of this dissertation. He has always been a friend and mentor.

I would also like to gratefully acknowledge the following people: my advisory committee members, Professor J. Bugg, Professor R. Burton, Professor R. Fotouhi, Professor J. Sharma, and Professor C. Zhang for their time and advice as committee members; Dr. C. Ross for proposal of the motivating application for this research; Professor Dolovich for financial support through a research grant from the Natural Sciences and Engineering Research Council of Canada (NSERC); the University of Saskatchewan for financial support through a graduate scholarship and the Canadian Federation of University Women for financial support through the Newstead Doctoral Scholarship.

Dedication

This dissertation is dedicated to my husband Bruce and son Connor for their continued support and understanding throughout my educational pursuits.

Table of Contents

List of Figures

List of Tables

Glossary

$\aleph$	Penalty term in total potential energy functional for near incompressibility
β	Parameter in the Babuška-Brezzi inequality condition
$\boldsymbol{\beta}$	Vector of coefficients in the linear combination of nullspace vectors
β_i	Coefficients in the linear combination of nullspace vectors
γ_{xy}, γ_{yz}, γ_{zx}	Components of shear strain in the Cartesian coordinate system
ε_x, ε_y, ε_z	Normal strain components in the *x*-, *y*- and *z*- directions, respectively
ε_i	Normal strains at a point
$\tilde{\varepsilon}_i$	Normal strains associated with the volumetric part of the strain energy density
$\boldsymbol{\varepsilon}$	Column vector of strain components
$\varepsilon^{(i)}$	Strain field in element *i*
$\hat{\boldsymbol{\varepsilon}}$	Deviatoric strain vector for plane strain
φ	Tolerance
κ	Bulk modulus
$\boldsymbol{\Lambda}$	Diagonal matrix of eigenvalues of the compliance tensor
λ	Lagrange multiplier
λ_{E}	Eigenvalues of $\tilde{\boldsymbol{A}}$
λ_{L}	Lamé parameter
$\lambda_{\min}$	Smallest eigenvalue of $\tilde{\boldsymbol{A}}$
$\lambda_{\max}$	Largest eigenvalue of $\tilde{\boldsymbol{A}}$
μ	Lamé parameter

ν	Poisson's ratio
Π	Total potential energy of a system
θ	Angle between two vectors; polar coordinate of cylinder
Θ_{xy}	Rigid body rotation
σ_x, σ_y, σ_z	Normal stress components in the *x*-, *y*- and *z*- directions, respectively
σ_i	Normal stresses at a point
$\tilde{\sigma}_i$	Normal stresses associated with the volumetric part of the stress state
$\boldsymbol{\sigma}$	Column vector of stress components
σ_{vM}	von Mises stress
$\hat{\boldsymbol{\sigma}}$	Deviatoric stress vector for plane strain
τ_{xy}, τ_{yz}, τ_{zx}	Components of shear stress in the Cartesian coordinate system
$\tilde{\tau}_{ij}$	Shear stresses associated with the volumetric part of the stress state
τ	Shear stress
τ_0	Value of shear stress for simple shear example
Ω	Potential energy of external forces applied to a system
ξ, η	Natural coordinate directions
$\boldsymbol{A}$	Matrix of stiffnesses corresponding to the second partial derivatives of the distortional strain energy
$\tilde{\boldsymbol{A}}$	Coefficient matrix for finite element equations that have only pressure as the unknown
a	Arbitrary component of matrix
$\boldsymbol{B}$	Matrix containing derivatives of the shape functions used to relate strains to displacements in an element
B_x, B_y, B_z	Body forces in the *x*, *y*, and *z* directions

$\hat{\boldsymbol{B}}$	Deviatoric strain-displacement matrix for plane strain
B_{ij}	Individual components of the standard strain-displacement matrix $\boldsymbol{B}$
$\tilde{\boldsymbol{B}}$	Portion of $\boldsymbol{B}$ used for enforcing incompressibility
$\boldsymbol{b}$	$\begin{bmatrix}\boldsymbol{b}_1 & \boldsymbol{b}_2\end{bmatrix}^{\mathrm{T}}$
b	Length of plate in x-direction
$\boldsymbol{b}_1$	Load vector after imposition of the displacement boundary conditions
$\boldsymbol{b}_2$	Vector in bottom block on right hand side of incompressible finite element equations
$\boldsymbol{b}_3$	Vector in derivation relating to the Babuška-Brezzi condition
$\tilde{\boldsymbol{b}}$	Subvector of $\boldsymbol{Q}^{\mathrm{T}}\boldsymbol{b}$
CSM	Cervical spine manipulation
CMT	Cervical manipulative therapy
C	Column space of a matrix
$\boldsymbol{C}$	Compliance tensor relating normal stresses to normal strains
c_k	Generalised displacements
CN	Condition number of a matrix
$\boldsymbol{D}$	Matrix that relates stresses to strains in an element (inverse of $\boldsymbol{C}$)
$\hat{\boldsymbol{D}}$	Deviatoric stress-strain matrix for plane strain
$\boldsymbol{d}$	Vector of normal strains multiplied by Young's Modulus
$\boldsymbol{d}'$	Modified vector of normal strains related to $\boldsymbol{s}'$ by $\boldsymbol{\Lambda}$
E	Young's modulus
e	Volumetric change per volume of an element
$\bar{e}$	Approximate volumetric change per volume of an element

FEM	Finite element method
F_i	Nodal forces
$\boldsymbol{F}$	Column vector of nodal forces
F^*	Single force boundary condition
$\boldsymbol{f}$	Force vector
$\boldsymbol{G}$	Matrix whose terms relate the change in volume per volume of an element due to deflection of a single displacement degree of freedom
G_{ij}	Individual components of $\boldsymbol{G}$, each referring to the change in volume of element i per unit displacement j
G	Shear modulus
$\boldsymbol{H}$	Householder matrix
$\tilde{\boldsymbol{H}}_i$	Matrix containing a Householder matrix
h	Length of plate in y-direction
$\boldsymbol{I}$	Identity matrix
$\boldsymbol{J}$	Jacobian matrix
J_{ij}	Individual component of Jacobian matrix
$\hat{\boldsymbol{J}}$	Matrix relating strains to derivative of displacements with respect to natural coordinates
$\boldsymbol{K}$	Coefficient/stiffness matrix
$\hat{\boldsymbol{K}}$	Global stiffness matrix with order of columns reversed
K_{ij}	Individual components of stiffness matrix
$\tilde{\boldsymbol{K}}$	Nonsingular submatrix of $\boldsymbol{K}$ with displacements as unknowns
$\boldsymbol{K}_{\text{free}}$	Global stiffness matrix for free variables
k	Degree of indeterminacy

$\hat{\boldsymbol{L}}$	Lower triangular matrix in LU decomposition
$\boldsymbol{M}$	Interpolation matrix for the pressures in the bottom block of incompressible finite element equations
m	Number of elements in the finite element mesh
N	Nullspace of a matrix
$N_j^{(i)}$	Traditional linear shape function corresponding to node j and element (i)
$\boldsymbol{N}'$	Matrix containing derivatives of shape functions to relate the nodal displacement vector to vector of derivative of displacements with respect to natural coordinates
n	Variable denoting size of a matrix
$\hat{n}$	Unit vector
n_{o}	Number of displacement unknowns for Dirichlet case
n_{p}	Number of parameters defining the pressure field
n_{u}	Number of parameters defining the displacement field
n_z	Number of zero rows in a matrix
P	Pressure
$\boldsymbol{P}$	Permutation matrix
p	Hydrostatic pressure
$\not{p}$	Number of pressure unknowns
$\boldsymbol{p}$	Pressure vector in incompressible finite element matrix equations
$\boldsymbol{p}_{\mathrm{c}}$	Constant pressure vector
p_{i}	Internal pressure of cylinder
p_{o}	External pressure of cylinder
$\boldsymbol{q}$	Pressure mode vector

q	Dimension of the nullspace of a matrix
q_o	Dimension of the nullspace for a model in which displacements are prescribed on the entire boundary
$\boldsymbol{Q}$	Orthogonal matrix
$\boldsymbol{R}$	Upper triangular matrix in QR decomposition
R	Row space of a matrix
r_i	Inner radius of cylinder
r_o	Outer radius of cylinder
r_0	Rank of $\boldsymbol{G}$ for Dirichlet case
r	Polar coordinate on cylinder
$\boldsymbol{S}_{\text{elim}}$	Final matrix of coefficients of eliminated variables
$\boldsymbol{S}^*_{\text{elim}}$	Intermediate matrix of coefficients of eliminated variables
$\boldsymbol{S}_{\text{free}}$	Final matrix of coefficients of free variables
$\boldsymbol{S}^*_{\text{free}}$	Intermediate matrix of coefficients of free variables
$\boldsymbol{s}$	Vector of normal stresses
$\boldsymbol{s'}$	Modified vector of normal stresses multiplied by $\boldsymbol{\Lambda}$ to get $\boldsymbol{b'}$
$\boldsymbol{T}$	Matrix relating elemental degrees of freedom to free variables
$\boldsymbol{T}_{\text{glob}}$	Matrix relating all of the nodal displacements to the free variables
U	Internal strain energy of a system
$\hat{U}$	Deviatoric component of internal strain energy
$\hat{\boldsymbol{U}}$	Upper triangular matrix in LU decomposition
$\hat{\boldsymbol{U}}_r$	Upper triangular matrix in LU decomposition after removal of hydrostatic pressures

u, v	Displacements in x- and y- directions, respectively
$\boldsymbol{u}$	Column vector of nodal displacements in an element
$\boldsymbol{u}_{\mathrm{BC}}$	Displacement boundary conditions
$\boldsymbol{u}_{\mathrm{elim}}$	Final vector of eliminated variables
$\mathbf{u}^{*}_{\mathrm{e\,lim}}$	Intermediate vector of eliminated variables
$\boldsymbol{u}_{\mathrm{free}}$	Final vector of free variables
$\boldsymbol{u}^{*}_{\mathrm{free}}$	Intermediate vector of free variables
$\boldsymbol{u}_{\mathrm{glob}}$	Vector of all nodal displacements
u_k	Displacement unknown corresponding to single force boundary condition
$\boldsymbol{u}^{*}_{\mathrm{perm}}$	Permuted vector of free variables
u_i	Nodal displacements
$\boldsymbol{u}_{\mathrm{p}}$	Particular solution for nodal displacements in the constraint equations
$\boldsymbol{u}_0$	Vector in the nullspace of $\boldsymbol{G}$
$u^{(\mathrm{i})}$	Displacement field in element (i)
$\hat{\boldsymbol{u}}$	Vector of nodal displacements in final step of modified LU decomposition
$u_{\max}$	Maximum displacement
$\boldsymbol{u}'$	Vector of derivatives of displacements for an element with respect to natural coordinates
V	Volume
$\boldsymbol{V}$	Matrix of nullspace vectors
$\boldsymbol{v}_{\mathrm{R}}$	Row space vector
$\boldsymbol{v}$	Arbitrary vector

W	Strain energy density
$\hat{W}$	Deviatoric strain energy density
$\tilde{W}$	Volumetric strain energy density
$\boldsymbol{w}$	Vector associated with the finite element equations and defined by $\boldsymbol{w} = \boldsymbol{A}^{1/2}\boldsymbol{u}$
x, y, z	Cartesian coordinates
x_i	Generic unknowns that may be pressures or displacements
$\boldsymbol{x}$	Arbitrary vector
$\hat{\boldsymbol{x}}$	Vector of unknowns in finite element matrix equations with order of rows reversed
$\tilde{\boldsymbol{x}}$	Vector of displacement unknowns
$\boldsymbol{y}$	Vector in intermediate step of LU decomposition or arbitrary vector in definition of Householder matrix
$\boldsymbol{z}$	Vector associated with the finite element equations and defined by $\boldsymbol{z} = \boldsymbol{A}^{-1/2}\boldsymbol{G}^{\mathrm{T}}\boldsymbol{p}$; Vector in Householder transformation

Chapter 1

Introduction

1.1 Motivation

For centuries, the principles and techniques of applied mechanics have been developed and applied successfully to many engineering problems. Traditionally, methods of stress analysis have mainly focussed on steel and aluminum structures. More recently, however, these principles and techniques are being extended to the medical sciences. There is tremendous potential for researchers in engineering mechanics to make fundamental contributions in this area. One area in particular is the field of biomechanics of soft tissue. In most problems involving the mechanics of soft tissue, advanced theories and methodologies are required in almost all aspects: constitutive laws, kinematic relations, and stable and efficient numerical implementations.

The graduate work underlying this thesis is motivated by a particular problem in biomechanical modelling: arterial deformation during chiropractic manipulation of the cervical spine. This problem is of great concern to practitioners in both chiropractic and traditional medicine since strokes, leading in some cases to death, have occurred following chiropractic manipulation of the cervical spine. There is dispute among the

practitioners regarding the incidence of these events and whether the chiropractic manipulation itself caused the stroke in any given case. Medical researchers have performed numerous case studies and have used various imaging modalities to observe physiological and morphological changes to arteries in the neck region subsequent to manipulation. However, there is still a need to develop quantitative research methods for establishing the cause of these changes. The purpose of the research described in this thesis is to provide a foundation for performing detailed engineering analyses of this problem.

1.2 General Research Approach and Thesis Outline

To realise the long-term goal of analysing the vertebral artery under actual loading conditions will require multiple research projects and a highly interdisciplinary approach. The objective of this thesis is to intiate the process by making vital conceptual connections between biology, engineering, and applied mathematics to develop a means for analysis. This dissertation follows a path that begins with assessment of the biomedical problem, suggests a long-term plan towards finite element modelling, identifies issues within the mathematics associated with combining tissue properties and existing finite element solution techniques, and finally contributes new mathematical approaches which eliminate obstacles to future modelling. This format is designed specifically to solve an important problem, the solution to which may otherwise remain inaccessible. It is true that the literature already contains medical studies of the vertebral artery as well as numerous mathematical treatments of the finite element method. By following an open-ended path towards tailoring a finite element

approach to this specific problem, however, the thesis provides an avenue through which a greater understanding into the consequences of neck manipulation may ultimately be achieved.

In Chapter 2, a biomedical literature review provides the context for the work. Anatomical details of the cervical spine and the vertebral artery are presented, together with a brief description of the neck manipulation used by chiropractors in clinical practice. The controversy surrounding this procedure is studied, with references to the literature in both the biomedical and chiropractic areas. This review, which is the first contribution of the dissertation, is used to establish the societal interest in the problem, as well as the pressing need for an engineering approach and method of quantitative analysis. In addition, the description of the anatomical detail and the chiropractic technique is used as a basis for suggesting a new direction towards physical modelling and analysis of the problem. The suggested direction is to combine *in vivo* measurements of arterial deformation together with data analysis by special-purpose finite element algorithms developed within this thesis.

The biomedical literature review of Chapter 2 is followed by an assessment in Chapter 3 of issues surrounding finite element analysis of the problem. Although there are many issues that researchers in biomechanics will encounter as they attempt to understand and analyse the chiropractic problem, the fundamental issue identified as the focal point for this thesis is the nearly incompressible behaviour of soft tissue and, in particular, the potential of this behaviour to seriously affect the reliability of finite element solutions. It is well known within the area of finite element analysis that near-incompressibility can

lead to catastrophic calculation and/or modelling errors in the form of artificial over-stiffening referred to as *displacement locking* and numerical instability in terms of *physical and spurious pressure modes*. (Displacement locking and pressure modes will be explained with reference to the literature in Chapter 3.) For over thirty years, a vast literature has been amassed in mathematics and engineering to develop special-purpose methods for dealing with these specific issues. It is hypothesised here, however, that for the specific conditions required for *in vivo* analysis of the vertebral artery, existing finite element techniques are insufficient to ensure reliable solutions.

Chapter 3 tests this hypothesis by reviewing the state-of-the-art in finite element techniques designed specifically for nearly and fully incompressible materials, and then testing these techniques on numerically generated displacement data. Since these methods are all mathematical in nature, the review is primarily in the language of mathematics. Within this description, the author has contributed new or alternative derivations and proofs which may provide new perspectives of the methods and, in some cases, make the governing principles accessible to a wider engineering audience. These derivations and proofs will be identified to the reader as they arise in the Chapter. The numerical experiments are used to test the performance of existing algorithms for different element types and a range of compressibility. The result of these experiments is to demonstrate the need for developing a new robust approach.

Chapters 4 and 5, which represent the culmination of the author's research, provide a path towards a robust approach for stress analysis of nearly-incompressible materials from measured displacement data. Chapter 4 begins with a general strategy for

eliminating the source of numerical instability. This strategy is based on the concept of replacing the original nearly incompressible material with a fully incompressible model. This then permits clear identification of the source of instability as a singularity which can be more easily removed. The implementation of this concept is then developed through a series of specific mathematical methods. These methods are variations of well known methods in applied mathematics and include a modified LU decomposition (Chapter 4), a modified QR decomposition (Chapter 4), and a new variational formulation (Chapter 5). In this progression of methods, the order is such that each successive method improves upon the previous techniques. These chapters also include numerical experiments which demonstrate the cost, in terms of accuracy, of modelling a nearly incompressible material with one that is fully incompressible.

Finally, Chapter 6 presents an additional, though potentially useful, theorem based on the approach of Chapter 5. This mathematical result assesses catastrophic displacement locking when a single force boundary condition is known and the remainder of the boundary conditions consist of measured displacements. It has potential application for addressing certain *inverse problems* in biomechanics where material properties are to be determined from measured boundary displacements in response to a load transducer applied at various locations in the body of tissue. Numerical experiments in this chapter demonstrate how the theorem may be used to identify unacceptable finite element models for property determination.

1.3 Specific Research Objectives

In summary, the research objectives that form the basis of this dissertation are as follows:

(1) to review and assess the biomedical research pertinent to chiropractic manipulation of the cervical spine, confirm the societal need for resolution of the issue, and establish a foundation for physical modelling and finite element analysis;

(2) to review and assess the state-of-the-art in finite element methods for nearly incompressible materials and test the hypothesis that improvements are needed to deal with the specific conditions posed by *in vivo* analysis of the vertebral artery from measured displacement data;

(3) to provide alternate mathematical descriptions and proofs which the author has developed to enhance the presentation of certain existing finite element methods for analysing nearly incompressible materials;

(4) to develop robust finite element methods for analysing nearly incompressible materials from displacement data by using a fully incompressible model and eliminating the resulting singularity; and

(5) to demonstrate the proposed methods with numerical examples.

Chapter 2

The Chiropractic Problem – Manipulation of the Cervical Spine

2.1 Introduction

According to the Canadian Chiropractic Association, “Chiropractic today is one of the largest primary care health professions in Canada with over 6,000 practicing chiropractors. Approximately four and a half million Canadians use the services of a chiropractor each year” [www.ccachiro.org]. Despite their prevalence, however, some chiropractic procedures have been criticised with regard to their safety. In particular, there is considerable controversy regarding manipulation of the cervical spine.

The first objective of this thesis is to review and assess the biomedical research pertinent to chiropractic manipulation of the cervical spine, confirm the societal need for resolution of the relevant issues, and establish a foundation for physical modelling and finite element analysis. In this chapter, the nature of debate between chiropractors and medical doctors is explored. This establishes the degree to which medical professionals are uncertain about the true risks associated with neck manipulation. A description of the anatomy associated with the problem and a review of applicable scientific studies lead to the conclusion that resolution requires a methodology combining medical imaging with engineering stress analysis.

2.2 Background Information

Manipulation of the cervical spine is used to treat patients with head and neck disorders, including neck pain and stiffness, muscle-tension headache and migraine [Di Fabio, 1999]. It involves the application of a thrusting force that moves the spinal joints beyond the normal range of motion [Vautravers and Maigne, 2000]. Most complications of cervical spine manipulation (CSM) are vascular [Vautravers and Maigne, 2000]. One of the risks is the possibility of having a stroke or cerebrovascular accident caused by vertebral artery dissection following cervical spine manipulation. The actual incidence of complications has been estimated from a variety of studies to be within the range of 1 in 50000 to 1 in 5 million [Di Fabio, 1999]. Considering chiropractic and medical sources, a commonly agreed upon number appears to be one incident per million adjustments. However, a report from the World Chiropractic Alliance argues that even this is an overestimation since a temporal relationship between two events (the chiropractic adjustment and the stroke) does not mean that one was caused by the other [World Chiropractic Alliance, 2001]. On the other hand, Frisoni and Anzola [1991] suggest that the estimates are low since not all cases are reported in the medical or chiropractic literature.

Although the incidence of complications is rare, the outcome is often unfavourable. In a study of 182 published cases; death occurred in 29 cases, 86 people had permanent neurologic impairment, 44 people recovered and in six cases, the outcome was unknown [Vautravers and Maigne, 2000]. From various reviews of case studies in the literature, it has been found that most of the cases of vertebral artery dissection are in people less than 45 years of age and in those that have had more than one cervical spine

manipulation [Frisoni and Anzola, 1991; Hufnagel *et al.*, 1999; Di Fabio, 1999; Rothwell *et al.*, 2001]. Reviews have also shown that when the type of manipulation was identified, rotational thrust was the mechanism of manipulation [Plaugher, 1994; Di Fabio, 1999; Smith and Estridge, 1962].

A pre-manipulative test, called the extension-rotation test, has been developed to determine those at risk of stroke. This test has the patient in a supine position with the head extended beyond the end of the table. The head is then rotated to each side while in the extended position. The patient then rotates his head to the extreme range of motion keeping his eyes open. While these movements are being performed, the patient is watched for signs of blanching, nystagmus or cyanosis around the mouth. If any of these occur or the patient complains of dizziness or nausea, manipulation in this position is contraindicated [Gatterman, 1990]. Unfortunately, the pre-manipulative test may not identify whether a patient is at risk since the adjustment will move the joints farther than the test and the rapid thrust of the manipulation is missing in the test [Di Fabio, 1999; Rothwell *et al*, 2001]. Also, the pre-manipulative test itself may cause a stroke [Plaugher, 1994; Di Fabio, 1999].

Key to understanding mechanisms by which a stroke could be caused by CSM is the anatomy of the vertebral artery. A pair of vertebral arteries runs through the cervical spine and supplies the brain stem which plays an important role in numerous physiologic functions, such as regulating the heart and lungs [Mader, 1985]. Each vertebral artery winds around the uppermost vertebra to enter the skull. At this point it is vulnerable to torsion injury and abrupt rotation may stretch the artery and tear the

inner lining of the artery [Norris *et al.*, 2000]. In fact, in cases where angiography has been performed, vertebral artery dissection has been observed most often at the joint of the upper two vertebrae [Norris *et al.*, 2000; Frisoni and Anzola, 1991; Hufnagel *et al.*, 1999]. However, this does not explain why some people have strokes but most do not.

Several hypotheses have been proposed to explain the predisposition of some people to vertebral artery dissection caused by cervical spine manipulation. Smith and Estridge [1962] proposed that pre-existing vascular abnormalities (such as, hypoplasia of one of the vertebral arteries) or bony abnormalities (such as, osteophyte formation or calcification of the atlantooccipital ligaments) would cause trauma to the vertebral artery when the head is rotated and hyperextended. Frisoni and Anzola [1991] suggested that repeated manipulations might cause small lesions in the arterial wall leading to a final lesion. They also proposed possible risk factors: vertebral artery size asymmetry, irregular vertebral artery anatomy, atherosclerosis, osteoarthritis, vertebral ligament laxity and risk factors for vascular disease, such as hypertension, stroke, diabetes, oral contraceptive use, migraine or transient ischemic attack [Frisoni and Anzola, 1991]. Komiyama *et al.* [2001] found a correlation between a left vertebral artery of aortic origin and arterial dissection. They hypothesised that this correlation may be caused by larger shear stress in the artery due to the anatomical differences.

A need for further research in this area is made evident by the above discourse. Clearly, there is not a reliable scientific paradigm which can be used as a basis for safe and effective practice. Since chiropractic medicine has become commonplace in society, this situation must be remedied. Towards this end, the rest of this chapter aims to

further explore the relevant anatomy, describe the existing scientific studies, and then, finally, to propose a direction for the remainder of the thesis and future research in the area.

2.3 Relevant Anatomy, Properties and Kinematics

Anatomy of the neck is well established, with similar descriptions found in several medical sources [e.g., Heller and Pedlow, 1998; Cramer and Darby, 1995]. The cervical spine consists of seven vertebrae: four typical (Figure 2.1) and three atypical (e.g. Figures 2.2 and 2.3). The cervical vertebrae are numbered starting with C1, on which the head rests, and then continuing in the inferior direction. The typical cervical vertebrae, shown in Figure 2.1, are C3 to C6. They are comprised of a vertebral body, vertebral arch and processes (articular, transverse and spinous) that allow for muscle attachment. The vertebral body gives strength and support for two thirds of the vertebral load [Heller and Pedlow, 1998]. It is composed of a cancellous (porous) core surrounded by a thin shell. All vertebrae possess a vertebral foramen which is the central “hole” forming the spinal canal. In contrast, only cervical vertebrae C1 to C6 possess transverse foramina (Figures 2.1, 2.2 and 2.3) which form a pathway and support structure (Figures 2.4, 2.5 and 2.6) for the vertebral arteries feeding the brain stem. Typically, each of the two vertebral arteries enters a transverse foramen of C6 and continues superiorly to pass through each subsequent foramen, from C5 to C1.

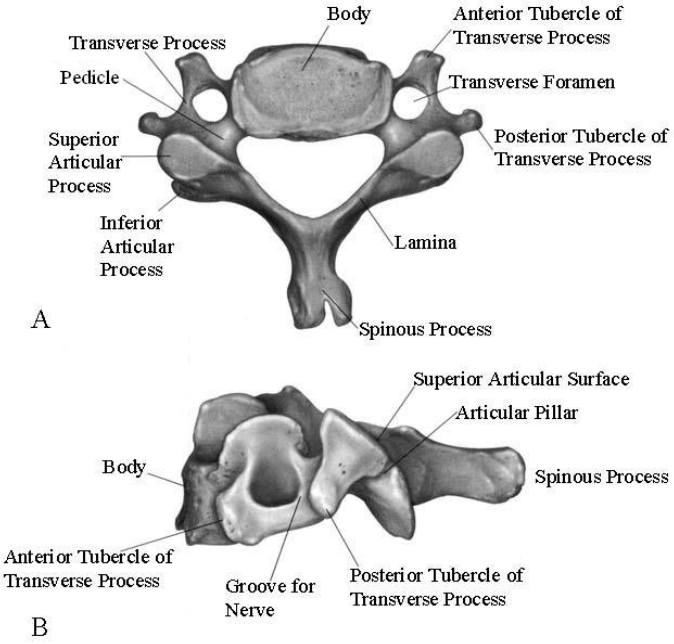

Figure 2.1: Typical Cervical Vertebra A. Superior View B. Lateral View (from Heller and Pedlow, 1998).

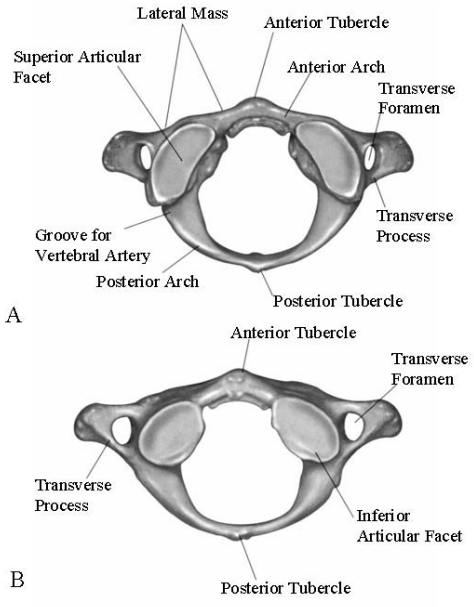

Figure 2.2: Atlas (C1) A. Superior View B. Inferior View (from Heller and Pedlow, 1998).

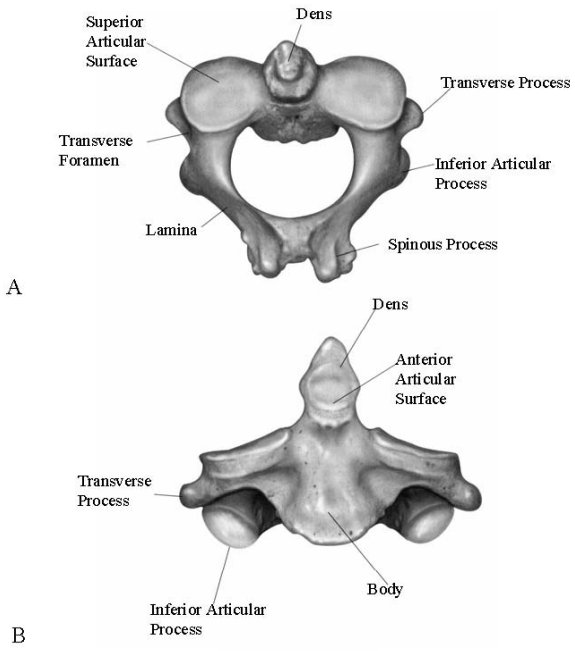

Figure 2.3: Axis (C2) A. Superior View B. Anterior View (from Heller and Pedlow, 1998).

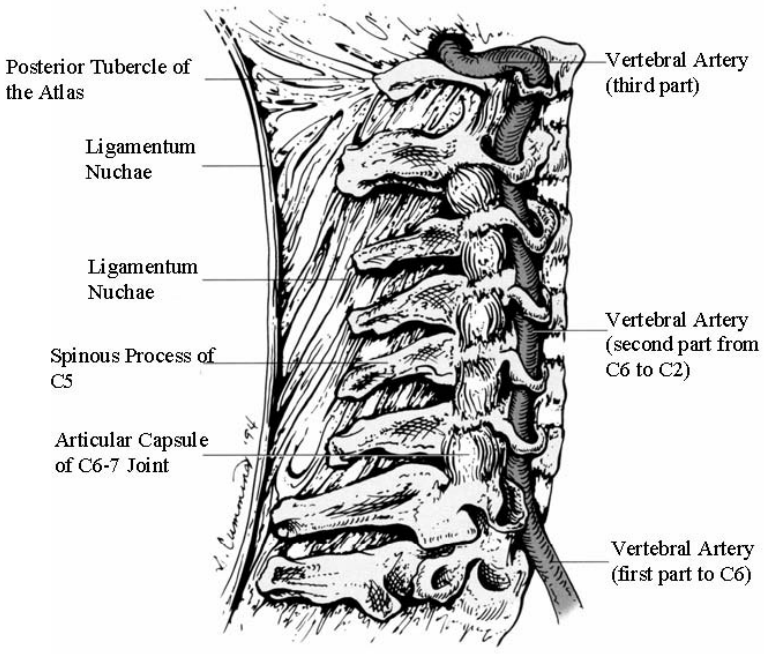

Figure 2.4: Second and Third Parts of the Vertebral Artery (from Cramer and Darby, 1995).

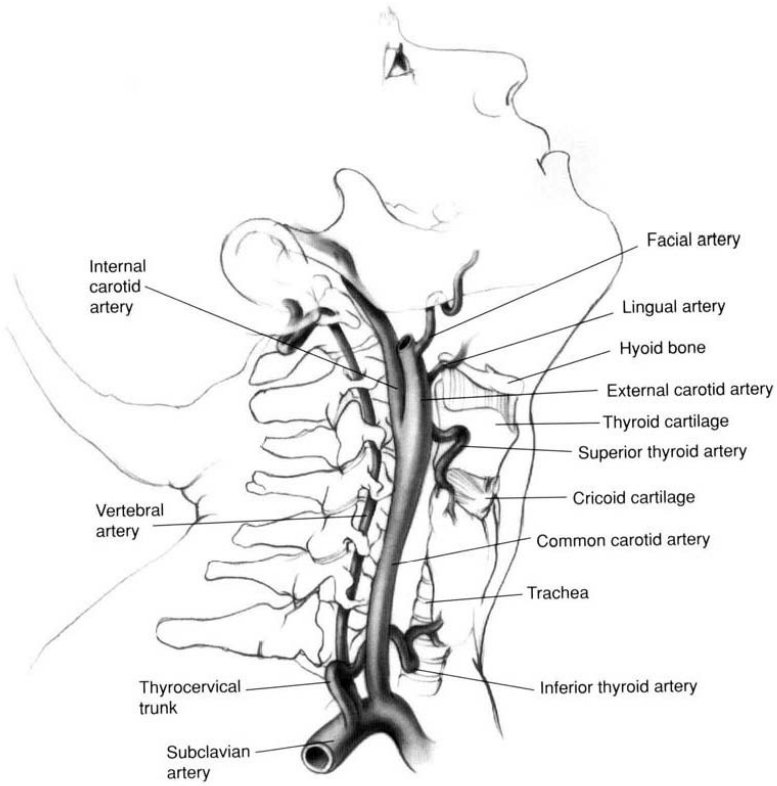

Figure 2.5: Arteries of the Neck (from Heller and Pedlow, 1998).

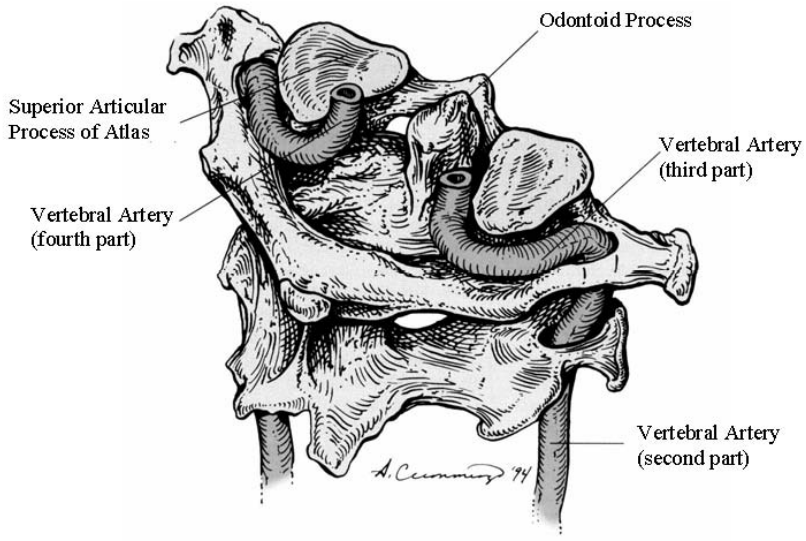

Figure 2.6: Third and Fourth Parts of the Vertebral Artery (from Cramer and Darby, 1995).

The atypical vertebrae are C1, C2 and C7. The geometric path of the vertebral arteries in and around C1 and C2 is particularly complex. C1, or the atlas (shown in Figure 2.2), is composed of two lateral masses joined by an anterior arch and a posterior arch. On the superior surface of the posterior arch, a groove exists for the vertebral artery. The vertebral artery proceeds superiorly through the transverse foramen of C1, around the superior articular process and lies on top of the posterior arch (Figure 2.6). The groove is sometimes covered either completely or partially by bone, which results in the formation of an additional foramen [Heller and Pedlow, 1998].

C2, known as the axis, is shown in Figure 2.3 and has a process or dens that projects upward from the body to articulate with the posterior side of the anterior arch of C1. The superior articular processes of the axis articulate with the inferior articular facets of C1. The configuration of these joints allows for much rotation (approximately 45° to each side) between the atlas and axis [Cramer and Darby, 1995].

Taken together, then, the geometry and supporting structures of the vertebral artery pose a considerable challenge for any attempts at stress analysis. This challenge is intensified by characteristics associated with arterial properties and spine kinematics. The vertebral artery has a complex material structure which is described in detail by Fung [1993]. Like other arteries, or blood vessels in general, it consists of three layers: the intima, media and adventitia. The intima is the innermost layer and contains endothelial cells. The media is the middle layer and contains smooth muscle cells. The adventitia is the outermost layer and contains collagen and ground substances. The stiffness of the inner

two layers is greater than that of the outer layer. The stress-strain relationship of this nonhomogeneous, composite structure is nonlinear and exhibits hysteresis. Creep occurs under constant stress and stress relaxation occurs under constant strain. Fung [1993] also suggests that the stresses and strains in an arterial wall may be related by a strain-energy function.

In terms of kinematics, the large rotation at the C1-C2 level of the spine has been shown to cause problems with kinking of the vertebral artery. Selecki [1969] found that after 30 degrees of rotation, there is kinking and stretching of the contralateral vertebral artery. At 45 degrees of rotation, kinking of the ipsilateral artery also occurs [Selecki, 1969]. This kinking and stretching may be caused by the fact that during axial rotation, the atlantoaxial joint on the ipsilateral side of rotation is relatively fixed, and on the contralateral side the atlas moves forward on the axis [Thiel, 1991]. This may also cause the opening of the vertebral artery to be stretched.

2.4 Previous Studies of the Cervical Spine and Vertebral Artery

The cervical spine has been the subject of numerous research studies. Not all, however, have been related to the vertebral artery or cervical manipulative therapy (CMT). For example, the anatomy of various portions of the cervical spine has been quantified. Oh *et al.* [1996] and Panjabi *et al.* [1991] quantified the three-dimensional anatomy of the mid to lower cervical spine (C3 to C7) to provide guidelines to the surgeon and improve safety of surgery in that area. Doherty and Heggeness [1994; 1995] had the same objective for their studies of the atlas and axis. The biomechanics of the cervical spine

has been studied using physical experiments on cadavers to determine injury mechanisms [Yoganandan *et al.* 1990], as well as static and dynamic bending responses [Voo *et al.*, 1998].

In addition to physical experiments, the spine has been studied using finite element models outside the context of CMT. In 1996, Yoganandan *et al.* wrote a review of the current finite element models of the human cervical spine, including models treating the vertebrae as rigid masses and the connective tissues as spring elements. At that time, they reported five new models with a higher level of technical detail. This included two-dimensional static analysis [Saito *et al.* 1991], three-dimensional static and dynamic analyses [Kleinberger, 1993; Bozic *et al.*, 1994; Teo *et al*., 1994], and finally a three-dimensional, linear, static stress analysis of the C4-C5-C6 spinal unit including discs, endplates and all ligaments [Yoganandan *et al.*, 1996].

Since that review of the finite element models existing prior to 1996, other models have been produced. Maurel *et al.* [1997] created a three-dimensional parameterised finite element model of the cervical spine from C3 to C7. They parameterised the geometry of the vertebrae to study the effect of different geometry on the mechanical behaviour of the cervical spine. This model included intervertebral discs, ligaments and some geometric and material nonlinearities. They found that the behaviour of their model varied greatly with small changes in the geometry [Maurel *et al.*, 1997]. In 1997, Yoganandan *et al.* created a three-dimensional finite element model of C4 to C6 using a computed tomography (CT) scan. Their model was geometrically accurate but did not include the ligaments. They used linear, isotropic, homogeneous material properties and

performed a parametric study by varying the properties of the vertebral endplates and the intervertebral discs. The same model was used to study various biomechanic effects, including laminectomy and facetectomy [Kumaresan *et al.*, 1997], responses of a paediatric neck by modifying the anatomy and material properties [Kumaresan *et al.*, 1997; Kumaresan et al., 2000], and changes in the external and internal responses of the model that occurred from varying Young's modulus of the cortical shell and cancellous core of the vertebral body, endplates, intervertebral disc and the ligaments [Kumaresan *et al.*, 1999]. Clausen *et al.* [1997] created a model of the C5-C6 motion segment from CT scans to study the effect of uncinate processes and uncovertebral joints on the biomechanics of the cervical spine. Sadegh *et al.*, [2000] used a dynamic load and viscoelastic material properties within their finite element models to predict the stresses in each vertebra and intervertebral disc.

In 2002, Fagan *et al*. created a review of spinal finite element models. Their review included whole spine models, vertebral body models, disk models, and cervical and lumbar spine models. The cervical spine models reviewed were mainly used for assessment of spinal cord injury. Using CT images, Brolin and Halldin [2004] created a finite element model of the upper cervical spine to study ligament characteristics. Tropiano *et al*. [2004] analysed the cervical spine in whiplash conditions using a finite element model of the entire human body (HUMOS). This model includes all bones, ligaments, tendons, skin, muscle and internal organs. Greaves et al. [2008] created a three-dimensional cervical spine model which included vertebrae, ligaments, discs and the spinal cord to investigate injury mechanisms. The spinal cord was modelled as linear, elastic and nearly incompressible (i.e. $\nu = 0.49$). Forces were applied to the

vertebrae and resulting reaction forces to the spinal cord. Finally, Wheeldon *et al*. [2008] modelled the lower cervical spine to determine the internal response of the spine to external loading. This used nonlinear material properties for the ligaments and vertebral discs thereby improving on previous models. These finite element models illustrate the biomechanics of the cervical spine for various movements and different loads. While these models show stresses and interactions between the vertebrae, intervertebral discs and some ligaments and muscles, they do not include the vertebral artery or aspects of CMT.

Studies which have included the vertebral artery have largely examined blood flow dynamics only, without analysing stresses or deformation within the arterial wall. Both experimental and numerical investigations have been conducted. A major category of experimental inquiry has employed imaging modalities. Duplex Doppler sonography has been used to visualise and evaluate blood flow in the extracranial portion [Trattnig *et al.*, 1990] as well as the intracranial portion [Kaps *et al.*, 1992] of the vertebral arteries. Doppler measurements have also been used to assess the effect of disk degeneration on vertebral arterial flow [Bayrak *et al*., 2009]. These studies confirmed the validity of this type of sonography in imaging the vertebral arteries, and other researchers have used it to study the flow with various types of spinal movements.

Refshauge [1994], for example, used duplex Doppler sonography to study the blood flow in the vertebral and internal carotid arteries. He found that blood velocity increased in 45 degree contralateral rotation and decreased in full rotation, but this was not consistent across all vessels studied. He concluded that sustained rotation influences

blood velocity in the extracranial vessels. Thiel [1991] used duplex Doppler sonography to study the blood flow in the vertebral artery while Wallenberg's test was performed. (Wallenberg's test is a pre-manipulative chiropractic procedure that places the head and neck in a position of sustained extension with rotation to screen for vertebrobasilar insufficiency.) Licht *et al.* [1998; 1999; and 2000] have used Doppler ultrasound extensively to study the effect of manipulation on the flow in the vertebral artery. In 1998, they studied the flow velocity to determine whether changes occur after spinal manipulation. They found no change in peak flow velocity. In 1999, they measured the volume blood flow in the vertebral artery of pigs during spinal manipulation and pre-manipulative testing. They found that the flow increased significantly after cervical manipulation for 40 seconds and then returned to normal, but the pre-manipulative tests did not change the flow significantly. In 2000, they studied vertebral artery blood flow in patients with positive pre-manipulative tests that were referred by chiropractors. They measured the flow velocities in both vertebral arteries but found no significant differences with different head positions. They concluded that a positive pre-manipulative test is not necessarily a contraindication to manipulation of the cervical spine.

Rivett *et al.* [1999] also used duplex Doppler sonography with colour flow imaging to determine the effect of pre-manipulative testing on the vertebral and internal carotid arteries. In contrast to the previous studies mentioned, they found that there were significant changes of flow velocity in the vertebral arteries in end-range positions involving rotation and extension. They concluded that the use of pre-manipulative testing is supported by their research.

To the best of the author's knowledge, the only numerical studies of blood flow in specifically the vertebral arteries are the finite element analyses by Krijger *et al.*, [1992] and Ravensbergen *et al.*, [1996], [1997]. In both cases, the vertebral artery was modelled to study the flow at the junction of the vertebral and basilar arteries. Neither of these investigations included the interaction between the arteries and the cervical spine.

Many of the experimental and numerical flow studies outlined above could be pertinent in future discussions of chiropractic manipulation of the cervical spine and its inherent risks. However, none of these investigations directly address the issue of CMT in terms of stresses in the arterial wall, and potential consequences including arterial dissection and dislodging of plaque.

Although little research has been conducted into arterial stresses during CMT, there have been studies into the properties and morphological response of the vertebral artery itself. Kawchuk *et al.* [2004] established an "experimental platform" for using intravascular ultrasound to provide two dimensional and three dimensional representations of the vertebral artery. They developed their platform using sedated canine subjects. Magnetic resonance imaging (MRI) has also been used to provide various images of the vertebral artery and arterial dissection [Kansagra *et al.*, 2008; Jacobs *et al.*, 1997; Mascalchi *et al.*, 1997]. Johnson *et al.* [2000] considered biomechanics of the artery. They compared the tensile behaviour in longitudinal and circumferential extension. Four biomechanical parameters were studied: percent extension required to break the sample, tensile strength, peak load and Young's

modulus. They found that the tensile strength of the longitudinal specimens was significantly lower than that of the circumferential specimens, possibly explaining why hyperextension or rotation of the neck can damage the vertebral artery by stretching it. They also found that the biomechanical parameters change along the length of the artery.

Less common is a study performed by Sheth *et al.* [2001] that considered the rotational changes in the morphology of the vertebral artery. They used magnetic resonance angiograms to study, *in vivo*, the normal rotational anatomy of the vertebral arteries and the bone at the C1-C2 junction. They found that when the head is rotated by 45°, the calibre of the contralateral artery as it exits the transverse foramen of C1 is decreased compared to the ipsilateral artery and when the head is in neutral position. This narrowing caused approximately seven percent elongation of the artery from C2 to the dural entry point. They did not consider this a significant change. They concluded that the likely site of vertebral artery dissection is the exit of the transverse foramen of C1 as opposed to the C1-C2 junction as other studies identify [Sheth *et al.*, 2001].

In terms of work directly targeting the effect of CMT on the potential for stroke or other injury, numerous case studies have been conducted [Ernst *et al*., 2002; Ernst, 2007; Kawchuk *et al*., 2008], but most are based on a qualitative medical methodology and are bereft of quantitative analysis. The quantitative research that has been identified from the author's examination of the literature is by researchers from the Human Performance Laboratory at the University of Calgary who are studying the biomechanics of spinal manipulative therapy. They have measured the forces exerted during different

techniques used for manipulation of the spine in the cervical, thoracic and sacroiliac regions of human volunteers. To take these measurements, they used a flexible pressure mat and found that the forces exerted on the cervical spine are considerably smaller than those exerted on the other two areas [Herzog *et al.*, 1993]. The same group of researchers also studied the effect of manipulation on the vertebral artery [Symons *et al.*, 2002]. They attached ultrasonic crystals to the vertebral arteries of unembalmed cadavers and performed manipulations while recording the strains. Mechanical testing was performed on the same arteries which had been removed from the bodies to determine the strain at failure. Comparing the strains *in situ* to the failure strain, they concluded that the artery does not experience enough strain during manipulation to "mechanically disrupt it" [Symons *et al.*, 2002]. The methods used for this study have been criticised by some chiropractors [Carstensen, 2004; Good, 2003].

2.5 A Plan for Engineering Analysis

In the preceding sections, the background and pertinent questions surrounding the "chiropractic problem" have been identified. Although the chiropractic problem is important to society and has generated considerable discussion and debate by professionals in both chiropractic and traditional medicine, it is clear that existing research has not answered the key questions. In this section, the information from §2.1 to §2.4 is compiled and assessed with a goal of establishing a direction for future biomechanical research in the field.

The literature is rife with case studies based on qualitative methodology and statistical "evidence" in attempts to establish the cause and incidence of vertebral artery dissection in connection with chiropractic manipulation of the cervical spine. The result has been a series of conflicting opinions and conclusions without a definitive resolution. Clearly, a bias exists in that the conclusions drawn depend on which group, i.e. chiropractic or traditional medicine, is conducting the study.

Quantitative research beyond statistics has either focused on aspects which do not directly address the issue of vertebral artery dissection, or make assumptions which leave the validity of the results in question. Although the studies of arterial flow provide important information regarding scenarios where blood flow could be impeded, they do not consider the stress field or potential failure of the arterial wall. The analyses that have focused on the arterial wall depend on cadavers and employ questionable procedures. The ultrasonic crystal data which has been collected corresponds to locations on the artery which, according to other studies, are not critical to the problem. The time of propagation values provide, at best, a rough estimate of some average strain measure along an artery during manipulation. This value is then compared to a failure load which was obtained for a specific material orientation in a tension test. No reference is made to the specific components of the strain tensor, the anisotropy of tissue properties, or failure measures from established theories in the mechanics of deformable bodies. The relevance of existing research, therefore, must be questioned and yet this research has been used as a basis for strongly concluding that a single thrust during spinal manipulative therapy is "unlikely to tear or otherwise mechanically disrupt the VA [vertebral artery]" [Symons *et al*., 2002].

To provide a more meaningful quantitative analysis, engineering principles and, specifically, the methods of advanced stress analysis can be applied. It is practically impossible, however, to obtain an analytical solution to the governing equations of stress and strain for a problem of this complexity. Referring to §2.3, and in particular Figures 2.4, 2.5, and 2.6, the intricacy of geometry and boundary conditions of the vertebral artery requires numerical solution of the corresponding boundary value problem. In solid mechanics, the most widely used and accepted technique is the finite element method. With a *suitable* finite element formulation, the stress field resulting from cervical manipulative therapy could be evaluated, and there would be potential to answer a number of fundamental questions: Are some people predisposed to arterial dissection from cervical spine manipulation due to anomalous anatomy and variations in arterial properties? What type of manipulation (i.e., loading) causes the damage? Does the change in blood pressure from systolic to diastolic within the artery affect the chances of a vertebral artery dissection? Can the pre-manipulative test cause a stroke and does it accurately predict those that might have a stroke, since the thrust component of the chiropractic manipulation is missing?

A suitable finite element formulation for this application must satisfy certain requirements. First and foremost, it must be appropriate for the analysis of soft tissue and, therefore, nearly-incompressible material [Vito & Dixon, 2003; Weinberg & Kaazempur-Mofrad, 2006]. Next, the formulation must accommodate the effects of large deformation (i.e., geometric nonlinearity) that is indicated by the rotations associated with head movement and CMT, as described in §2.3 and §2.4. Many commercial finite element codes are capable of an analysis of this type. However, an

added challenge occurs due to the complex nature of the loading conditions experienced by the vertebral artery during cervical manipulative therapy. The forces applied directly to the artery are unknown without modelling the anatomical detail between the practitioners hands on the surface of the neck and the resulting forces on the artery due to both the bony structures (vertebrae and transverse foramina) and soft tissues (ligaments and musculature). Due to anatomical differences, this modelling would be required for each individual person (as confirmed by the work of Maurel et al. [1997] reviewed in §2.4). While forces on the neck have been measured (as reviewed in §2.4), the forces on the artery, *in vivo*, cannot be inferred from these measurements. This fact alone could preclude finite element analysis of the vertebral artery. Fortunately, the review in §2.4 shows that useful boundary information in the form of measured displacements can be obtained with imaging techniques such as ultrasonography or magnetic resonance imaging (MRI). Thus, the finite element formulation appropriate to modelling the vertebral artery, *in vivo*, must incorporate near-incompressibility, geometric nonlinearity, displacement boundary conditions, and the associated uncertainty in the measured displacements. As demonstrated in the next chapter, achieving this result with existing finite element methods is problematic and necessitates a new approach.

Chapter 3

Fundamental Issues with Finite Element Modelling

3.1 Preliminary Comments on the Finite Element Method

The finite element method (FEM) has been a work in progress for several decades. Its evolution has come from several disciplines. Mathematicians use the method for numerical solution of partial differential equations in boundary value problems. Originally, engineers used the FEM in the form of the flexibility method mainly for aircraft design in which forces were the primary unknowns or the stiffness method in which displacements were the primary unknowns [Felippa, 2001]. Calculations at this time were performed by hand. For nonstructural applications, such as the analysis of solids, fluid flow or heat transfer, variational principles used an extension of the Rayleigh-Ritz method and Castigliano's First Theorem by minimisation of a potential functional. In applications where a variational principle is not appropriate, such as mass transport, Galerkin's Residual Method was applied [Logan, 1993].

Although there are many different implementations or formulations of the FEM and many different areas of application, there is a common thread throughout. An unknown field is discretised or divided into a set of smaller and simpler interconnected bodies or

elements. For example, the variation of a certain quantity over the entire field may be unknown, whereas over an element its variation may be approximated as linear. The governing equations, such as equilibrium and compatibility, are satisfied either approximately or exactly throughout the discretised field and boundary conditions are applied. Finally, values of the quantity at discrete points in the field are determined by solving a system of simultaneous linear equations which is formed from the individual element equations. Whatever the formulation or application, the appeal of the finite element method is due to its ability to produce an approximate solution to a problem with complicated geometry, loading or material properties for which an analytical solution is not available. However, as shown in the next section, finite element calculations become unreliable when dealing with the parameters chosen to model the vertebral artery during chiropractic manipulation: near-incompressibility, measured displacement data, and geometric nonlinearity.

3.2 A Motivating Example – FEM of a Simple Patch

The remainder of this chapter and subsequent chapters will explore the pertinent technical aspects of the finite element method in detail. It will be instructive, however, to first show the results of a preliminary simulation demonstrating the fundamental shortcomings of applying the finite element method in the present context. Consider a loaded rectangular plate of thickness t and in-plane dimensions b and h, as shown in Figure 3.1. The plate is subjected to pressure P along two opposite sides and is constrained in the z-direction to create a uniform state of plane strain in the x-y plane. A rudimentary finite element mesh, consisting of four rows and four columns of identical

rectangular elements, is also shown in the figure. The objective of the analysis is to determine unknown stresses and displacements over each element from known conditions on the boundary of the plate. This simple test case is an example of a broader series of classical tests, known as the patch test, used to assess finite element convergence. (The patch test will be discussed in more detail later in the thesis.) For a method to be reliable for analysing complicated problems, it must be robust for the simplest fields, including a uniform distribution.

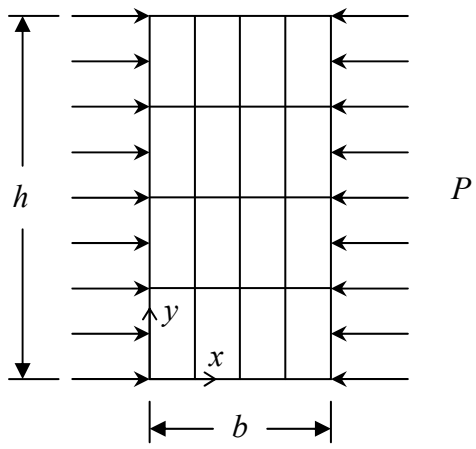

Figure 3.1: Plane strain compression of rectangular plate by pressure P (finite element mesh included).

For a linear elastic material, the analytical solution to this problem may be obtained directly from generalised Hooke's law and the classical strain-displacement relations, giving

$$\sigma_x = -P\,, \tag{3.1}$$

$$\sigma_y = 0\,, \tag{3.2}$$

$$\sigma_z = -\nu P\,, \tag{3.3}$$

$$u = -P\frac{\left(1-\nu^2\right)}{E}\left(x-\frac{b}{2}\right), \tag{3.4}$$

and

$$v = P\frac{\nu\left(1+\nu\right)}{E}\left(y-\frac{h}{2}\right), \tag{3.5}$$

where E is Young's modulus, ν is Poisson's ratio, σ_x, σ_y, and σ_z are the normal stresses, and u and v are the displacements in the x- and y-directions, respectively. For the arbitrarily selected values of P = 0.1 kN/mm^2, E = 70 kN/mm^2, b = 100 mm, and h = 200 mm, equations (3.4) and (3.5) were used to produce displacement boundary conditions so that the problem could be recast as a Dirichlet boundary value problem where, on the boundary, u and v are known but P is unknown as would be encountered in the chiropractic problem. As will be discussed in detail later in this chapter, a material is "nearly incompressible" when Poisson's ratio is "close to 0.5". ANSYS®, a commercially available finite element software package, was used to solve the test problem for values of Poisson's ratio from 0.4 to 0.4999. For this preliminary simulation, a standard linear elastic, plane strain, displacement formulation with classical four node quadrilateral elements was used. To simulate uncertainty in the boundary displacement data, a random error distribution with a maximum value of 1% was applied to the data. The results for σ_x, σ_y, and σ_z are given in Tables 3.1, 3.2, and 3.3, respectively.

The purpose of considering a range of Poisson's ratio values is to compare the performance of the finite element method for compressible materials versus materials that approach incompressibility. For each case, the theoretical stress field is uniform over the plate, while ANSYS® gives a stress variation as shown in the tables. For

$\nu = 0.4$ and $\nu = 0.45$, the error in the stress values calculated by ANSYS® are of the same order of magnitude as the uncertainty in the data. However, for $\nu = 0.49$ and $\nu = 0.4999$, the results indicate a fundamental problem with obtaining usable stress values from displacement data for Poisson's ratio in this range, precisely the range normally used in modelling soft tissue [Baldewsing, 2006]. A relatively small uncertainty in the given data was used to produce these results, and further simulations would show that changing the specific error distribution causes erratic changes in the solution for Poisson's ratio close to 0.5. Furthermore, for problems which exhibit geometric nonlinearity, iterative methods are typically used. Each iteration would require solution of a linearised system, and any erratic behaviour would be magnified with each step in the process.

Table 3.1: Comparison of Theoretical and Finite Element Values for σ_x.

ν	Theoretical Value (MPa)	Maximum FEM Value (MPa)	Minimum FEM Value (MPa)
0.4000	-100.0	-98.98	-102.7
0.4500	-100.0	-98.81	-104.1
0.4900	-100.0	-60.91	-65.72
0.4999	-100.0	-227.0	-488.9

Table 3.2: Comparison of Theoretical and Finite Element Values for σ_y.

ν	Theoretical Value (MPa)	Maximum FEM Value (MPa)	Minimum FEM Value (MPa)
0.4000	0	0.4307	-1.854
0.4500	0	0.1447	-3.461
0.4900	0	41.31	37.47
0.4999	0	-127.4	-389.8

Table 3.3: Comparison of Theoretical and Finite Element Values for σ_z.

ν	Theoretical Value (MPa)	Maximum FEM Value (MPa)	Minimum FEM Value (MPa)
0.4000	-40.00	-39.74	-41.82
0.4500	-45.00	-44.75	-48.39
0.4900	-49.00	-9.128	-12.71
0.4999	-49.90	-177.2	-439.3

For over 40 years, this numerical instability has been the subject of a major research effort in the finite element community. As a result, much has been achieved toward this problem. One of the goals of this thesis, however, is to show that even the most advanced finite element formulations specifically designed for nearly incompressible materials are inadequate for the combination of conditions posed by the chiropractic problem. In the remainder of this chapter, a presentation of the underlying theory is developed to form a basis for: identifying the fundamental source of numerical instability; assessing the pertinent finite element formulations; and, most importantly, extending the theory to resolve the instability issue. In the remainder of this thesis, these mathematical developments and extensions, together with the theorems, proofs, and algorithms that result, constitute the majority of the research contribution. Simple numerical examples are used throughout only to demonstrate and reinforce the fundamental concepts embodied in the mathematics.

3.3 FEM and Incompressibility

3.3.1 Constitutive Modelling

The most accurate model of biological materials would account for several properties. Accordingly, numerous constitutive models have been developed to include: material and geometric nonlinearity; anisotropy; incompressibility; time dependence; inhomogeneity; and multiaxial effects. For reviews of methods used to determine soft tissue material properties and soft tissue constitutive models, see [Sacks and Sun, 2003] and [Vito and Dixon, 2003], respectively. See also Simon *et al.* [1998], McAfee *et al.*, [1994], Itskov and Aksel [2002], and Fung [1993] which has been a standard for many years. Linear elasticity, or more specifically Hooke's law, has also been used with success to model soft tissue [Fung 1993; Coley, 2000]. Although linear elasticity is clearly an approximation, Fung [1993] found that the stress-strain curve for soft tissue has a very shallow curve initially and then slopes upward at a steep angle. Even in cases where hyperelasticity is usually assumed, the relationship between stresses and strains is often linear, or close to linear. The stress-strain curve can remain approximately linear for strains up to 40 percent [Coley *et al.*, 2000]. Depending on the magnitude of the rigid body rotations, material linearity can also hold true while the deformation is geometrically nonlinear.

These constitutive models all focus on certain aspects of soft tissue properties, but all rely on the assumption of near-incompressibility. The issues surrounding near-incompressibility are manifest in both linear and nonlinear cases and, in addition, the iterative solution of nonlinear problems involves a series of linearised substeps. Therefore, the ramifications of near-incompressibility, i.e., numerical instability, can be

examined within the context of linear elasticity theory and, in particular, the governing equations for a Hookean material.

The first approach that was used in this research to investigate the mathematical cause of instability was an examination of the eigenvalues associated with generalised Hooke's law. For isothermal processes, the linearly elastic, isotropic constitutive relation between normal stresses and strains can be written as

$$\boldsymbol{C}\boldsymbol{s} = \boldsymbol{d} \tag{3.6}$$

where

$$\boldsymbol{C} = \begin{bmatrix} 1 & -\nu & -\nu \\ -\nu & 1 & -\nu \\ -\nu & -\nu & 1 \end{bmatrix}, \tag{3.7}$$

$$\boldsymbol{s} = \begin{bmatrix} \sigma_x \\ \sigma_y \\ \sigma_z \end{bmatrix}, \tag{3.8}$$

$$\boldsymbol{d} = \begin{bmatrix} E\varepsilon_x \\ E\varepsilon_y \\ E\varepsilon_z \end{bmatrix}, \tag{3.9}$$

ν is Poisson's ratio, E is Young's modulus, σ_i are the normal stresses at a point and ε_i are the normal strains at that point. Matrix $\boldsymbol{C}$ in equation (3.7) has eigenvalues $1 + \nu$, $1 + \nu$ and $1 - 2\nu$. Mathematically, relative to the basis of matrix $\boldsymbol{C}$, the eigenvectors corresponding to the repeated eigenvalue, $1 + \nu$, lie in a plane perpendicular to the unit vector, $\hat{n} = \frac{1}{\sqrt{3}}\begin{bmatrix} 1 & 1 & 1 \end{bmatrix}^{\mathrm{T}}$ while the eigenvector corresponding to $1 - 2\nu$ falls on a line parallel to $\hat{n}$.

Accordingly, $\boldsymbol{C}$ can be diagonalised by writing

$$\boldsymbol{C} = \boldsymbol{Q}\boldsymbol{\Lambda}\boldsymbol{Q}^{\mathrm{T}} \tag{3.10}$$

where $\boldsymbol{Q}$ is chosen to be the orthogonal matrix

$$\boldsymbol{Q} = \frac{1}{\sqrt{6}}\begin{bmatrix} 1 & \sqrt{3} & \sqrt{2} \\ 1 & -\sqrt{3} & \sqrt{2} \\ -2 & 0 & \sqrt{2} \end{bmatrix} \tag{3.11}$$

and

$$\boldsymbol{\Lambda} = \begin{bmatrix} 1+\nu & 0 & 0 \\ 0 & 1+\nu & 0 \\ 0 & 0 & 1-2\nu \end{bmatrix}. \tag{3.12}$$

Equation (3.6) can be rewritten, therefore, as

$$\boldsymbol{\Lambda}\,\boldsymbol{s}' = \boldsymbol{d}' \tag{3.13}$$

where

$$\begin{aligned} \boldsymbol{s}' &= \boldsymbol{Q}^{\mathrm{T}}\boldsymbol{s} \\ &= \frac{1}{\sqrt{6}}\begin{bmatrix} \sigma_x + \sigma_y - 2\sigma_z \\ \sqrt{3}\left(\sigma_x - \sigma_y\right) \\ \sqrt{2}\left(\sigma_x + \sigma_y + \sigma_z\right) \end{bmatrix} \end{aligned} \tag{3.14}$$

and

$$\begin{aligned} \boldsymbol{d}' &= \boldsymbol{Q}^{\mathrm{T}}\boldsymbol{d} \\ &= \frac{1}{\sqrt{6}}\begin{bmatrix} E\varepsilon_x + E\varepsilon_y - 2E\varepsilon_z \\ \sqrt{3}\left(E\varepsilon_x - E\varepsilon_y\right) \\ \sqrt{2}\left(E\varepsilon_x + E\varepsilon_y + E\varepsilon_z\right) \end{bmatrix}. \end{aligned} \tag{3.15}$$

For full incompressibility, the volume change in a body during deformation is zero. To demonstrate the significance of this, consider the classical expression for dilatation [Beer *et al.*, 2002] given by

$$e = \varepsilon_x + \varepsilon_y + \varepsilon_z , \tag{3.16}$$

where e is the change in volume per volume of an infinitesimal element, and (3.16) is valid within the context of linear elasticity. From the third linear algebraic equation of (3.13),

$$\varepsilon_x + \varepsilon_y + \varepsilon_z = \frac{1-2\nu}{E}(\sigma_x + \sigma_y + \sigma_z) , \tag{3.17}$$

and for fully incompressible materials, by definition, $e = 0$ for any loading, and therefore ν must be 0.5. This also implies that the sum $\sigma_x + \sigma_y + \sigma_z$ is arbitrary and the hydrostatic component of stress (also called the hydrostatic pressure),

$$p = \frac{\sigma_x + \sigma_y + \sigma_z}{3} , \tag{3.18}$$

is undetermined by the constitutive relations; i.e., an infinite number of mathematically consistent solutions exist. This conclusion is valid for both three dimensional fields and and states of plane strain. Furthermore, the diagonalised form of matrix $\boldsymbol{C}$ shown in equation (3.12) clearly shows that for $\nu = 0.5$, $\boldsymbol{C}$ has a zero eigenvalue, a determinant of zero and is singular. For nearly incompressible materials, ν is close to 0.5 and $\boldsymbol{C}$ is therefore ill-conditioned; i.e., small variations or uncertainty in strain values can result in large variations in the calculated values of stress. The ramifications of this indeterminacy within the context of finite element modelling will be reviewed in the next sub-section.

3.3.2 Classical Finite Element Formulation

Many FEM formulations in solid mechanics are based on the classical principle of stationary potential energy [Budynas, 1999; Hughes, 1987]. This principle, based on a potential energy functional, is reviewed here to identify the relationship between finite element analysis and the issues associated with nearly incompressible materials. This review also provides the foundation for a new method, based on a modified potential energy functional, which is introduced later in the thesis. Typically, for compressible materials, the principle of stationary potential energy [Budynas, 1999] states that the equilibrium configuration can be obtained by minimising

$$\Pi = U + \Omega \ , \tag{3.19}$$

where

Π = the total potential energy of the system in static equilibrium,

U = the internal strain energy,

Ω = the potential energy of the external forces,

and, for the standard FEM formulation, Π is considered to be a function of only the nodal displacement degrees of freedom.

The numerical instability arises in the derivation of the strain energy which for linear elastic materials is given by

$$U = \int \left[\frac{1}{2}\sigma_{xx}\varepsilon_{xx} + \frac{1}{2}\sigma_{yy}\varepsilon_{yy} + \frac{1}{2}\sigma_{zz}\varepsilon_{zz} + \frac{1}{2}\tau_{xy}\gamma_{xy} + \frac{1}{2}\tau_{yz}\gamma_{yz} + \frac{1}{2}\tau_{zx}\gamma_{zx} \right] \mathrm{d}V \ . \tag{3.20}$$

or $$U = \frac{1}{2}\int \boldsymbol{\sigma}^{\mathrm{T}} \boldsymbol{\varepsilon}\, \mathrm{d}V \tag{3.21}$$

where $\boldsymbol{\sigma} = \left[\sigma_{xx}\ \sigma_{yy}\ \sigma_{zz}\ \tau_{xy}\ \tau_{yz}\ \tau_{zx}\right]^{\mathrm{T}}$, $\boldsymbol{\varepsilon} = \left[\varepsilon_{xx}\ \varepsilon_{yy}\ \varepsilon_{zz}\ \gamma_{xy}\ \gamma_{yz}\ \gamma_{zx}\right]^{\mathrm{T}}$, V is volume, σ_{ij} are the normal stress components, τ_{ij} are the shear stress components, ε_{ij} are the normal strain components, and γ_{ij} are the shear strain components.

When the body is discretised into nodes and elements in the FEM, the standard strain-displacement relations become

$$\boldsymbol{\varepsilon} = \boldsymbol{B}\,\boldsymbol{u} \tag{3.22}$$

where $\boldsymbol{B}$ is the matrix which contains derivatives of the shape functions used to relate nodal position to nodal displacements in an element and $\boldsymbol{u}$ is the column vector of nodal displacements for that element. The stress-strain relations are

$$\boldsymbol{\sigma} = \boldsymbol{D}\boldsymbol{\varepsilon} = \boldsymbol{D}\boldsymbol{B}\boldsymbol{u} \tag{3.23}$$

where $\boldsymbol{D}$ is the material relation between stresses and strains. When equations (3.22) and (3.23) are substituted into equation (3.21) the expression for the strain energy becomes

$$U = \frac{1}{2}\int \boldsymbol{u}^{\mathrm{T}}\boldsymbol{B}^{\mathrm{T}}\boldsymbol{D}^{\mathrm{T}}\boldsymbol{B}\,\boldsymbol{u}\, \mathrm{d}V\,. \tag{3.24}$$

The total potential energy Π is found by adding U to $\Omega = -\Sigma F_i u_i$ where F_i are the nodal forces and u_i are the associated nodal displacements. When this is minimised with respect to $\boldsymbol{u}$, the result is the usual finite element formulation [Budynas, 1999]

$$\boldsymbol{K}\boldsymbol{u} = \boldsymbol{F}\,, \tag{3.25}$$

where $\boldsymbol{K}$ is the coefficient or stiffness matrix, and $\boldsymbol{F}$ is the column vector of nodal forces. For compressible materials, there are generally no problems with this formulation. The problem with near incompressibility arises from the determination of the matrix $\boldsymbol{D}$, which relates stresses to known strains and is the mathematical inverse of $\boldsymbol{C}$ given in equation (3.7). As was shown previously, for three-dimensional and plane strain formulations under the idealisation of full incompressibility, $\boldsymbol{C}$ is singular and therefore has no inverse (but may have a generalised inverse [Loredo & Klocker, 1997; Zheng, 2002]). Thus, $\boldsymbol{D}$ does not exist. For nearly incompressible materials, $\boldsymbol{C}$ is ill-conditioned and it may be shown that its inverse $\boldsymbol{D}$ is ill-conditioned to the same degree.

The analysis above demonstrates that the mathematical distinction between full incompressibility and near incompressibility is a fine one. From a practical standpoint, the problem is the same for the two cases; either way the result is a system of equations that cannot be relied upon to give numerically stable solutions. That is, any small numerical perturbation can lead to a dramatic change in calculated values, as was shown in Section 3.2. This necessitates a deviation from the standard FEM formulation. Consequently, research over the past thirty years to resolve this issue has resulted in numerous methods for both fully and nearly incompressible materials. However, a distinction between near incompressibility and full incompressibility is not always emphasised. In the review to follow, the word "incompressibility" will be used to denote both, except where a distinction is required.

3.4 Prototypical Methods for Incompressible Materials

As shown in the preceding sections, the hydrostatic pressure for incompressible materials is either indeterminate or numerically unstable in the constitutive law of the standard FEM. To solve this problem, the pressure p is often treated as an unknown, like the displacements, and determined as part of the solution. This is referred to as a mixed formulation of the FEM [Weissman *et al.*, 1992]. The manner in which the mixed method is applied has been a major topic in finite element analysis. A journal paper by Kumaresan *et al.* [1994] reviews various mixed methods including applications and a comparison of the methods.

3.4.1 Full Incompressibility

For full incompressibility, the indeterminacy of p and singularity of matrix $\boldsymbol{C}$ may be circumvented by separating the internal strain energy into its deviatoric and hydrostatic components. Therefore, equation (3.19) becomes

$$\Pi(u_i, p) = \hat{U} + \int p\, e \, \mathrm{d}V + \Omega \tag{3.26}$$

where $\hat{U}$ is the deviatoric component of the internal strain energy, the second term represents the hydrostatic component, and both $\hat{U}$ and Ω are functions of u_i only. Component $\hat{U}$ is not related to classical matrix $\boldsymbol{D}$ and therefore is not ill-conditioned. In addition, if the discretised field consists of a single element for which the hydrostatic pressure is constant, then the p may come outside of the integral. To find a solution to the problem, Π is minimised by setting

$$\frac{\partial \Pi}{\partial u_i} = 0 = \frac{\partial \hat{U}}{\partial u_i} + p \int \frac{\partial e}{\partial u_i} \mathrm{d}V - F_i \tag{3.27}$$

and

$$\frac{\partial \Pi}{\partial p} = 0 = \int e \, dV \, . \tag{3.28}$$

By optimising with respect to both u_i and p, minimisation of the potential energy is still achieved and the hydrostatic component of the constitutive law, $e = 0$, is enforced in an approximate sense through integration over each element. The description given by equations (3.26), (3.27), and (3.28), involving a decomposition of U into hydrostatic and deviatoric components, is standard and may be found in a number of sources [Hughes, 1987; Bathe, 1996]. Furthermore, it is usually posed as an application of the classical Lagrange multiplier method [Hughes, 1987; Bathe, 1996; Bonet & Wood, 1997; Oden and Key, 1970].

The Lagrange multiplier method is used in mathematics to optimise a function subject to a constraint [Trim, 2004]. In this method, a constrained optimisation problem is converted to an unconstrained optimisation problem with extra unknown(s). For instance, when a function $f(x_i)$ is to be minimised with respect to variables x_i subject to the constraint $g(x_i) = 0$, it may be converted to the minimisation of

$$\Im(x_i, \lambda) = f(x_i) + \lambda g(x_i) \tag{3.29}$$

where λ is a scalar parameter, the Lagrange multiplier, whose physical meaning depends on the problem being considered. Minimising $\Im(x_i, \lambda)$ with respect to x_i and λ gives

$$\frac{\partial \mathfrak{I}}{\partial x_i} = 0 = \frac{\partial f}{\partial x_i} + \lambda \frac{\partial g}{\partial x_i}, \tag{3.30}$$

and

$$\frac{\partial \mathfrak{I}}{\partial \lambda} = 0 = g(x_i). \tag{3.31}$$

By comparing (3.26) and (3.29) and using the correspondence

$$\mathfrak{I}(x_i, \lambda) = \Pi(u_i, p), \tag{3.32}$$

$$g = \int e \mathrm{d}V, \tag{3.33}$$

and

$$f = \hat{U} + \Omega, \tag{3.34}$$

the Lagrange multiplier equations (3.30) and (3.31) give the mixed FEM formulation (3.27) and (3.28) for full incompressibility. In the literature, the above correspondence is usually implied directly from equations (3.27) and (3.28) without addressing the subtlety introduced by equation (3.34), where the function to be minimised is $\hat{U} + \Omega$ rather than the total potential energy $U + \Omega$, as required by the principle of stationary potential energy. While this may seem to be inconsistent, it is easily reconciled. By the Lagrange multiplier method, a function is minimised within the constraint space. In this case, the constraint space is a subspace where the volume does not change. By definition, the hydrostatic (volumetric) component of strain energy is zero within this subspace, and therefore the total strain energy U is equal to the deviatoric strain energy $\hat{U}$.

The Lagrange multiplier approach described above leads to global finite element systems of the form [Hughes, 1987; Zienkiewicz *et al*., 1986; Zienkiewicz & Taylor, 1997]

$$\left[\begin{array}{c|c} \boldsymbol{A} & \boldsymbol{G}^{\mathrm{T}} \\ \hline \boldsymbol{G} & \boldsymbol{0} \end{array}\right]\left[\begin{array}{c} \boldsymbol{u} \\ \hline \boldsymbol{p} \end{array}\right]=\left[\begin{array}{c} \boldsymbol{b}_1 \\ \hline \boldsymbol{b}_2 \end{array}\right], \tag{3.35}$$

where the system of equations from the top block of (3.35), i.e. $\boldsymbol{Au} + \boldsymbol{G}^{\mathrm{T}}\boldsymbol{p} = \boldsymbol{b}_1$, represents the equilibrium equations, and the bottom block, i.e. $\boldsymbol{Gu} = \boldsymbol{b}_2$, represents the constraint equations. $\boldsymbol{A}$ is a matrix of stiffnesses corresponding to the second partial derivatives of the distortional strain energy, and the matrix $\boldsymbol{G}$ contains geometric terms each of which relates the change in volume per volume of an element due to a deflection of a single displacement degree of freedom. The vector $\boldsymbol{b}_1$ is the load vector after imposition of the displacement boundary conditions, and the vector $\boldsymbol{b}_2$ is equal to zero until the displacement boundary conditions are imposed.

3.4.2 Near Incompressibility

In the literature, functionals for near incompressibility have been devised using a number of different approaches, including general variational forms [Rong *et al.*, 2001; Bathe, 1996; Herrmann, 1965; Reissner, 1950] and "penalty" methods [Bonet & Wood, 1997; Hughes, 1987; Hughes *et al.*, 1979)]. However, the variational forms are usually introduced without using the principle of stationary potential energy as the starting point, and the penalty formulations do not always follow the classical penalty approach of applied mathematics. This section presents an alternative derivation which follows the same steps as those used above to derive the functional for full incompressibility, with a goal of providing a formulation which is accessible to a broader engineering audience and may be useful for future pedagogical and research applications.

Using equation (3.19), the variational principle for the standard displacement finite element formulation may be written as

$$\Pi(\boldsymbol{u}) = \int W \, \mathrm{d}V + \Omega \tag{3.36}$$

where W is the strain energy per volume. The notation $\Pi(\boldsymbol{u})$ indicates that the potential energy functional, Π, depends only on displacement field $\boldsymbol{u}$. The stress and strain fields are not independent variables since in the context of the standard formulation, both the strain-displacement and the stress-strain (constitutive) relations are enforced exactly at all points. Mathematically, the point-wise enforcement of these relations may be indicated by writing that $\boldsymbol{\varepsilon} = \boldsymbol{\varepsilon}(\boldsymbol{u})$, $\boldsymbol{\sigma} = \boldsymbol{\sigma}(\boldsymbol{\varepsilon})$ and, therefore, $\boldsymbol{\sigma} = \boldsymbol{\sigma}(\boldsymbol{u})$. The strain energy density, W, may be decomposed into distortional and volumetric parts giving

$$W = \hat{W} + \widetilde{W} \tag{3.37}$$

and therefore, equation (3.36) can be rewritten as

$$\Pi(\boldsymbol{u}) = \int \hat{W} \, \mathrm{d}V + \int \widetilde{W} \, \mathrm{d}V + \Omega \tag{3.38}$$

where $\hat{W}$ is the distortional part of the strain energy density and $\widetilde{W}$ is the volumetric part. By definition, for the volumetric component of a stress state, $\widetilde{\sigma}_x = \widetilde{\sigma}_y = \widetilde{\sigma}_z = p$ and $\widetilde{\tau}_{xy} = \widetilde{\tau}_{yz} = \widetilde{\tau}_{zx} = 0$, where $\widetilde{\sigma}_i$ and $\widetilde{\tau}_{ij}$ are, respectively, the normal and shear stresses associated with the volumetric part of the stress state. Referring to equation (3.20), the classical expression for strain energy density within a linear elastic material then gives

$$\widetilde{W} = \frac{1}{2}\widetilde{\sigma}_x\widetilde{\varepsilon}_x + \frac{1}{2}\widetilde{\sigma}_y\widetilde{\varepsilon}_y + \frac{1}{2}\widetilde{\sigma}_z\widetilde{\varepsilon}_z \tag{3.39}$$

where from Hooke's law, as given by equations (3.6) to (3.9) and (3.17), the volumetric normal strain components, $\widetilde{\varepsilon}_i$ are

$$\tilde{\varepsilon}_x = \tilde{\varepsilon}_y = \tilde{\varepsilon}_z = \frac{1-2\nu}{E} p = \frac{p}{3\kappa} \tag{3.40}$$

and κ is the bulk modulus given by

$$\kappa = \frac{E}{3(1-2\nu)} \quad . \tag{3.41}$$

Thus, equation (3.39) becomes

$$\tilde{W} = \frac{p^2}{2\kappa} \quad . \tag{3.42}$$

Equation (3.42) can be found in a number of sources. The manner in which (3.42) is rearranged algebraically is the key to obtaining the equations for near incompressibility. Although not an obvious choice, let (3.42) be written as

$$\tilde{W} = \frac{p^2}{\kappa} - \frac{p^2}{2\kappa} \quad . \tag{3.43}$$

The volumetric component of the constitutive law is

$$p = \kappa\, e \tag{3.44}$$

and so equation (3.43) can become

$$\tilde{W} = p\, e - \frac{p^2}{2\kappa} \quad . \tag{3.45}$$

Substituting (3.45) into (3.38) gives

$$\Pi(u_i, p) = \hat{U} + \int pe \,\mathrm{d}V - \int \frac{p^2}{2\kappa} \mathrm{d}V + \Omega\,, \tag{3.46}$$

where p is now treated as an independent unknown and the relationship between deviatoric strain energy $\hat{U}$ and deviatoric strain energy density $\hat{W}$ is given by

$$\hat{U} = \int \hat{W} \,\mathrm{d}V \quad . \tag{3.47}$$

To demonstrate that equation (3.46) is the prototypical functional for near incompressibility, $\Pi(u_i, p)$ is minimised in similar fashion to the approach that was used for full incompressibility, giving

$$\frac{\partial \Pi}{\partial u_i} = 0 = \frac{\partial \hat{U}}{\partial u_i} + p \int \frac{\partial e}{\partial u_i} \mathrm{d}V - F_i \tag{3.48}$$

and

$$\frac{\partial \Pi}{\partial p} = 0 = \int \left(e - \frac{p}{\kappa} \right) dV \,. \tag{3.49}$$

Comparing these equations to (3.27) and (3.28), the same energy minimisation with respect to u_i is achieved, but the hydrostatic component of the constitutive law is $p = \kappa e$, rather than the fully incompressible equation $e = 0$. Again, this part of the constitutive law is enforced only approximately instead of point-wise.

Through discretisation, equations (3.48) and (3.49) lead to the matrix form

$$\left[\begin{array}{c|c} \boldsymbol{A} & \boldsymbol{G}^{\mathrm{T}} \\ \hline \boldsymbol{G} & \boldsymbol{M} \end{array}\right] \left[\begin{array}{c} \boldsymbol{u} \\ \hline \boldsymbol{p} \end{array}\right] = \left[\begin{array}{c} \boldsymbol{b}_1 \\ \hline \boldsymbol{b}_2 \end{array}\right]. \tag{3.50}$$

where $\boldsymbol{M}$ is the interpolation matrix for the pressures and is related to the bulk modulus. As incompressibility is approached, $\boldsymbol{M}$ approaches zero and (3.50) is equivalent to (3.35).

In Bonet & Wood [1997], the formulation given by (3.46) is described as a "penalty" approach (with Bonet and Wood placing the quotation marks) where

$$\aleph = -\int \frac{p^2}{2\kappa} \mathrm{d}V \tag{3.51}$$

is the penalty term and κ is the penalty parameter. The quantity $\aleph$, however, does not satisfy the conditions for a true penalty term [Stoeker, 1980] as it is not positive semi-definite and therefore does not actually penalise the minimisation of functional Π.

In the literature, selection of the penalty parameter seems to be somewhat arbitrary. The quantity κ is not viewed as having a specific value for a particular material, but rather as a parameter which is given a value large enough to approximate full incompressibility yet small enough to avoid mathematical singularity. This deviates substantially from the perspective taken in this thesis where real materials may be viewed as nearly incompressible, and $\nu = 0.5$ is regarded as the theoretical upper limit of incompressibility.

3.5 Issues Regarding Incompressibility

Both prototypical methods presented in the previous section resolve the problem of indeterminacy in the constitutive law by circumventing point-wise enforcement of the volumetric constraint in favour of an averaged, approximate form. However, it has long been recognised that these approaches may still encounter serious problems during implementation. In this section, the pertinent issues are discussed leading to a review in subsequent sections of the more advanced finite element methods for incompressibility.

These methods are then assessed in terms of their suitability for the chiropractic problem.

The first consideration which affects performance is the choice of element. This is defined by the number of nodes per element and the degree of integration for the displacements and hydrostatic pressures. For compatibility, the displacements must be continuous across the element boundaries. The pressures may be either continuous or discontinuous. However, the combination of interpolations for the displacements and pressures is not arbitrary [Hughes, 1987; Huang *et al*, 2004]. Many elements are considered unsuitable for analysis of incompressible materials and may be subject to displacement locking and pressure modes.

Displacement locking occurs when the final displacements are calculated to be artificially small for a given problem. The combination of restricted motion which is implied by the finite element discretisation and the constraint on the displacements due to the constant volume condition creates a mesh which is unable to distort as it should [Armero, 2000]. In other words, discretisation of a deformable body (with an infinite number of kinematic degrees of freedom) leads to a model with a finite number of degrees-of-freedom. This can, in some cases, result in a finite element model which has insufficient flexibility to simultaneously respond to applied loads and satisfy the constant volume requirement of incompressibility. The same phenomenon occurs for both full incompressibility and near incompressibility [Belytschko, 1986].

A pressure mode is a mathematical manifestation of the non-uniqueness of the pressure solution in an incompressible problem. A pressure mode distribution, as an additive part of a particular solution to the governing equations, creates an incorrect pressure field. However, the governing equations are still satisfied. If the indeterminacy is encountered in solving the original partial differential equations of equilibrium, then a "physical mode" exists. If the indeterminacy is encountered in solving the matrix equations of the finite element model, this may be due to a discrete version of the physical mode, or "spurious modes" introduced by the details of the discretisation process, or both.

Since the pressures for an incompressible analysis are unknown degrees of freedom, they must be determined with reliance on force or stress traction boundary conditions. If insufficient force boundary condition information is available, the indeterminacy of the hydrostatic component of stress will manifest itself as pressure modes. According to Dvorkin [2001], pressure modes exist when, from either equation (3.35) or (3.50)

$$\boldsymbol{G}^{\mathrm{T}}\boldsymbol{p} = \boldsymbol{0}. \tag{3.52}$$

They may also by predicted by the existence of zero eigenvalues in the matrix equation (3.35) [Zienkiewicz *et al.*, 1997]. In the 4-node, bilinear displacement, discontinuous constant pressure element, the spurious mode is in the form of a checkerboard pressure distribution [Zienkiewicz *et al.*, 1997; Dvorkin, 2001]. The calculated solution consists of a linear combination of the actual expected pressure plus the constant hydrostatic pressure mode and the checkerboard spurious pressure mode. It may be questioned, then, whether any of the unknown quantities in the problem can be obtained. Malkus in Appendix 4.II of Hughes [1987] offers a theorem and proof that unique solutions for the

displacements exist despite the existence of pressure modes. Part of this proof is reworked here as the author feels that it may be more accessible to some readers than the one offered by Malkus. It begins with two Lemmas (3.1 and 3.2) which are based on results from classical linear algebra in terms of the fundamental subspaces of a matrix (see Appendix A for review). It is then followed by a theorem stating conditions under which solutions exist.

Consider the system given by equation (3.35). This system may be rewritten as

$$\boldsymbol{K}\boldsymbol{x} = \boldsymbol{b}\,, \tag{3.53}$$

or

$$\boldsymbol{A}\boldsymbol{u} + \boldsymbol{G}^{\mathrm{T}}\boldsymbol{p} = \boldsymbol{b}_1\,, \tag{3.54}$$

and

$$\boldsymbol{G}\boldsymbol{u} = \boldsymbol{b}_2\,. \tag{3.55}$$

Lemma 3.1: A solution to the system (3.55) exists if and only if for every pressure mode vector, $\boldsymbol{q}$, in the nullspace of $\boldsymbol{G}^{\mathrm{T}}$, $\boldsymbol{b}_2^{\mathrm{T}}\boldsymbol{q} = 0$.

Proof: Assume that $\boldsymbol{G}\boldsymbol{u} = \boldsymbol{b}_2$ has at least one solution. Then, $\boldsymbol{b}_2$ is in $C(\boldsymbol{G})$, the column space of $\boldsymbol{G}$ [Strang, 1976]. Equivalently, $\boldsymbol{b}_2$ is in $R\left(\boldsymbol{G}^{\mathrm{T}}\right)$, the row space of $\boldsymbol{G}^{\mathrm{T}}$. Every member of $R\left(\boldsymbol{G}^{\mathrm{T}}\right)$ is orthogonal to every member of $N\left(\boldsymbol{G}^{\mathrm{T}}\right)$, the nullspace of $\boldsymbol{G}^{\mathrm{T}}$. Thus, for $\boldsymbol{q} \in N\left(\boldsymbol{G}^{\mathrm{T}}\right)$, $\boldsymbol{b}_2{}^{\mathrm{T}}\boldsymbol{q} = \boldsymbol{0}$ (by the definition of orthogonality). Now, conversely, assume that for every $\boldsymbol{q} \in N\left(\boldsymbol{G}^{\mathrm{T}}\right)$ that $\boldsymbol{b}_2{}^{\mathrm{T}}\boldsymbol{q} = \boldsymbol{0}$, then $\mathbf{b}_2 \in R\left(\boldsymbol{G}^{\mathrm{T}}\right)$ (since $N\left(\boldsymbol{G}^{\mathrm{T}}\right)$ and $R\left(\boldsymbol{G}^{\mathrm{T}}\right)$ are orthogonal complements) or equivalently, $\boldsymbol{b}_2 \in C(\boldsymbol{G})$. Thus, $\boldsymbol{G}\boldsymbol{u} = \boldsymbol{b}_2$ has a solution. ■

Lemma 3.2: If $\boldsymbol{v}_R \in R(\boldsymbol{G})$ and $\boldsymbol{A}$ is a positive-definite matrix, then $\boldsymbol{G}\boldsymbol{A}^{-1}\boldsymbol{v}_R = \boldsymbol{0}$ if and only if $\boldsymbol{v}_R = \boldsymbol{0}$.

Proof. Since $\boldsymbol{A}^{-1}$ is positive-definite, it is non singular and $\boldsymbol{A}^{-1}\boldsymbol{v}_R = \boldsymbol{0}$ if and only if $\boldsymbol{v}_R = \boldsymbol{0}$. Now, assume that $\boldsymbol{A}^{-1}\boldsymbol{v}_R$ is entirely in the nullspace of $\boldsymbol{G}$. Since $\boldsymbol{v}_R$ is entirely in the row space of $\boldsymbol{G}$, $\boldsymbol{v}_R^T\left(\boldsymbol{A}^{-1}\boldsymbol{v}_R\right) = \boldsymbol{0}$. This, however, is a contradiction since for positive-definite $\boldsymbol{A}^{-1}$, $\boldsymbol{v}^T\boldsymbol{A}^{-1}\boldsymbol{v} > \boldsymbol{0}$ for all $\boldsymbol{v}$. Thus $\boldsymbol{A}^{-1}\boldsymbol{v}_R$ is not entirely in the nullspace of $\boldsymbol{G}$ and $\boldsymbol{G}\left(\boldsymbol{A}^{-1}\boldsymbol{v}_R\right) = \boldsymbol{0}$ if and only if $\boldsymbol{A}^{-1}\boldsymbol{v}_R = \boldsymbol{0}$; i.e., if and only if $\boldsymbol{v}_R = \boldsymbol{0}$. ■

Theorem 3.1: Given (3.53) with $\boldsymbol{A}$ positive-definite, the system has solutions if and only if for every $\boldsymbol{q} \in N\left(\boldsymbol{G}^T\right)$, $\boldsymbol{b}_2{}^T\boldsymbol{q} = \boldsymbol{0}$.

Proof: From Lemma 3.1, $\boldsymbol{G}\boldsymbol{u} = \boldsymbol{b}_2$ has solutions if and only if $\boldsymbol{b}_2{}^T\boldsymbol{q} = \boldsymbol{0}$. These solutions may be written as

$$\boldsymbol{u} = \boldsymbol{u}_p + \boldsymbol{u}_0, \tag{3.56}$$

where $\boldsymbol{u}_p$ is a particular solution and $\boldsymbol{u}_0$ is in $N\left(\boldsymbol{G}\right)$. Therefore,

$$\boldsymbol{G}\boldsymbol{u}_p = \boldsymbol{b}_2 \tag{3.57}$$

and

$$\boldsymbol{G}\boldsymbol{u}_0 = \boldsymbol{0}. \tag{3.58}$$

Substituting equation (3.56) into (3.54),

$$\boldsymbol{A}\left(\boldsymbol{u}_p + \boldsymbol{u}_0\right) + \boldsymbol{G}^T\boldsymbol{p} = \boldsymbol{b}_1, \tag{3.59}$$

and

$$\boldsymbol{A}\boldsymbol{u}_{\mathrm{p}} + \boldsymbol{A}\boldsymbol{u}_0 + \boldsymbol{G}^{\mathrm{T}}\boldsymbol{p} = \boldsymbol{b}_1 . \tag{3.60}$$

To prove that the system (3.53) has solutions, therefore, it must be shown that for every $\boldsymbol{u}$ given by (3.56) (which already satisfies the constraint equations), there is at least one $\boldsymbol{p}$ for which the equilibrium equations (3.60) are also satisfied. Since $\boldsymbol{A}$ is positive-definite, $\boldsymbol{A}^{-1}$ exists and premultiplying (3.60) by $\boldsymbol{A}^{-1}$ gives,

$$\boldsymbol{A}^{-1}\boldsymbol{A}\boldsymbol{u}_{\mathrm{p}} + \boldsymbol{A}^{-1}\boldsymbol{A}\boldsymbol{u}_0 + \boldsymbol{A}^{-1}\boldsymbol{G}^{\mathrm{T}}\boldsymbol{p} = \boldsymbol{A}^{-1}\boldsymbol{b}_1 , \tag{3.61}$$

and this becomes

$$\boldsymbol{u}_{\mathrm{p}} + \boldsymbol{u}_0 + \boldsymbol{A}^{-1}\boldsymbol{G}^{\mathrm{T}}\boldsymbol{p} = \boldsymbol{A}^{-1}\boldsymbol{b}_1 . \tag{3.62}$$

Premultiplying (3.62) by **G**,

$$\boldsymbol{G}\boldsymbol{u}_{\mathrm{p}} + \boldsymbol{G}\boldsymbol{u}_0 + \boldsymbol{G}\boldsymbol{A}^{-1}\boldsymbol{G}^{\mathrm{T}}\boldsymbol{p} = \boldsymbol{G}\boldsymbol{A}^{-1}\boldsymbol{b}_1 . \tag{3.63}$$

Substituting (3.57) and (3.58) into (3.63),

$$\boldsymbol{b}_2 + \boldsymbol{G}\boldsymbol{A}^{-1}\boldsymbol{G}^{\mathrm{T}}\boldsymbol{p} = \boldsymbol{G}\boldsymbol{A}^{-1}\boldsymbol{b}_1 , \tag{3.64}$$

and rearranging,

$$\left(\boldsymbol{G}\boldsymbol{A}^{-1}\boldsymbol{G}^{\mathrm{T}}\right)\boldsymbol{p} = \left(\boldsymbol{G}\boldsymbol{A}^{-1}\boldsymbol{b}_1 - \boldsymbol{b}_2\right). \tag{3.65}$$

Now, the objective has become one of showing that there exists at least one solution to (3.65). Applying Lemma 3.1, (3.65) has solutions if and only if the vector $\boldsymbol{G}\boldsymbol{A}^{-1}\boldsymbol{b}_1 - \boldsymbol{b}_2$ is orthogonal to $N\left(\left(\boldsymbol{G}\boldsymbol{A}^{-1}\boldsymbol{G}^{\mathrm{T}}\right)^{\mathrm{T}}\right)$. Noting that $\boldsymbol{A}$ and therefore, $\boldsymbol{A}^{-1}$ are symmetric, $\left(\boldsymbol{G}\boldsymbol{A}^{-1}\boldsymbol{G}^{\mathrm{T}}\right)^{\mathrm{T}} = \boldsymbol{G}\boldsymbol{A}^{-1}\boldsymbol{G}^{\mathrm{T}}$ (i.e. $\boldsymbol{G}\boldsymbol{A}^{-1}\boldsymbol{G}^{\mathrm{T}}$ is itself symmetric). Now, assume that there is a vector, $\boldsymbol{v} \in N\left(\boldsymbol{G}\boldsymbol{A}^{-1}\boldsymbol{G}^{\mathrm{T}}\right)$. Then, by definition, $\boldsymbol{G}\boldsymbol{A}^{-1}\boldsymbol{G}^{\mathrm{T}}\boldsymbol{v} = \boldsymbol{0}$. Since $\boldsymbol{G}^{\mathrm{T}}\boldsymbol{v}$ gives a linear combination of the rows of $\boldsymbol{G}$, Lemma 3.2 states that $\boldsymbol{G}\boldsymbol{A}^{-1}\boldsymbol{G}^{\mathrm{T}}\boldsymbol{v} = \boldsymbol{0}$ if and only if $\boldsymbol{G}^{\mathrm{T}}\boldsymbol{v} = \boldsymbol{0}$; that is $N\left(\boldsymbol{G}^{\mathrm{T}}\right) = N\left(\boldsymbol{G}\boldsymbol{A}^{-1}\boldsymbol{G}^{\mathrm{T}}\right)$. Therefore, (3.65) has solutions if and only if

$\boldsymbol{GA}^{-1}\boldsymbol{b}_1 - \boldsymbol{b}_2$ is orthogonal to $N\left(\boldsymbol{G}^{\mathrm{T}}\right)$ where, by definition, $\boldsymbol{q} \in N\left(\boldsymbol{G}^{\mathrm{T}}\right)$. The test for orthogonality involves the inner product of $\boldsymbol{q}$ and $\boldsymbol{GA}^{-1}\boldsymbol{b}_1 - \boldsymbol{b}_2$, or

$$\boldsymbol{q}^{\mathrm{T}}\left(\boldsymbol{GA}^{-1}\boldsymbol{b}_1 - \boldsymbol{b}_2\right) = \boldsymbol{q}^{\mathrm{T}}\boldsymbol{GA}^{-1}\boldsymbol{b}_1 - \boldsymbol{q}^{\mathrm{T}}\boldsymbol{b}_2 . \tag{3.66}$$

Since $\boldsymbol{q}$ is in $N\left(\boldsymbol{G}^{\mathrm{T}}\right)$, $\boldsymbol{G}^{\mathrm{T}}\boldsymbol{q} = \boldsymbol{0}$ or, equivalently, $\boldsymbol{q}^{\mathrm{T}}\boldsymbol{G} = \boldsymbol{0}$. Therefore,

$$\boldsymbol{q}^{\mathrm{T}}\left(\boldsymbol{GA}^{-1}\boldsymbol{b}_1 - \boldsymbol{b}_2\right) = -\boldsymbol{q}^{\mathrm{T}}\boldsymbol{b}_2 . \tag{3.67}$$

and (3.65) has solutions if and only if $\boldsymbol{q}^{\mathrm{T}}\boldsymbol{b}_2 = 0$. ■

Malkus then continues in a corollary to prove that the displacement solution is unique. Therefore, he has proved that solutions exist to (3.35) if $\boldsymbol{b}_2$ is orthogonal to the pressure modes. Also, when the system is solvable, the displacement part of the solution is unique and the pressure part may consist of the actual pressure plus a pressure mode. (A more complete description of pressure modes may be found in [Sani *et al.*, 1981, Part 1; Sani *et al.*, 1981, Part 2].)

In the remainder of the chapter, strategies for dealing with pressure modes, as well as displacement locking, are reviewed. These issues are related to element selection and therefore the next section establishes the conditions under which elements are considered suitable for incompressibility.

3.6 Assessing Finite Element Suitability for Incompressibility

To assess whether an element's interpolations are suitable for incompressibility, simple count conditions, the patch test, or the more mathematical inf-sup condition may be used [Zienkiewicz *et al.*, 1986]. These conditions determine whether a mixed finite element discretisation is stable and will lead to a physically meaningful solution. Elements that fail these conditions may be subject to the issues discussed above, displacement locking or pressure modes. Other criteria also exist that more simply relate constraints and degrees of freedom to predict convergence and accuracy of finite element solutions.

3.6.1 Count Conditions

Count conditions may be used as a simple method for predicting problems related to specific finite element formulations. To check their finite element meshes for plasticity applications, Nagtegaal *et al.* [1974] found that "convergence will only occur if the total number of degrees of freedom increases faster than the total number of constraints". In other words, the ratio of displacement degrees of freedom to the number of constraints as a finite element mesh is refined should be greater than one. Hughes [1987] opts for an alternate constraint counting method to determine the ability of an element to perform well in incompressible and nearly incompressible applications. Although he admits that it is not a "precise mathematical method" for assessing the suitability of elements, it is able to predict locking.

Hughes' constraint counting method states that the optimal ratio of equilibrium equations (the top half of the system in equation (3.35)) to the linearly independent constraint equations (the bottom half) is generally assumed to be 2 in two dimensions.

This is related to the original continuous boundary value problem in which the ratio of equilibrium equations to constraint equations is two, i.e. the equilibrium of forces in the x- and y-directions to the constant volume of the body [Hughes, 1987]. If the ratio is less than two, the element will tend to lock since there are more constraints on the displacements than there are displacement degrees of freedom. If the ratio is greater than two, not enough incompressibility conditions exist to approximate incompressibility satisfactorily.

3.6.2 The Patch Test

The original patch test verified that an arbitrary patch of elements would behave exactly like an elastic solid material subjected to boundary displacements consistent with constant straining [Taylor *et al.*, 1986]. Taylor *et al.* extended the original patch test so that it would not only be a necessary condition for finite element convergence but also a sufficient condition. Zienkiewicz *et al.* [1986] applied the patch test to mixed formulations and showed that the same necessary and sufficient convergence conditions were still upheld by testing for consistency and stability. The consistency requirement ensures that the finite element approximation will exactly represent the differential equations of equilibrium and compatibility as the size of the elements approaches zero [Zienkiewicz & Taylor, 1989].

The stability requirement is tested by a count condition. The count condition of Zienkiewicz and Taylor [1997] is such that

$$n_{\mathrm{u}} \geq n_{\mathrm{p}} \tag{3.68}$$

where n_u is the number of parameters defining the displacement field and n_p is the number of parameters defining the pressure field of a patch of elements in which all the displacements on the boundary and one pressure is prescribed. This is a necessary condition for the solution to be unique. In addition to this count condition, the coefficient matrix $\boldsymbol{A}$ from (3.35) must be non singular for all patches if stable solutions are to exist [Zienkiewicz & Taylor, 1997].

3.6.3 The Inf-Sup Condition

Satisfaction of the inf-sup condition, also known as the Babuška-Brezzi condition (B-B condition), is equivalent to the satisfaction of the patch test as given by Zienkiewicz and Taylor [1997]. This condition is the mathematical criterion that determines whether a finite element formulation is stable and convergent [Zienkiewicz *et al*., 1986]. Satisfaction of this criterion guarantees that the finite element grid will not lock and will be free of spurious pressure modes. However, even if an element satisfies the B-B condition, a grid subjected to complete displacement boundary conditions will still result in the physical (constant) pressure mode. A mathematical derivation of the B-B condition may be found in various sources [Babuška & Narasimhan, 1997; Chapelle & Bathe, 1993]. One perspective that is within the context of the results to be shown in this dissertation is the relationship between the B-B condition and the condition number of the stiffness matrix for a particular grid.

Following the form of the mixed finite element method given in (3.35), one statement of the B-B condition is [Strang, 2007]: for every $\boldsymbol{p}$ there must be a $\boldsymbol{u}$ so that

$$\boldsymbol{u}^{\mathrm{T}}\boldsymbol{G}^{\mathrm{T}}\boldsymbol{p} \geq \beta\sqrt{\boldsymbol{u}^{\mathrm{T}}\boldsymbol{A}\boldsymbol{u}}\sqrt{\boldsymbol{p}^{\mathrm{T}}\boldsymbol{p}} \tag{3.69}$$

for a fixed $\beta > 0$. The following lemma is a variation of material found in [Strang, 2007] and it leads to a theorem relating the B-B condition to the condition number of the stiffness matrix given in (3.35). First, consider the matrix equations given by (3.35), i.e., (3.54) and (3.55). Since $\boldsymbol{A}$ is positive definite, its inverse exists. Therefore, if (3.54) is rearranged and solved for **u**, the result is

$$\boldsymbol{u} = \boldsymbol{A}^{-1}\boldsymbol{b}_1 - \boldsymbol{A}^{-1}\boldsymbol{G}^{\mathrm{T}}\boldsymbol{p} \quad . \tag{3.70}$$

Substituting (3.70) into (3.55) and rearranging gives

$$\boldsymbol{G}\boldsymbol{A}^{-1}\boldsymbol{G}^{\mathrm{T}}\boldsymbol{p} = \boldsymbol{G}\boldsymbol{A}^{-1}\boldsymbol{b}_1 - \boldsymbol{b}_2 \, . \tag{3.71}$$

This may be rewritten as

$$\widetilde{\boldsymbol{A}}\boldsymbol{p} = \boldsymbol{b}_3 \, , \tag{3.72}$$

where $\widetilde{\boldsymbol{A}} = \boldsymbol{G}\boldsymbol{A}^{-1}\boldsymbol{G}^{\mathrm{T}}$ and $\boldsymbol{b}_3 = \boldsymbol{G}\boldsymbol{A}^{-1}\boldsymbol{b}_1 - \boldsymbol{b}_2$. Since (3.72) represents (3.35), the condition number of $\widetilde{\boldsymbol{A}}$ is the important parameter where the stability of (3.35) is concerned. If $\widetilde{\boldsymbol{A}}$ has a zero eigenvalue, it will have a nontrivial nullspace and therefore pressure modes can occur.

Lemma 3.3: If the B-B condition is satisfied, then the eigenvalues of $\widetilde{\boldsymbol{A}}$ are all positive and

$$\left\| \widetilde{\boldsymbol{A}}^{-1} \right\| \leq \frac{1}{\beta^2} \, . \tag{3.73}$$

Proof: Let

$$\boldsymbol{w} = \boldsymbol{A}^{1/2}\boldsymbol{u} \, . \tag{3.74}$$

Then

$$\boldsymbol{u} = \boldsymbol{A}^{-1/2}\boldsymbol{w}\,. \tag{3.75}$$

Using definition (3.75), the terms of the B-B condition may be rewritten as follows,

$$\begin{aligned}\boldsymbol{u}^{\mathrm{T}}\boldsymbol{A}\boldsymbol{u} &= \left(\boldsymbol{A}^{-1/2}\boldsymbol{w}\right)^{\mathrm{T}}\boldsymbol{A}\left(\boldsymbol{A}^{-1/2}\boldsymbol{w}\right) \\ &= \boldsymbol{w}^{\mathrm{T}}\left(\boldsymbol{A}^{-1/2}\right)^{\mathrm{T}}\boldsymbol{A}\boldsymbol{A}^{-1/2}\boldsymbol{w}\end{aligned}\,. \tag{3.76}$$

Since $\boldsymbol{A}$ is symmetric, then $\boldsymbol{A}^{\mathrm{T}} = \boldsymbol{A}$ and (3.76) becomes

$$\begin{aligned}\boldsymbol{u}^{\mathrm{T}}\boldsymbol{A}\boldsymbol{u} &= \boldsymbol{w}^{\mathrm{T}}\boldsymbol{A}^{-1/2}\boldsymbol{A}\boldsymbol{A}^{-1/2}\boldsymbol{w} \\ &= \boldsymbol{w}^{\mathrm{T}}\boldsymbol{w}.\end{aligned} \tag{3.77}$$

The norm of a vector, as defined by Strang [1976], is $\|\boldsymbol{w}\| = \sqrt{\boldsymbol{w}^{\mathrm{T}}\boldsymbol{w}}$ and therefore $\|\boldsymbol{w}\|^2 = \boldsymbol{w}^{\mathrm{T}}\boldsymbol{w}$. Now, (3.77) becomes

$$\boldsymbol{u}^{\mathrm{T}}\boldsymbol{A}\boldsymbol{u} = \|\boldsymbol{w}\|^2\,. \tag{3.78}$$

Similarly,

$$\|\boldsymbol{p}\| = \sqrt{\boldsymbol{p}^{\mathrm{T}}\boldsymbol{p}}\,. \tag{3.79}$$

Also,

$$\begin{aligned}\boldsymbol{u}^{\mathrm{T}}\boldsymbol{G}^{\mathrm{T}}\boldsymbol{p} &= \left(\boldsymbol{A}^{-1/2}\boldsymbol{w}\right)^{\mathrm{T}}\boldsymbol{G}^{\mathrm{T}}\boldsymbol{p} \\ &= \boldsymbol{w}^{\mathrm{T}}\boldsymbol{A}^{-1/2}\boldsymbol{G}^{\mathrm{T}}\boldsymbol{p}\,.\end{aligned} \tag{3.80}$$

By substituting (3.78), (3.79) and (3.80) into (3.69), the B-B condition becomes

$$\boldsymbol{w}^{\mathrm{T}}\boldsymbol{A}^{-1/2}\boldsymbol{G}^{\mathrm{T}}\boldsymbol{p} \geq \beta\|\boldsymbol{w}\|\cdot\|\boldsymbol{p}\|\,. \tag{3.81}$$

Dividing both sides by $\|\mathbf{w}\|$ gives a more useful form of the B-B condition to prove the lemma and (3.81) becomes

$$\frac{\boldsymbol{w}^{\mathrm{T}}\boldsymbol{A}^{-1/2}\boldsymbol{G}^{\mathrm{T}}\boldsymbol{p}}{\|\boldsymbol{w}\|} \geq \beta \|\boldsymbol{p}\|. \tag{3.82}$$

Let $\boldsymbol{z} = \boldsymbol{A}^{-1/2}\boldsymbol{G}^{\mathrm{T}}\boldsymbol{p}$, then (3.82) becomes

$$\frac{\boldsymbol{w}^{\mathrm{T}}\boldsymbol{z}}{\|\boldsymbol{w}\|} \geq \beta \|\boldsymbol{p}\|. \tag{3.83}$$

Since $\boldsymbol{w}^{\mathrm{T}}\boldsymbol{z}$ is the inner product between $\boldsymbol{w}$ and $\boldsymbol{z}$, (3.83) may be rewritten as

$$\frac{\|\boldsymbol{w}\| \cdot \|\boldsymbol{z}\| \cos\theta}{\|\boldsymbol{w}\|} \geq \beta \|\boldsymbol{p}\|, \tag{3.84}$$

where θ is the angle between $\boldsymbol{w}$ and $\boldsymbol{z}$. The $\|\boldsymbol{w}\|$ terms on the left hand side of (3.84) may be cancelled leaving the term $\|\boldsymbol{z}\|\cos\theta$. Since the range of $\cos\theta$ is -1 to 1, the largest value of $\|\boldsymbol{z}\|\cos\theta$ is $\|\boldsymbol{z}\|$. Therefore,

$$\max \frac{\boldsymbol{w}^{\mathrm{T}}\boldsymbol{z}}{\|\boldsymbol{w}\|} = \|\boldsymbol{z}\| = \left\|\boldsymbol{A}^{-1/2}\boldsymbol{G}^{\mathrm{T}}\boldsymbol{p}\right\|. \tag{3.85}$$

So another form of the B-B condition is

$$\left\|\boldsymbol{A}^{-1/2}\boldsymbol{G}^{\mathrm{T}}\boldsymbol{p}\right\| \geq \beta \|\boldsymbol{p}\|, \tag{3.86}$$

or when both sides are squared,

$$\left\|\boldsymbol{A}^{-1/2}\boldsymbol{G}^{\mathrm{T}}\boldsymbol{p}\right\|^2 \geq \beta^2 \|\boldsymbol{p}\|^2. \tag{3.87}$$

Expanding the norms by the definition given above, (3.87) becomes

$$\boldsymbol{p}^{\mathrm{T}}\boldsymbol{G}\left(\boldsymbol{A}^{-1/2}\right)^{\mathrm{T}}\boldsymbol{A}^{-1/2}\boldsymbol{G}^{\mathrm{T}}\boldsymbol{p} \geq \beta^2 \boldsymbol{p}^{\mathrm{T}}\boldsymbol{p}. \tag{3.88}$$

Since $\boldsymbol{A}$ is symmetric, $\left(\boldsymbol{A}^{-1/2}\right)^{\mathrm{T}} = \left(\boldsymbol{A}^{-1/2}\right)$,

$$\boldsymbol{p}^{\mathrm{T}}\boldsymbol{G}\boldsymbol{A}^{-1}\boldsymbol{G}^{\mathrm{T}}\boldsymbol{p} \geq \beta^2 \boldsymbol{p}^{\mathrm{T}}\boldsymbol{p}, \tag{3.89}$$

and, using the definition of $\widetilde{\boldsymbol{A}}$,

$$\boldsymbol{p}^{\mathrm{T}}\widetilde{\boldsymbol{A}}\boldsymbol{p} \geq \beta^2 \boldsymbol{p}^{\mathrm{T}}\boldsymbol{p}, \tag{3.90}$$

or

$$\boldsymbol{p}^{\mathrm{T}}\widetilde{\boldsymbol{A}}\boldsymbol{p} \geq \boldsymbol{p}^{\mathrm{T}}\beta^2\boldsymbol{p}. \tag{3.91}$$

In the set of all $\boldsymbol{p}$ vectors, let $\hat{\boldsymbol{p}}$ be those that are also eigenvectors of $\widetilde{\boldsymbol{A}}$. Then

$$\widetilde{\boldsymbol{A}}\hat{\boldsymbol{p}} = \lambda_{\mathrm{E}}\hat{\boldsymbol{p}}, \tag{3.92}$$

where λ_{E} are the eigenvalues of $\widetilde{\boldsymbol{A}}$. Equation (3.91) can be written for the eigenvalues and eigenvectors of $\widetilde{\boldsymbol{A}}$, as in (3.92), and rearranged as

$$\hat{\boldsymbol{p}}^{\mathrm{T}}\left(\lambda_{\mathrm{E}}\hat{\boldsymbol{p}} - \beta^2\hat{\boldsymbol{p}}\right) \geq 0. \tag{3.93}$$

When $\hat{\boldsymbol{p}}^{\mathrm{T}}$ is distributed, this equation becomes

$$\lambda_{\mathrm{E}}\hat{\boldsymbol{p}}^{\mathrm{T}}\hat{\boldsymbol{p}} - \beta^2\hat{\boldsymbol{p}}^{\mathrm{T}}\hat{\boldsymbol{p}} \geq 0 \tag{3.94}$$

or

$$\left(\lambda_{\mathrm{E}} - \beta^2\right)\left\|\hat{\boldsymbol{p}}\right\|^2 \geq 0. \tag{3.95}$$

Therefore,

$$\lambda_{\mathrm{E}} \geq \beta^2, \tag{3.96}$$

where by definition $\beta > 0$. So, if the form of the B-B condition given by (3.87) is to be satisfied for all $\boldsymbol{p}$'s including eigenvectors of $\widetilde{\boldsymbol{A}}$, then the eigenvalues of $\widetilde{\boldsymbol{A}}$ must satisfy (3.96) and are all positive. Furthermore, if all the eigenvalues are greater than or equal to β^2, then

$$\lambda_{\min} \geq \beta^2, \tag{3.97}$$

where $\lambda_{\min}$ is the smallest eigenvalue of $\widetilde{\boldsymbol{A}}$. Taking the reciprocal, (3.97) becomes

$$\frac{1}{\lambda_{\min}} \leq \frac{1}{\beta^2}. \tag{3.98}$$

The norm of a symmetric matrix with positive eigenvalues is defined as the maximum eigenvalue [Strang, 1976]. Therefore, if

$$\left\| \widetilde{\boldsymbol{A}} \right\| = \lambda_{\max}, \tag{3.99}$$

then, it follows that

$$\left\| \widetilde{\boldsymbol{A}}^{-1} \right\| = \frac{1}{\lambda_{\min}}, \tag{3.100}$$

and

$$\left\| \widetilde{\boldsymbol{A}}^{-1} \right\| \leq \frac{1}{\beta^2}. \ \blacksquare \tag{3.101}$$

Theorem 3.2: If the B-B condition is satisfied, then the condition number (*CN*) of $\widetilde{\boldsymbol{A}}$ is bounded.

Proof: The condition number of a matrix is defined as [Strang, 1976]

$$CN\left(\widetilde{\boldsymbol{A}}\right) = \left\| \widetilde{\boldsymbol{A}} \right\| \cdot \left\| \widetilde{\boldsymbol{A}}^{-1} \right\|. \tag{3.102}$$

Since $\widetilde{\boldsymbol{A}}$ is positive definite,

$$\left\| \widetilde{\boldsymbol{A}} \right\| = \lambda_{\max} \tag{3.103}$$

where $\lambda_{\max} < \infty$; i.e. $\lambda_{\max}$ is bounded. Now, substituting (3.103) into (3.102)

$$CN\left(\widetilde{\boldsymbol{A}}\right) = \lambda_{\max} \left\| \widetilde{\boldsymbol{A}}^{-1} \right\|, \tag{3.104}$$

and by Lemma 3.3,

$$CN\left(\tilde{\boldsymbol{A}}\right) \leq \frac{\lambda_{\max}}{\beta^2}. \tag{3.105}$$

for a fixed $\beta > 0$. Therefore, if the B-B condition is satisfied, it follows that $CN(\tilde{\boldsymbol{A}})$ is bounded and the finite element solution will be free of pressure modes. ■

Ideally, all finite element formulations would be free of pressure modes and displacement locking. The B-B condition, patch test, and/or count conditions can be used to identify the expected performance of a given formulation, but the actual design of stable methods to satisfy these criteria has required considerable research over the past thirty years. The major methods currently available are reviewed in the following section.

3.7 Methods for Addressing the Issues Associated with Incompressibility

3.7.1 Element Selection

The choice of element can determine whether displacement locking or pressure modes occur. Whether Hughes' count condition [Hughes, 1987], the patch test [Zienkiewicz *et al.*, 1986; Zienkiewicz & Taylor, 1997] or the B-B condition [Bathe, 1996] is applied, the consensus is that the continuous biquadratic displacement, discontinuous linear pressure element (i.e. 9-node quadrilateral element with 3 internal pressure interpolation nodes or Q9P3) shown in Figure 3.2 is the optimal quadrilateral for incompressible analysis. Although this is the 'best' element, other elements may still be used and are found in practice. For example, the bilinear displacement, constant pressure element

(Q4P1), shown in Figure 3.3, is widely used even though it does not pass the B-B condition [Simo, *et al*. 1993], but it passes the patch test [Zienkiewicz & Taylor, 1997] and Hughes' count condition in some configurations [Hughes, 1987]. As a result, much research has been performed to make this element more robust for various applications and leads to other methods for addressing incompressibility issues.

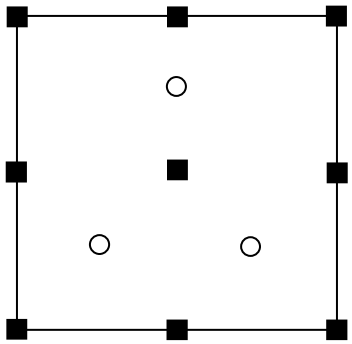

Figure 3.2: Biquadratic displacement, linear pressure element (■ represents displacement node, ○ represents pressure interpolation node).

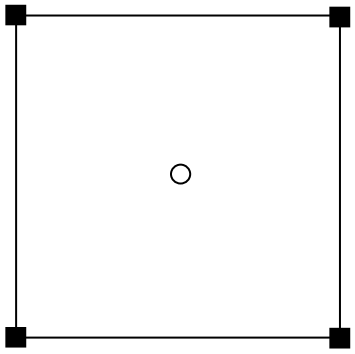

Figure 3.3: Bilinear displacement, constant pressure element (■ represents displacement node, ○ represents pressure interpolation node).

3.7.2 Reduced/Selective Integration

The reduced integration method was an early approach for addressing the issues of incompressibility [Yu, 1991]. It may be applied to near incompressibility and standard elements with only displacement unknowns to address the issue of displacement locking that is often exhibited by these elements. To accomplish this, the material properties matrix (i.e., $\boldsymbol{D}$ in equation (3.23)) is divided into a μ (shear modulus) part and a λ_L (volumetric) part where μ and λ_L are the Lamé parameters. Then, either both parts are treated with a reduced order of numerical quadrature (uniform reduced integration) or only the volumetric part is under-integrated (selective reduced integration). For example, in a four-node quadrilateral element where 'exact' integration uses a 2×2 quadrature, a 1-point quadrature would be used instead. In doing this, the effects of incompressibility are relaxed. This method is similar to the mixed formulation where the stiffness matrix is separated into deviatoric and volumetric parts. In fact, the mixed formulation and reduced integration have been shown to be equivalent [Malkus & Hughes, 1978], however, only for plane strain and three-dimensional analyses, not axisymmetry [Yu, 1991].

Reduced integration, whether uniform or selective, may have the effect of producing spurious zero-energy displacement modes, also called mechanisms or hourglass modes [Reese *et al.*, 2000]. An hourglass mode occurs when a numerically valid displacement field manifests in the solution but has no associated strain energy. In other words, there is no change in the energy associated with a particular part of the displacement solution. Hourglass modes are so named due to the shape that an element may take (see Figure

3.4). To suppress these modes, other elements may be used or methods may be used to counteract their effects; i.e., use of a stabilisation matrix [Belytschko & Bachrach, 1986]. Armero [2000] presents an extensive account of hourglassing in a four-node element subjected to plane strain using insight from a spectral analysis.

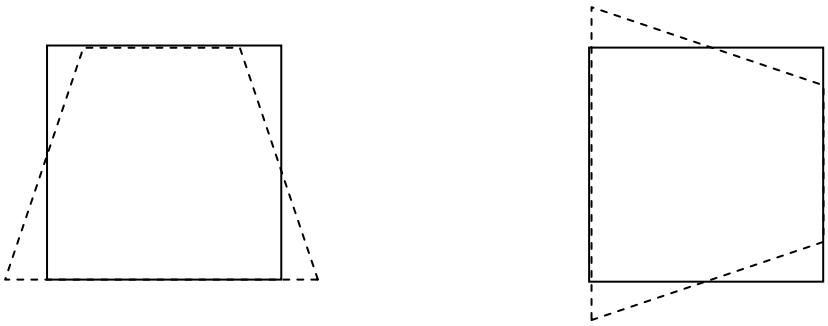

Figure 3.4: Hourglass or zero energy modes (dotted lines represent possible distorted shape).

Another problem with reduced integration is that the incompressibility is satisfied only at a limited number of integration points. This means that the calculated stress field is accurate at the integration points but in error on the remainder of the element [Yu & Netherton, 2000].

The B-bar approach is an extension of selective reduced integration which was developed to be effective for more general geometries [Belytschko & Bachrach, 1986]. Instead of changing the material properties matrix, this method works on the strain-displacement matrix in the displacement finite element method by dividing the $\boldsymbol{B}$ matrix (relating strains to displacements) into deviatoric and dilatational components

[Belytschko *et al*., 1986]. The dilational part is then "improved" by using reduced quadrature.

3.7.3 Variational Principles

A number of researchers have addressed displacement locking and spurious pressure modes by developing alternative variational formulations to replace the prototypical methods presented in Section 3.4. The two most well-known variational principles are the Hellinger-Reissner and the Hu-Washizu methods. The Hu-Washizu functional is defined in terms of three types of independent variables; displacement, stress, and strain [Weissman & Taylor, 1992 (b)]. The Hellinger-Reissner method is a special case of the Hu-Washizu method in which only the displacements and stresses are independent variables and may be recovered from the Hu-Washizu principle by enforcing the constitutive equations point-wise [Weissman & Taylor, 1992(a)].

The approach that was introduced in Section 3.4.2 for developing the prototypical formulation of near incompressibility has the added advantage that it can be used to describe other variational methods [Reissner, 1950] in applied mechanics. It is used here to develop the Hu-Washizu three-field form and provide a basis for explaining how the Hu-Washizu principle alleviates the effects of displacement locking and spurious pressure modes. The specific form of this presentation provides an alternative from that normally found in the literature [Lee *et al.*, 1998]. Starting with equation (3.42),

$$\widetilde{W} = \frac{p^2}{2\kappa} \quad , \tag{3.106}$$

and using the relation $p = \kappa e$ gives

$$\widetilde{W} = \frac{\kappa e^2}{2} \ . \tag{3.107}$$

Through judicious manipulation of (3.107), the volumetric component of the strain energy density may be written as

$$\widetilde{W} = \frac{\kappa e^2}{2} - pe + pe \ . \tag{3.108}$$

The key to obtaining the Hu-Washizu three-field form is to introduce another independent unknown $\bar{e}$ which approximates the point-wise volumetric strain e in an average sense over each element. Equation (3.108) can be approximated as

$$\widetilde{W} = \frac{\kappa \bar{e}^2}{2} - p\bar{e} + pe \ , \tag{3.109}$$

and from equation (3.38),

$$\Pi = \hat{U} + \int \widetilde{W} \, \mathrm{d}V + \Omega \tag{3.110}$$

or

$$\Pi(u_i, p, \bar{e}) = \hat{U} + \int \frac{\kappa \bar{e}^2}{2} \mathrm{d}V + \int p(e - \bar{e}) \mathrm{d}V + \Omega \ , \tag{3.111}$$

which is the Hu-Washizu functional. Minimising Π with respect to u_i, p, and $\bar{e}$ gives

$$\frac{\partial \Pi}{\partial u_i} = 0 = \frac{\partial \hat{U}}{\partial u_i} + p \int \frac{\partial e}{\partial u_i} \mathrm{d}V - F_i \ , \tag{3.112}$$

$$\frac{\partial \Pi}{\partial p} = 0 = \int (e - \bar{e}) \mathrm{d}V \ , \tag{3.113}$$

and

$$\frac{\partial \Pi}{\partial \bar{e}} = 0 = \int (\kappa \bar{e} - p) \mathrm{d}V \ . \tag{3.114}$$

Equation (3.112) is the same potential energy minimisation that was obtained for the two-field (***u-p***) formulations developed earlier in the chapter. Equation (3.113) defines mathematically the relationship between $\bar{e}$ and e, while (3.114) provides a relaxed expression of the hydrostatic component of the constitutive law in terms of $\bar{e}$. The purpose of this relaxation is to mitigate the effects of displacement locking and spurious modes at a fundamental level.

3.7.4 Incompatible Modes/Enhanced Strain Methods

Another approach to relaxing the severity of the incompressibility constraint and its tendency towards locking is to approximate the displacement field with an assumed form which includes additional terms that are discontinuous between elements [Bathe, 1996]. Any inaccuracy introduced by the consequent violation of compatibility is usually outweighed by the increase in numerical flexibility in arriving at solutions which can approximately satisfy both the constant volume requirement and equilibrium. Kouhia and Stenberg [1995] have applied this method to linear triangles in which the conforming part of the displacement field has the usual degrees of freedom at the element nodes, and in the nonconforming part the continuity is relaxed at the nodes but maintained midside. Although incompatible modes are used successfully for linear analysis, they are not as successfully applied to nonlinear analyses due to the additional shape functions and static condensation necessary [Hughes, 1987].

The method of incompatible modes was a precursor to the enhanced strain technique [Reese & Wriggers, 2000]. Whereas in the incompatible modes method part of the displacement field is nonconforming, in the enhanced strain technique the strain field is

divided into a compatible part and a local enhancement. The concept of strain enhancement which is *local* and *nonconforming* may be explained with the following simple but illustrative example. Consider two adjacent one-dimensional finite elements, each with two nodes. See Figure 3.5.

Let the displacement distribution in each element be given by

$$u^{(1)}(x) = N_1^{(1)}(x)u_1 + N_2^{(1)}(x)u_2 \tag{3.115}$$

$$u^{(2)}(x) = N_2^{(2)}(x)u_2 + N_3^{(2)}(x)u_3 \tag{3.116}$$

where $u^{(i)}(x)$ is the displacement field in element (i), $N_j^{(i)}$ is the traditional linear shape function corresponding to node j and element (i), and u_j is the displacement corresponding to node j. By using this conventional definition, the displacement field is

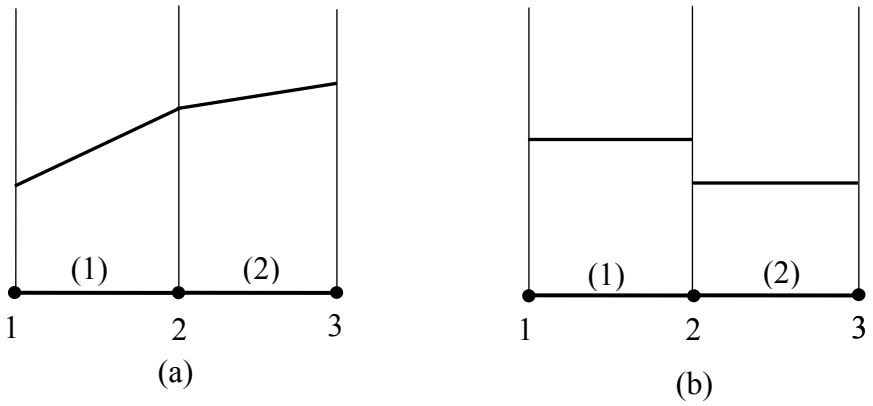

Figure 3.5: (a) Traditional continuous displacement functions, (b) corresponding strains.

continuous at interelement boundaries as shown in Figure 3.5(a). By virtue of the classical strain-displacement relations, the elemental strains, $\varepsilon_x^{(i)}$, are given by

$$\varepsilon_x^{(1)} = \frac{\partial u^{(1)}}{\partial x} = \frac{\partial N_1^{(1)}}{\partial x} u_1 + \frac{\partial N_2^{(1)}}{\partial x} u_2 \tag{3.117}$$

and

$$\varepsilon_x^{(2)} = \frac{\partial u^{(2)}}{\partial x} = \frac{\partial N_2^{(2)}}{\partial x} u_2 + \frac{\partial N_3^{(2)}}{\partial x} u_3 \ . \tag{3.118}$$

While the strain field is not continuous between elements (Figure 3.5(b)), there is still a connection between the elemental strains; as can be seen in equations (3.117) and (3.118), they are related by u_2. The expressions for $\varepsilon_x^{(1)}$ and $\varepsilon_x^{(2)}$ can now be 'enhanced' by incorporating additional terms to give

$$\varepsilon_x^{(1)} = \frac{\partial u^{(1)}}{\partial x} = \frac{\partial N_1^{(1)}}{\partial x} u_1 + \frac{\partial N_2^{(1)}}{\partial x} u_2 + c_1 + c_2 x \tag{3.119}$$

$$\varepsilon_x^{(2)} = \frac{\partial u^{(2)}}{\partial x} = \frac{\partial N_2^{(2)}}{\partial x} u_2 + \frac{\partial N_3^{(2)}}{\partial x} u_3 + c_3 + c_4 x \tag{3.120}$$

where c_k, k = 1 to 4, are generalised displacements. Since c_k are independent, the enhancement for each element is local and unrelated to adjacent elements. Furthermore, the displacements that would result from integrating the enhanced part of the strain field would be, in general, discontinuous (nonconforming) between elements. A number of researchers have applied this concept to incompressible finite element analysis with marked success [Simo & Rifai, 1990; Simo & Armero, 1992; Pantuso & Bathe, 1995; Simo, *et al*, 1993; Wriggers & Reese, 1996; Reese & Wriggers, 2000; Auricchio *et al*, 2004; Lovadina & Auricchio, 2003; Armero, 2000]. The method has encountered some difficulties however, when applied to nonlinear problems and, in particular, fields with a significant compressive component [Lovadina & Auricchio, 2003].

3.7.5 Pressure Smoothing

The methods mentioned previously in this section alter the finite element formulation to address the issues of incompressibility. For example, in the selective reduced integration method, the constitutive model is changed; in the B-Bar method, the strain-displacement relation is changed; etc. Pressure smoothing is a method that is applied to 'smooth' the pressure oscillations that occur due to the spurious pressure modes [Chen *et al*., 1995]. In one approach, the smoothed pressure distribution is written in terms of nodal pressures and the displacement shape functions, and the difference between the smoothed field and the original calculated pressures is minimised in a least squares sense [Lee *et al.*, 1979]. In general, smoothing is performed as a post-processing procedure [Sani *et al.*, 1981, Part 1; Sani *et al.*, 1981, Part 2] and, as it is applied only to the pressure oscillations, has no effect on the constant/physical pressure mode. One example of removing the checkerboard mode (pressure oscillation) applies a procedure similar to the stabilisation matrix for hourglass modes of Belytschko and Bachrach [1986]. In this approach, the checkerboard pressures are filtered without affecting the non-checkerboarding pressure and then a pressure recovery procedure is employed after the fact [Chen *et al.*, 1995]. This method also leaves the constant pressure mode, if it exists, unaffected.

3.7.6 Other Methods

The literature related to the analysis of incompressible materials is fairly extensive. This subsection will describe some other methods that do not fall under the broad categories discussed previously in this chapter, but generally make use of more than one of the categories. See, for example, Reese *et al.* [2000].

An approach by Wu *et al.* [1999] combines a different variational formulation with incompatible modes to eliminate the pressures at the elemental level. The new variational principle includes the distortional part of the complementary energy. They also include a strategy for eliminating zero energy modes (hourglass modes).

In the analysis of incompressible materials, the shear stresses and difference of normal stresses can be determined but the sum of the normal stresses cannot be computed directly. Szabó *et al.* [1989] use an indirect method of solving Laplace's equation to determine the sum of normal stresses and thereby find the entire stress field.

Boroomand and Khalilian [2004] replace the original incompressible problem with the sum of two compressible problems each having the same shear modulus as the original. One of the sub-problems has fictitious boundary conditions which are determined iteratively so that the volume changes of the two sub-problems cancel, thereby enforcing incompressibility.

Rong and Liu [2001] have an interesting approach for finding the pressures which uses l'Hôpital's rule from calculus. To address the rank deficiency leading to the checkerboard mode they begin with the dilatational component of the constitutive law

$$p = \kappa e \tag{3.121}$$

or

$$p = \frac{E}{3(1-2\nu)} e \tag{3.122}$$

and then interpret the right hand side as a $\frac{0}{0}$ indeterminate form. L'Hôpital's rule can therefore be invoked to give an expression for the hydrostatic pressure, namely

$$p = \lim_{\nu \to 0.5} \left(-\frac{E}{6} \right) \frac{\mathrm{d}e}{\mathrm{d}\nu} . \tag{3.123}$$

Other techniques include: formulations with special purpose shape functions designed specifically for axisymmetric problems [Yu & Netherton, 2000]; time-marching schemes [Zienkiewicz & Wu, 1991]; and techniques employing macroelements which relax the constant volume restriction [Needleman & Shih, 1978; Nascimbene & Venini, 2002].

Most recently, Oñate *et al.* [2003; 2004] have developed a very promising finite calculus approach where the separation of deviatoric and dilatational effects occurs at the fundamental level of the governing differential equations. A major advantage of this method is circumvention of numerical instabilities and locking from the onset of the formulation. However, it does constitute a new formulation and would not be simply a modification to existing techniques.

Another recent method which also endeavours to resolve the problem at a fundamental level is that proposed by Chiumenti *et al.* [2002]. In this work, the full space of continuous functions is decomposed into the finite element space and an additional complementary subspace. The complementary subspace contains the portion of the pressure function whose omission in the conventional finite element analysis results in rank deficiency. To implement this approach, the variational principle is replaced by the

minimisation of two functionals; one in the finite element space and one in the complementary subspace.

3.8 Assessment of FEM and the Chiropractic Problem

As outlined at the end of Chapter 2, a finite element model of the vertebral artery subjected to chiropractic manipulation must incorporate near-incompressibility, geometric nonlinearity, displacement boundary conditions, and the associated uncertainty in the displacements determined from imaging. By exploring the pertinent technical aspects of the finite element method and the relevant literature, it is clear that the standard finite element technique experiences difficulties under these conditions. In this chapter, the techniques specifically designed to alleviate the problems of displacement locking and spurious pressure modes associated with incompressible materials are examined. The question to be answered in this section is whether any of these methods are suitable for the specific conditions of the chiropractic problem described above.

Rather than considering each method individually, this question can be answered by addressing fundamental concepts that are common to all. For example, displacement locking is a potential problem for all of the methods designed for incompressible materials. However, for the case where the boundary conditions are restricted to displacements, as is the case in the chiropractic problem, locking is not an issue since it refers to artificially small displacements in response to given applied force boundary

conditions. The other fundamental problem is the ability of the methods to treat pressure modes.

The Babuška-Brezzi condition, patch test and the count condition are used to predict whether an element will be subject to pressure modes. The modes are then "treated" by avoiding the elements that are susceptible. Other methods use different techniques to relax the volumetric constraint and stabilise the pressure modes. The Hu-Washizu and other variational principles are applied at the formulation stage of the variational principle. Reduced integration methods underintegrate specific parts of the stress-strain relations. Enhanced strain targets the strain field description. In the incompatible mode methods, the displacement field is affected. Finally, the pressure smoothing technique filters the pressures after solutions have already been reached. While all of these methods can lessen the effect of spurious modes with varying degrees of success, the key challenge identified in this section is that under the conditions of the chiropractic problem, the nonuniqueness of solution due to the physical mode is not eliminated by any of these methods. This may be proven with respect to both the governing partial differential equations and the discrete finite element equations.

To prove the nonuniqueness of solution in the governing partial differential equations due to the physical mode, the goal is to show that under displacement boundary conditions an arbitrary hydrostatic pressure p can be added to the normal stresses without violating the equations of equilibrium or the displacements on the boundary. The equilibrium equations are given by

$$\frac{\partial \sigma_{xx}}{\partial x} + \frac{\partial \tau_{xy}}{\partial y} + \frac{\partial \tau_{xz}}{\partial z} + B_x = 0\,, \tag{3.124}$$

$$\frac{\partial \tau_{yx}}{\partial x} + \frac{\partial \sigma_{yy}}{\partial y} + \frac{\partial \tau_{yz}}{\partial z} + B_y = 0\,, \tag{3.125}$$

and

$$\frac{\partial \tau_{zx}}{\partial x} + \frac{\partial \tau_{zy}}{\partial y} + \frac{\partial \sigma_{zz}}{\partial z} + B_z = 0\,, \tag{3.126}$$

where B_x, B_y, and B_z are the body forces in the x, y, and z directions. For the physical mode, the same p is added to every normal stress at every point. Since p is constant throughout the field, when it is differentiated with respect to x, y and z the result is zero and the equilibrium equations are still satisfied. Also, a hydrostatic pressure, by definition, can only affect a volume change. For an incompressible material, the volume is constant, and therefore a hydrostatic pressure has no effect on the displacements.

For the discrete finite element equations, nonuniqueness of solution may be proven by showing that, in cases where all boundary conditions are measured displacements, a vector $\boldsymbol{p}_c = [p \quad p \quad \ldots \quad p]^T$ with p a constant, will give $\boldsymbol{G}^T \boldsymbol{p}_c = \boldsymbol{0}$. Before boundary conditions are imposed, the discrete finite element equations are

$$\boldsymbol{A}\boldsymbol{u} + \boldsymbol{G}^T \boldsymbol{p} = \boldsymbol{f} \tag{3.127}$$

and

$$\boldsymbol{G}\boldsymbol{u} = \boldsymbol{0}\,, \tag{3.128}$$

where $\boldsymbol{f}$ is the force vector. Each equation in (3.128) defines the change in volume of a particular element. After imposing the displacement boundary conditions, the right hand sides of (3.127) and (3.128) become $\boldsymbol{b}_1$ and $\boldsymbol{b}_2$, respectively. Since all of the displacements on the boundary have been specified, the left hand side of each equation of $\boldsymbol{G}\boldsymbol{u} = \boldsymbol{b}_2$ gives the change in volume of an element due to internal displacements only.

The individual components of $\boldsymbol{G}$, G_{ij}, refer to the change in volume of element i per unit displacement j. In the case of matrix $\boldsymbol{G}^{\mathrm{T}}$, each row of the matrix corresponds to the elemental volume changes due to a particular internal displacement. If $\boldsymbol{G}^{\mathrm{T}}$ premultiplies $\boldsymbol{p}_{\mathrm{c}}$, the j^{th} row is given by

$$G_{1j}p + G_{2j}p + \cdots + G_{mj}p = \left(G_{1j} + G_{2j} + \cdots + G_{mj}\right)p \,. \tag{3.129}$$

The quantity $G_{1j} + G_{2j} + \cdots + G_{mj}$ gives the total volume change due to displacement j. Since displacement j can only affect the cluster of elements surrounding its corresponding node, the quantity $G_{1j} + G_{2j} + \cdots + G_{mj}$ is the volume change of the cluster due to displacement j. As shown in the example of Figure 3.6, displacement of an internal degree of freedom changes the volume of individual elements but not the cluster as a whole. Therefore, by adding a constant value of p to a solution of the finite element equations, the result is still a solution.

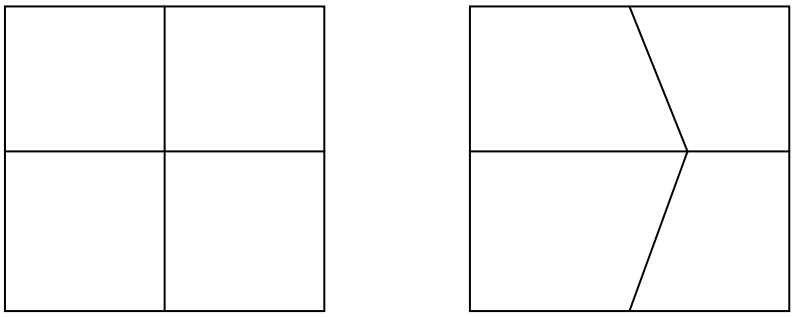

Figure 3.6: Distortion of an element cluster due to displacement of an internal degree of freedom.

After this proof was developed by the author, a closer examination of the literature revealed that a number of researchers have alluded to the physical mode issue without

addressing it in detail [Strang 2007; Bathe, 2006; Zienkiewicz *et al.*, 1991]. Most practical problems in stress analysis have mixed boundary conditions (i.e., displacements and forces) and therefore the physical mode does not exist. This is not the case in the chiropractic problem and the methods discussed previously are not designed to eliminate the physical mode. As an illustration, methods reviewed in this chapter were applied to the simple test case introduced in Section 3.2, with $\nu = 0.4999$. Like the patch test, satisfactory performance for this test case may be viewed as a necessary condition for accepting a method as suitable for analysing the chiropractic problem. These illustrations were performed using ANSYS®.

The methods considered are: use of a higher order element, selective reduced integration, and enhanced strain. Tables 3.4, 3.5 and 3.6 show the maximum and minimum values of σ_x, σ_y and σ_z obtained over the entire grid. To simulate uncertainty in the boundary displacement data, a random error distribution with a maximum value of 1% was applied to the data. In each case, two runs were performed, each with a different set of random errors applied to the data.

The stress values clearly show that despite using methods that are more advanced than the standard finite element method, an instability still exists. Signs of ill-conditioning are evident; a relatively small error in the data (1% maximum) results in a much larger error in the calculated values (up to 1000% in σ_x for the 8-node element and 850% for

Table 3.4: Comparison of Theoretical and Finite Element Values for σ_x.

Method	Data Set	Theoretical Value (MPa)	Maximum FEM Value (MPa)	Minimum FEM Value (MPa)
8-node Element	1	-100	838	-599
8-node Element	2	-100	929	743
Selective Reduced Integration	1	-100	-354	-918
Selective Reduced Integration	2	-100	747	460
Enhanced Strain	1	-100	-353	-921
Enhanced Strain	2	-100	748	460

Table 3.5: Comparison of Theoretical and Finite Element Values for σ_y.

Method	Data Set	Theoretical Value (MPa)	Maximum FEM Value (MPa)	Minimum FEM Value (MPa)
8-node Element	1	0	939	-497
8-node Element	2	0	1027	847
Selective Reduced Integration	1	0	-256	-818
Selective Reduced Integration	2	0	846	560
Enhanced Strain	1	0	-255	-820
Enhanced Strain	2	0	847	560

Table 3.6: Comparison of Theoretical and Finite Element Values for σ_z.

Method	Data Set	Theoretical Value (MPa)	Maximum FEM Value (MPa)	Minimum FEM Value (MPa)
8-node Element	1	-49.99	888	-545
8-node Element	2	-49.99	977	794
Selective Reduced Integration	1	-49.99	-305	-868
Selective Reduced Integration	2	-49.99	796	510
Enhanced Strain	1	-49.99	-304	-870
Enhanced Strain	2	-49.99	797	510

the other methods). Perhaps more significant is the variation from positive to negative extremes. In an iterative solution process, this can lead to fatal run-time errors. It is interesting to note that for the same data set, both selective reduced integration and enhanced strain give comparable values. This suggests that although the two methods address incompressibility differently, the outcome in response to a given data set is similar. To demonstrate that the instability is caused by the pressure modes, the von Mises stresses were calculated from the stresses given in Tables 3.4 to 3.6. The von Mises stress is defined as

$$\sigma_{\mathrm{vM}} = \frac{1}{\sqrt{2}}\left[\left(\sigma_x - \sigma_y\right)^2 + \left(\sigma_y - \sigma_z\right)^2 + \left(\sigma_z - \sigma_x\right)^2 + 6\left(\tau_{xy}^2 + \tau_{yz}^2 + \tau_{zx}^2\right)\right]^{1/2}, \qquad (3.130)$$

and is significant in this case because it is obtained only from distortional stress components (i.e. normal stress differences and shear stresses) and is independent of the hydrostatic pressure.

The calculated ANSYS values and exact solution are given in Table 3.7. Also included in this table are values for the von Mises stresses from the original illustration of Section 3.2.

Table 3.7: Comparison of Theoretical and Finite Element Values for σ_{vM}.

Method	Data Set	Theoretical Value (MPa)	Maximum FEM Value (MPa)	Minimum FEM Value (MPa)
8-node Element	1	86.6	88.8	83.2
8-node Element	2	86.6	90.3	84.4
Selective Reduced Integration	1	86.6	87.9	85.1
Selective Reduced Integration	2	86.6	87.6	86.1
Enhanced Strain	1	86.6	88.7	84.1
Enhanced Strain	2	86.6	87.9	85.6
Standard FEM	1	86.6	88.6	84.6

In all cases (including the standard finite element method demonstration of Section 3.2), the calculated von Mises stress is within 4.3% of the exact solution. This is consistent with the result of Malkus [Hughes, 1987] and Theorem 3.1 of this thesis which state that unique displacement solutions exist despite the existence of pressure modes. Since the distortional stresses are directly related in a point-wise fashion to the displacements, the solution for von Mises stress should be unique if pressure modes are the only source of instability. As Table 3.7 shows, this is clearly the case. It is also important to note that σ_{vM} is one of the most commonly used measures for failure theories in stress analysis.

This leads to the central realisation of this dissertation: although the evidence shows that it is impractical and numerically unstable to determine the complete stress state under the conditions of the chiropractic problem, a very useful stress measure, namely the von Mises stress, could be determined as long as the destabilising effects of both the physical and spurious modes are eliminated from the solution process so that fatal run-time errors are avoided.

This realisation by the author gave rise to a master's thesis by V.K. Nagarkal [2006] in which an extensive set of numerical tests verified that the von Mises stress is accurate under a wide range of both linear and nonlinear conditions associated with the chiropractic problem. In this master's thesis, results demonstrated that fatal run-time errors can occur in the case of iterative solution of nonlinear problems.

The remainder of this thesis is devoted to developing algorithms that are designed to remove the pressures, thus eliminating the possibility of either a spurious or physical pressure mode. The result will be a robust solution process for calculating distributions of von Mises stress.

Chapter 4

Decomposition Methods for Stable Finite Element Analysis

4.1 General Approach

In Chapter 3, it was established that a physical pressure mode, with its associated numerical instability, is inevitable when only displacements are specified on the boundary of an incompressible material. It was also established that a very useful quantity, the von Mises stress, can be accurately determined provided the numerical instability due to pressure modes is alleviated. The general strategy proposed here is to develop algorithms for solving the mixed finite element equations in such a way that the nodal displacements are obtained without calculating the pressure degrees of freedom. The von Mises stress can then be obtained from the strain-displacement and distortional constitutive relations.

All of the proposed algorithms have common features:

(1) The material is modelled as fully incompressible. Real tissue would have some degree of compressibility and a Poisson's ratio close to 0.5. Mathematically, this corresponds to systems of equations with coefficient matrices that are ill-conditioned but not strictly singular. By assuming the material has Poisson's ratio precisely equal to 0.5, the ill-conditioned matrices become singular (within round-off error) and sources of numerical instability are more easily identified and

eliminated. For example, small numerical values that theoretically approach zero in the incompressible limit can be identified with confidence. Adopting this approach introduces a small error in accuracy of the calculated displacements and von Mises stresses, but it will be shown that the cost of this approximation is small when compared to the benefit of stabilising the calculations.

(2) Each algorithm is designed for the specific structure of the mixed finite element equations (3.35). Numerous methods, including most notably the singular value decomposition (SVD), can be used to manipulate and analyse singular matrices. Special purpose methods, however, have the potential for greater efficiency in that they may require fewer operations during implementation.

(3) All of the algorithms rely upon fundamental approaches in linear algebra and produce nonsingular subsystems with nodal displacements as their only unknowns.

The first method, based on LU decomposition, is presented in the following section.

4.2 Modified LU Decomposition

4.2.1 Description of Method

One approach to calculating the nodal displacements while filtering out calculation of the hydrostatic pressures is to use a variation of LU decomposition (which writes a matrix as the product of a lower triangular matrix $\boldsymbol{L}$ and an upper triangular matrix $\boldsymbol{U}$ [Strang, 1976]). The proposed method begins with equation (3.35), which may be rewritten as

$$\boldsymbol{Kx} = \boldsymbol{F} \tag{4.1}$$

where

$$\boldsymbol{K} = \left[\begin{array}{c|c} \boldsymbol{A} & \boldsymbol{G}^{\mathrm{T}} \\ \hline \boldsymbol{G} & \boldsymbol{0} \end{array}\right] \quad , \tag{4.2}$$

$$\boldsymbol{x} = \left[\begin{array}{c} \boldsymbol{u} \\ \hline \boldsymbol{p} \end{array}\right], \tag{4.3}$$

and

$$\boldsymbol{F} = \left[\begin{array}{c} \boldsymbol{b}_1 \\ \hline \boldsymbol{b}_2 \end{array}\right]. \tag{4.4}$$

Adding to the discussion of Chapter 3, the matrix $\boldsymbol{K}$ is mixed-determined in an inverse problem sense [Gladwell, 1980]; the indeterminacy is related only to the hydrostatic pressures $\boldsymbol{p}$, while the nodal displacements $\boldsymbol{u}$ are exactly determined by the system of equations (4.1). A simple but effective method for avoiding the hydrostatic pressure values is to order the solution process so that the displacement unknowns are calculated first, and the process stops after $\boldsymbol{u}$ has been determined. The steps in the proposed procedure are as follows:

(i) The columns of matrix $\boldsymbol{K}$ and rows of vector $\boldsymbol{x}$ are placed in reverse order, producing $\hat{\boldsymbol{K}}$ and $\hat{\boldsymbol{x}}$, respectively. This reverses the order of unknowns in the system of equations and is necessary so that the unknown nodal displacements are calculated first, subsequent to LU decomposition. Unfortunately, this also has the effect of producing a matrix for which pivoting is problematic.

(ii) A least squares system is used to ensure nonzero diagonal entries. That is, the system

$$\hat{\boldsymbol{K}}\,\hat{\boldsymbol{x}} = \boldsymbol{F} \tag{4.5}$$

is replaced with

$$\hat{\boldsymbol{K}}^{\mathrm{T}}\hat{\boldsymbol{K}}\,\hat{\boldsymbol{x}} = \hat{\boldsymbol{K}}^{\mathrm{T}}\boldsymbol{F} \quad . \tag{4.6}$$

(iii) The matrix $\hat{\boldsymbol{K}}^{\mathrm{T}}\hat{\boldsymbol{K}}$ is decomposed using LU decomposition, so that

$$\hat{\boldsymbol{K}}^{\mathrm{T}}\hat{\boldsymbol{K}} = \hat{\boldsymbol{L}}\hat{\boldsymbol{U}} \tag{4.7}$$

and equation (4.6) becomes

$$\hat{\boldsymbol{L}}\hat{\boldsymbol{U}}\,\hat{\boldsymbol{x}} = \hat{\boldsymbol{K}}^{\mathrm{T}}\boldsymbol{F} \tag{4.8}$$

or,

$$\hat{\boldsymbol{L}}\,\boldsymbol{y} = \hat{\boldsymbol{K}}^{\mathrm{T}}\boldsymbol{F} \tag{4.9}$$

where

$$\hat{\boldsymbol{U}}\,\hat{\boldsymbol{x}} = \boldsymbol{y} \quad . \tag{4.10}$$

(iv) Equation (4.9) is solved for $\boldsymbol{y}$.

(v) Let m be the number of elements in the finite element mesh and therefore the number of unknown hydrostatic pressures. The system given by equation (4.10) is then reduced by eliminating the first m rows and m columns of matrix $\hat{\boldsymbol{U}}$ to produce the reduced matrix $\hat{\boldsymbol{U}}_{\mathrm{r}}$, and also by eliminating the first m elements of both $\hat{\boldsymbol{x}}$ and $\mathbf{y}$ to produce $\hat{\boldsymbol{u}}$ and $\boldsymbol{y}_{\mathrm{r}}$, respectively. This gives the system

$$\hat{\boldsymbol{U}}_{\mathrm{r}}\,\hat{\boldsymbol{u}} = \boldsymbol{y}_{\mathrm{r}} \tag{4.11}$$

which can be solved for $\hat{\boldsymbol{u}}$, a vector consisting only of nodal displacements.

4.2.2 Computer Code Implementation

To perform numerical examples demonstrating the modified LU method as well as other stabilising algorithms, a series of finite element codes were written by the author. Each code was written assuming a linear elastic, isotropic material model subjected to plane strain conditions. Plane strain was chosen since two-dimensional analysis of an arterial cross section would be more accurately modelled as plane strain, rather than plane stress. In addition, three-dimensional analyses would encounter ill-conditioning of the same type as that exhibited by plane strain. This may be shown by considering 3-D generalised Hooke's law in the form

$$\sigma_x = \frac{E}{(1+\nu)(1-2\nu)}\left[(1-\nu)\varepsilon_x + \nu\left(\varepsilon_y + \varepsilon_z\right)\right], \tag{4.12}$$

$$\sigma_y = \frac{E}{(1+\nu)(1-2\nu)}\left[(1-\nu)\varepsilon_y + \nu\left(\varepsilon_z + \varepsilon_x\right)\right], \tag{4.13}$$

$$\sigma_z = \frac{E}{(1+\nu)(1-2\nu)}\left[(1-\nu)\varepsilon_z + \nu\left(\varepsilon_x + \varepsilon_y\right)\right]. \tag{4.14}$$

As ν approaches 0.5, the same numerical instability is apparent whether $\varepsilon_z = 0$, or not. In contrast, the equations for plane stress have a different form completely, are not unstable in the neighbourhood of $\nu = 0.5$, and may be easily derived from the three-dimensional relations as

$$\sigma_x = \frac{E}{1-\nu^2}\left(\varepsilon_x + \nu\varepsilon_y\right), \tag{4.15}$$

and

$$\sigma_y = \frac{E}{1-\nu^2}\left(\varepsilon_y + \nu\varepsilon_x\right). \tag{4.16}$$

As a starting point and reference, a code using a classical finite element formulation with four node quadrilateral elements and isoparametric shape functions was developed [Budynas, 1999]. For this preliminary code, any value of Poisson's ratio could be specified.

Subsequent codes were based on the mixed formulation described in Chapter 3 leading to systems of the form given by equation (4.1). In this case, the four node bilinear displacement, constant pressure (Q4P1) element was chosen. This element does not pass the patch test or the B-B condition for mixed formulations [Zienkiewicz *et al*, 1986; Zienkiewicz & Taylor, 1997; Bathe, 1996]. However, it is still widely used [Chen *et al*, 1995; Kouhia & Stenberg, 1995] and intensively researched [Pantuso & Bathe, 1995] due to its "simplicity, reliability and good performance in the prediction of the displacement (velocity) field" [Dvorkin, 2001]. It is also easily extended to non-linear analyses [Malkus in Hughes, 1987]. Its use is further justified by the statement of Simo *et al.* [1993] referring to the "lack of robustness exhibited by high order elements in non-linear Lagrangian calculations".

The finite element formulation for the Q4P1 code is given in Appendix B and is similar in many respects to that for the standard quadrilateral element; i.e., they share the same displacement shape functions, implementation method for boundary conditions, and general assembly procedures for producing the global system from elemental systems. The Q4P1 codes developed for this thesis, however, are designed for full incompressibility and only the distortional component of the constitutive relation is enforced pointwise. As a result, generalised Hooke's law is replaced with a relationship

involving only the normal stress differences, normal strain differences, shear stress, and shear strain. By subtracting (4.13) from (4.12), and (4.14) from (4.13),

$$\sigma_x - \sigma_y = \frac{E}{1+\nu}\left(\varepsilon_x - \varepsilon_y\right) \tag{4.17}$$

and

$$\sigma_y - \sigma_z = \frac{E}{1+\nu}\left(\varepsilon_y - \varepsilon_z\right), \tag{4.18}$$

respectively. For plane strain, $\varepsilon_z = 0$ and in matrix form the distortional component of Hooke's law becomes

$$\begin{bmatrix} \sigma_x - \sigma_y \\ \sigma_y - \sigma_z \\ \sigma_z - \sigma_x \\ \sqrt{6}\tau_{xy} \end{bmatrix} = \frac{E}{1+\nu}\begin{bmatrix} 1 & 0 & 0 & 0 \\ 0 & 1 & 0 & 0 \\ 0 & 0 & 1 & 0 \\ 0 & 0 & 0 & 0.5 \end{bmatrix}\begin{bmatrix} \varepsilon_x - \varepsilon_y \\ \varepsilon_y \\ -\varepsilon_x \\ \sqrt{6}\gamma_{xy} \end{bmatrix} \tag{4.19}$$

or

$$\hat{\boldsymbol{\sigma}} = \hat{\boldsymbol{D}}\,\hat{\boldsymbol{\varepsilon}}\,, \tag{4.20}$$

where the fourth line of (4.19) expresses the classical linear elastic relationship between shear stress and shear strain.

As a result of the non-standard stress-strain relation, the strain-displacement relation must also be modified. It must now be written in terms of the deviatoric normal strains and shear strain, as

$$\hat{\boldsymbol{\varepsilon}} = \hat{\boldsymbol{B}}\,\boldsymbol{u} \tag{4.21}$$

where $\hat{\boldsymbol{B}}$ is given by

$$\hat{\boldsymbol{B}} = \begin{bmatrix} B_{11}-B_{21} & B_{12}-B_{22} & B_{13}-B_{23} & B_{14}-B_{24} & B_{15}-B_{25} & B_{16}-B_{26} & B_{17}-B_{27} & B_{18}-B_{28} \\ B_{21} & B_{22} & B_{23} & B_{24} & B_{25} & B_{26} & B_{27} & B_{28} \\ -B_{11} & -B_{12} & -B_{13} & -B_{14} & -B_{15} & -B_{16} & -B_{17} & -B_{18} \\ \sqrt{6}B_{31} & \sqrt{6}B_{32} & \sqrt{6}B_{33} & \sqrt{6}B_{34} & \sqrt{6}B_{35} & \sqrt{6}B_{36} & \sqrt{6}B_{37} & \sqrt{6}B_{38} \end{bmatrix} \tag{4.22}$$

and B_{ij} are individual components of the standard strain-displacement matrix $\boldsymbol{B}$. (See Appendix B.)

As discussed in Chapter 3, the volumetric constraint is enforced in an average sense over each element. For plane strain, this relation is defined as

$$\int \left(\varepsilon_x + \varepsilon_y\right) \mathrm{d}V = 0 \tag{4.23}$$

over each element where

$$\varepsilon_x + \varepsilon_y = B_{11}u_1 + B_{13}u_2 + B_{15}u_3 + B_{17}u_4 + B_{22}v_1 + B_{24}v_2 + B_{26}v_3 + B_{28}v_4 \tag{4.24}$$

or

$$\varepsilon_{\mathrm{x}} + \varepsilon_{\mathrm{y}} = \boldsymbol{u}^{\mathrm{T}} \widetilde{\boldsymbol{B}} \tag{4.25}$$

where

$$\widetilde{\boldsymbol{B}} = \begin{bmatrix} B_{11} & B_{22} & B_{13} & B_{24} & B_{15} & B_{26} & B_{17} & B_{28} \end{bmatrix}^{\mathrm{T}}. \tag{4.26}$$

The expression for stationary potential energy, as developed in equation (3.26), is given by

$$\Pi = \hat{U} + \Omega + p\int \left(\varepsilon_x + \varepsilon_y\right) \mathrm{d}V\,, \tag{4.27}$$

or

$$\Pi = \frac{1}{12G}\int \hat{\boldsymbol{\sigma}}^{\mathrm{T}}\hat{\boldsymbol{\sigma}}\,\mathrm{dV} + \Omega + \mathrm{p}\int\left(\varepsilon_{\mathrm{x}} + \varepsilon_{\mathrm{y}}\right)\mathrm{dV}\,, \tag{4.28}$$

and, as detailed in Appendix B, the final finite element formulation may be obtained by substituting (4.20), (4.21) and (4.25) into (4.28) and minimising to give

$$\left[\frac{1}{6G}\int \hat{\boldsymbol{B}}^{\mathrm{T}}\hat{\boldsymbol{D}}^{2}\hat{\boldsymbol{B}}\,\mathrm{dV}\right]\boldsymbol{u} - \boldsymbol{F} + \mathrm{p}\int\widetilde{\boldsymbol{B}}\,\mathrm{dV} = 0 \tag{4.29}$$

and

$$\boldsymbol{u}^{\mathrm{T}}\int\widetilde{\boldsymbol{B}}\,\mathrm{d}V = 0\,. \tag{4.30}$$

These integrals are performed using Gauss-Legendre quadrature where the Gauss points follow a 2×2 quadrature rule for exact integration [Zienkiewicz & Taylor, 1989]. This process is performed for each element in the finite element grid and then the equations are assembled into the global stiffness matrix which takes the form given in equation (4.1).

Once the equations are assembled, the system may be solved using the modified LU method, or a different approach, to eliminate the degrees of freedom. In the next section, three examples are employed to demonstrate that the LU method can be used to produce stable subsystems of linear equations which may be solved to obtain accurate values for nodal displacements and the von Mises stress.

4.2.3 Numerical Example 1 - Rectangular Block in Compression

The proposed strategy for material incompressibility was applied to the elementary example considered in Section 3.2. As a measure of numerical instability, the condition number (*CN*) of matrices $\boldsymbol{K}$ and $\hat{\boldsymbol{U}}_{\mathrm{r}}$ from equations (4.1) and (4.11) were calculated

according to the singular value decomposition (SVD), as reviewed in Appendix A. The SVD was used (instead of eigenvalue decomposition) to determine the condition numbers since $\boldsymbol{K}$ is not positive definite. Before applying the SVD, as is common practice, the matrices were scaled by dividing each row by its largest element in absolute value. The condition number was defined as the ratio of the largest to smallest singular value for the matrix, a method that has been used by other researchers for assessing numerical stability in the context of incompressible analysis [Canga & Becker, 1999]. The value of $CN(\boldsymbol{K})$ was calculated to confirm that the original unfiltered system in this example is singular, as expected. The calculated values are given in Table 4.1.

Table 4.1: Condition numbers for matrices used in calculating the displacements in a block in uniform plane strain compression.

Matrix	Condition Number
$\boldsymbol{K}$	6.01×10^{17}
$\hat{\boldsymbol{U}}_{\mathrm{r}}$	6.80

Recall that in the modified approach, the unknown nodal displacements are calculated using $\hat{\boldsymbol{U}}_{\mathrm{r}}$, which is constructed from matrix $\hat{\boldsymbol{U}}$ by eliminating the rows and columns corresponding to the hydrostatic pressures. Theoretically, the condition number for singular matrix $\boldsymbol{K}$ would approach infinity, and the calculated value in Table 4.1 is consistent with this, within the limitations of machine precision. The reduction to $\hat{\boldsymbol{U}}_{\mathrm{r}}$ achieves a dramatic decrease in the condition number, and therefore a significant increase in numerical stability. To confirm the von Mises stresses calculated with the modified LU method, the author's code was applied to three displacement data sets, each

with a different random error distribution of maximum of 1%. The calculated values are given in Table 4.2.

Table 4.2: Comparison of Theoretical and Finite Element Values for σ_{vM} Calculated Using the Modified LU Method.

Data Set	Theoretical Value (MPa) $\nu = 0.49$	Theoretical Value (MPa) $\nu = 0.4999$	Maximum FEM Value (MPa)	Minimum FEM Value (MPa)
1	86.608	86.602	87.541	85.802
2	86.608	86.602	87.546	86.490
3	86.608	86.602	87.367	85.610

The values in Table 4.2 clearly suggest that a nearly incompressible material with Poisson's ratio as low as 0.49 could be modeled as having $\nu = 0.5$ with little effect on σ_{vM}. That is, $\nu = 0.5$ can be used in the stabilisation process with little cost in accuracy.

4.2.4 Numerical Example 2 - Rectangular Block in Simple Shear

Consider the same block as in Section 4.2.3, however subjected to a simple shear as shown in Figure 4.1. The dimensions, Young's modulus and Poisson's ratio remain the same and the maximum displacement $u_{\max}$ at the top of the block is 1 mm. The analytical solution for this example is

$$u = \frac{u_{\max}}{h} y, \tag{4.31}$$

$$v = 0 \tag{4.32}$$

and

$$\sigma_{\text{vM}} = \sqrt{3}\tau, \tag{4.33}$$

where u and v are the x- and y-displacements, respectively and

$$\tau = \frac{E}{2(1+\nu)} \frac{u_{\max}}{h} . \tag{4.34}$$

Equations (4.31) and (4.32) were used to create the displacement boundary conditions that are a result of applying the simple shear τ_0 to the block. For linear elasticity, the maximum displacement $u_{\max}$, the shear strain γ_{xy}, and the rigid body rotation Θ_{xy}, must be small. To ensure this condition exists, $\tan \gamma_{xy} \approx \gamma_{xy}$. For $u_{\max}$ = 1 mm, linear elasticity is maintained.

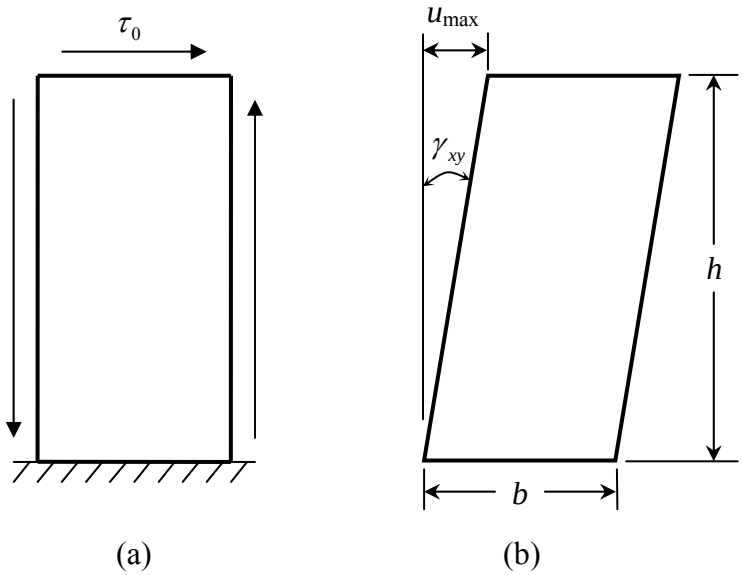

Figure 4.1: Rectangular block in simple shear (a) with boundary conditions, before deformation; (b) after deformation

Condition numbers for a regular grid of 10 × 10 elements are presented in Table 4.3 for $\boldsymbol{K}$, and $\hat{\boldsymbol{U}}_r$. Again, the calculated values indicate a dramatic change from the original ill-conditioned system to one that is numerically stable.

Table 4.3: Condition numbers for matrices used in calculating the displacements in a rectangular block in simple shear.

Matrix	Condition Number
$\boldsymbol{K}$	2.79×10^{17}
$\hat{\boldsymbol{U}}_{\mathrm{r}}$	54.6

4.2.5 Numerical Example 3 - Thick-walled Cylindrical Pressure Vessel

As a final example to demonstrate the modified LU approach, consider a thick-walled cylindrical pressure vessel of inner radius, r_{i}, outer radius, r_{o}, and subjected to internal pressure, p_{i}, and external pressure, p_{o}, shown in Figure 4.2. This is the classical Lamé problem [Budynas, 1999; Cook and Young, 1985]. If the cylinder is axially restrained (i.e., in plane strain) and is made of a linearly elastic, incompressible material, the analytical solution for displacements in the x- and y- directions is given by

$$u = \frac{3\left(r_i r_o\right)^2\left(p_i - p_o\right)}{2\,E\,r\left(r_o^{\,2} - r_i^{\,2}\right)}\,\cos\theta \tag{4.35}$$

and

$$v = \frac{3\left(r_i r_o\right)^2\left(p_i - p_o\right)}{2\,E\,r\left(r_o^{\,2} - r_i^{\,2}\right)}\,\sin\theta \tag{4.36}$$

where r and θ are the polar coordinates of a point, easily written as x- and y- coordinates. The von Mises stress is given by

$$\sigma_{\mathrm{vM}} = \left|\frac{\sqrt{3}\left(r_i r_o\right)^2\left(p_i - p_o\right)}{r^2\left(r_i^{\,2} - r_o^{\,2}\right)}\right| . \tag{4.37}$$

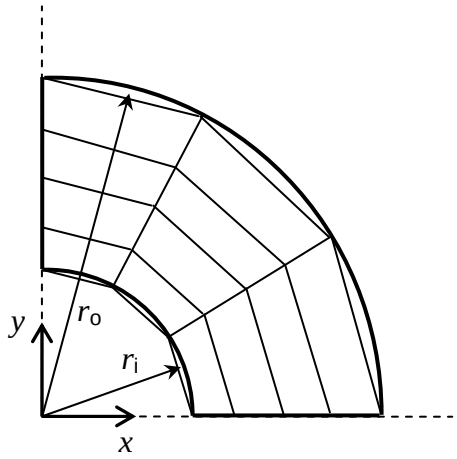

Figure 4.2: A plane within a thick-walled cylinder of inner radius r_i and outer radius r_o. The inner and outer radii are subjected to pressures p_i and p_o, respectively. A sample finite element grid is shown.

For the arbitrarily selected values of r_i = 100 mm, r_o = 200 mm, p_i = 0.2 kN/mm^2 and p_o = 0.1 kN/mm^2, equations. (4.35) and (4.36) were used to produce displacement boundary conditions in recasting the problem as a Dirichlet boundary value problem. Taking advantage of symmetry, one-quarter of the cylinder was modelled and results were produced for three grids (given as number of elements in the radial direction × the number of elements in the circumferential direction): 10×10, 15×15, and 20×20. The average (maximum) percent difference between the von Mises stress at the natural centres of the elements calculated using equation (4.37) and the values obtained using the finite element code for these grids are 0.491%(0.550%), 0.219%(0.245%), and 0.123%(0.138%), respectively. This verifies that the finite element model is providing a reasonable approximation to the field. The condition numbers for each of the grids is given in Table 4.4.

Table 4.4: Condition numbers for matrices used in calculating the displacements in a thick-walled cylinder for different FEM grids.

Matrix	10×10 Grid	15×15 Grid	20×20 Grid
$\boldsymbol{K}$	2.44×10^{15}	9.86×10^{15}	1.42×10^{16}
$\hat{\boldsymbol{U}}_{\mathrm{r}}$	59.4	171	336

Again, the condition number of $\hat{\boldsymbol{U}}_{\mathrm{r}}$ is significantly smaller than $CN(\boldsymbol{K})$ for all grids. All of the condition numbers increase with the grid size. This is expected, however, when going from a 10×10 grid to a 20×20, since the size of the stiffness matrix $\boldsymbol{K}$ increases from 262×262 to 1122×1122.

For all three of the examples in this chapter, the widely criticised but frequently used [Zienkiewicz & Taylor, 1997] bilinear displacement, constant pressure element has been employed. The results have demonstrated that by selectively eliminating those unknowns which are indeterminate, a reduced, non singular system of equations in terms of the unknown nodal displacements is produced. So, a stable subsystem does exist within the original mixed-determined system of equations.

Although the final reduced systems are nonsingular and stable, the intermediate calculations involved in decomposing a matrix into upper and lower triangular matrices ($\boldsymbol{L}$ and $\boldsymbol{U}$) includes division by a pivot (i.e., division by element K_{ii}, for each row i). The LU decomposition, therefore, may involve steps such as division by a small number, which could affect the numerical stability of the overall solution process. The extent of

this instability would depend on the specific nature of the matrix $\boldsymbol{K}$ and led to further study by the author. An alternative approach which avoids division by pivots and is based on a modification of QR decomposition is outlined in the following section.

4.3 Multi-level QR Solution Method

4.3.1 A Review of QR Decomposition

The QR method decomposes a matrix $\boldsymbol{K}$ into the product of an orthogonal matrix $\boldsymbol{Q}$ and an upper triangular matrix $\boldsymbol{R}$ such that

$$\boldsymbol{K} = \boldsymbol{Q}\boldsymbol{R}. \tag{4.38}$$

One method that may be used to decompose $\boldsymbol{K}$ is through a Gram-Schmidt process; however this process is known to be numerically unstable [Strang, 1976]. A more numerically stable process is through the use of Householder matrices. Householder matrices are used because they have properties that make them ideally suited for converting a full matrix into one that is upper triangular. These properties can be verified mathematically with proofs given in Strang [1976] but are listed here without proof. A Householder matrix, $\boldsymbol{H}$, is orthogonal and symmetric so that

$$\boldsymbol{H} = \boldsymbol{H}^{-1} = \boldsymbol{H}^{\mathrm{T}}. \tag{4.39}$$

Also, it has the form [Strang, 1976]

$$\boldsymbol{H} = \boldsymbol{I} - 2\frac{\boldsymbol{v}\boldsymbol{v}^{\mathrm{T}}}{\|\boldsymbol{v}\|^2} \tag{4.40}$$

where vector $\boldsymbol{v}$ may be defined as

$$\boldsymbol{v} = \boldsymbol{x} + \|\boldsymbol{x}\|\boldsymbol{z}\,, \tag{4.41}$$

with $\boldsymbol{x}$ an arbitrary vector, and

$$\boldsymbol{z} = \begin{bmatrix} 1 & 0 & 0 & \cdots & 0 \end{bmatrix}^{\mathrm{T}}. \tag{4.42}$$

Using these definitions,

$$\boldsymbol{H}\boldsymbol{x} = -\|\boldsymbol{x}\|\boldsymbol{z}\,, \tag{4.43}$$

or, if $\|\boldsymbol{x}\| = a$, then

$$\boldsymbol{H}\boldsymbol{x} = \begin{bmatrix} -a \\ 0 \\ 0 \\ \vdots \\ 0 \end{bmatrix}. \tag{4.44}$$

A series of Householder matrices $\boldsymbol{H}$ can be applied to a matrix $\boldsymbol{K}$ in a step-wise process that transforms $\boldsymbol{K}$, one column at a time, into an upper triangular matrix. Consider an example where $\boldsymbol{K}$ has 3 row and 3 columns. The first vector x_1 is the first column of $\boldsymbol{K}$ and the first Householder matrix, $\boldsymbol{H}_1$, is found from Equation (4.40). When this matrix is multiplied by $\boldsymbol{K}$, the result is of the form

$$\boldsymbol{H}_1\boldsymbol{K} = \begin{bmatrix} * & * & * \\ 0 & * & * \\ 0 & * & * \end{bmatrix}. \tag{4.45}$$

The next vector, $\boldsymbol{x}_2$, is the second column of $\boldsymbol{H}_1\boldsymbol{K}$ from the pivot down and the process is repeated, with a 2×2 Householder matrix applied to the 2×2 submatrix defined by

ignoring the first row and first column of $\boldsymbol{H}_1\boldsymbol{K}$. Therefore, the second step in the transformation requires a matrix of the form

$$\tilde{\boldsymbol{H}}_2 = \begin{bmatrix} 1 & 0 & 0 \\ 0 & * & * \\ 0 & * & * \end{bmatrix}, \tag{4.46}$$

where the 2×2 Householder matrix is represented with asterisks. When $\tilde{\boldsymbol{H}}_2$ is multiplied by $\boldsymbol{H}_1\boldsymbol{K}$, the result is

$$\tilde{\boldsymbol{H}}_2\boldsymbol{H}_1\boldsymbol{K} = \begin{bmatrix} * & * & * \\ 0 & * & * \\ 0 & 0 & * \end{bmatrix}. \tag{4.47}$$

This is the desired upper triangular matrix. Therefore, with the definition $\tilde{\boldsymbol{H}}_1 \equiv \boldsymbol{H}_1$,

$$\boldsymbol{R} = \tilde{\boldsymbol{H}}_2\tilde{\boldsymbol{H}}_1\boldsymbol{K} \tag{4.48}$$

and, comparing (4.48) and (4.47), the orthogonal matrix $\boldsymbol{Q}$ is

$$\boldsymbol{Q} = \tilde{\boldsymbol{H}}_1\tilde{\boldsymbol{H}}_2, \tag{4.49}$$

where the symmetric orthogonal property of Householder matrices has been used in obtaining (4.49). If the original system of equations was

$$\boldsymbol{K}\boldsymbol{x} = \boldsymbol{b}, \tag{4.50}$$

then by applying QR decomposition with Householder transformations, the new system of equations to be solved is

$$\boldsymbol{R}\boldsymbol{x} = \boldsymbol{Q}^{\mathrm{T}}\boldsymbol{b} \quad . \tag{4.51}$$

This decomposition may be applied to any arbitrarily sized $m \times n$ matrix and the number of iterations of the Householder transformation process required to arrive at an upper triangular matrix is the smaller of either $m - 1$ or n.

4.3.2 Multilevel QR Formulation

In this section, the method of QR decomposition is adapted by the author to produce an algorithm for stabilising the finite element equations for incompressible materials. As with the LU method presented in Section 4.2, the aim of the formulation developed here is to filter out the pressures, leaving only the displacements as unknowns. QR decomposition is applied to the system of equations given by (3.35) (and repeated here for convenience to the reader)

$$\left[\begin{array}{c|c} \boldsymbol{A} & \boldsymbol{G}^{\mathrm{T}} \\ \hline \boldsymbol{G} & \boldsymbol{0} \end{array}\right]\left[\begin{array}{c} \boldsymbol{u} \\ \hline \boldsymbol{p} \end{array}\right]=\left[\begin{array}{c} \boldsymbol{b}_1 \\ \hline \boldsymbol{b}_2 \end{array}\right]. \tag{4.52}$$

The steps for this procedure are as follows:

(i) The column blocks of the matrix, $\boldsymbol{K}$, are reversed so that the new system of equations is

$$\left[\begin{array}{c|c} \boldsymbol{G}^{\mathrm{T}} & \boldsymbol{A} \\ \hline \boldsymbol{0} & \boldsymbol{G} \end{array}\right]\left[\begin{array}{c} \boldsymbol{p} \\ \hline \boldsymbol{u} \end{array}\right]=\left[\begin{array}{c} \boldsymbol{b}_1 \\ \hline \boldsymbol{b}_2 \end{array}\right]. \tag{4.53}$$

(ii) QR decomposition is applied to each column block of the matrix separately; that is, QR decomposition is applied to $\left[\begin{array}{c} \boldsymbol{G}^{\mathrm{T}} \\ \hline \boldsymbol{0} \end{array}\right]$ and $\left[\begin{array}{c} \boldsymbol{A} \\ \hline \boldsymbol{G} \end{array}\right]$, separately. Column pivoting within each column block is applied to ensure that the norm of each remaining column from the pivot down, during the Householder transformation process, is as large as possible. This ensures that the process is numerically stable and will clearly identify the rank of each block. A permutation matrix is therefore required to properly order the displacement degrees of freedom after solution.

(iii) In the first column block, QR decomposition is terminated when the norm of a column from the pivot down is smaller than some tolerance φ (e.g., $\varphi = 0.0001$). QR decomposition is then resumed in the second column block and proceeds once again until the norm is too small, thereby completing the QR decomposition.

Numerical experiments by the author, using the code described in Section 4.2.2 and involving this procedure of reordering the unknowns followed by block-restricted column pivoting, led to the discovery that this process isolates a nonsingular submatrix that corresponds to a system of equations with the nodal displacements as the only unknowns. This submatrix is located in the second column block beginning at the row where QR decomposition is terminated in the first column block and extending for the same number of rows as displacement degrees of freedom. For an illustration of this, consider an arbitrary 4×4 matrix of the same form as equation (4.53) after QR decomposition has been performed, shown in Figure 4.3. This result is proven in the following theorem and corresponding proof.

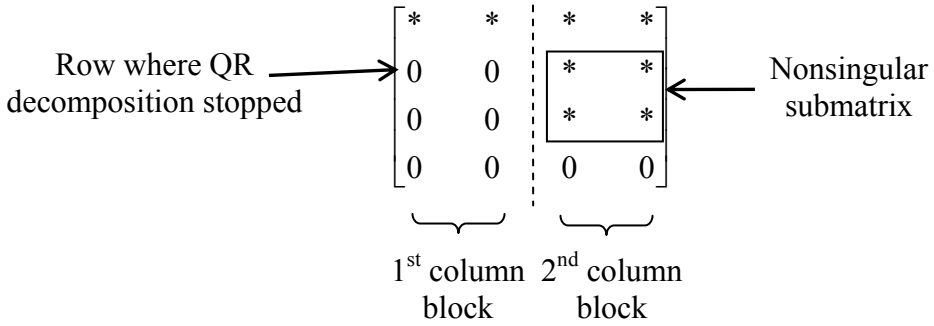

Figure 4.3: Illustration of location of non singular submatrix

Theorem 4.1: Given an $n \times n$ system of equations

$$\boldsymbol{K}\boldsymbol{x} = \boldsymbol{b}\,, \tag{4.54}$$

where x_1, x_2, ..., x_p are underdetermined by k and x_{p+1}, x_{p+2}, ..., x_n are exactly determined, if $\boldsymbol{K}$ is partitioned into 2 column blocks of size p and $n-p$ respectively, and is then decomposed by QR factorisation (via Householder matrices) with column pivoting restricted within each block, then the submatrix, $\tilde{\boldsymbol{K}}$, consisting of rows $p+1-k$ to $n-k$ within block 2 is nonsingular.

Proof: Since the variables x_1, x_2, ..., x_p are underdetermined by k, QR factorisation within the first block of p columns will result in $p-k$ nonzero upper-triangular rows within that block. Thus, rows 1 to $p-k$ of matrix $\boldsymbol{K}$ are linearly independent. Also, since variables x_{p+1}, x_{p+2}, ..., x_n are exactly determined, the rank of $\boldsymbol{K}$ equals $n-k$ and QR factorisation will lead to all zeros in rows $n-k+1$, ..., n of matrix $\boldsymbol{K}$. Since the rank of $\boldsymbol{K}$ is $n-k$, and the first $p-k$ rows are linearly independent, and the last k rows are zero, rows $p-k+1$ to $n-k$ must be linearly independent. ■

From the theorem, the author has shown that through this particular multi-level QR factorisation process, the first p elements in rows $p-k+1$ to $n-k$ are zero. Therefore,

$$\tilde{\boldsymbol{K}}\,\tilde{\boldsymbol{x}} = \tilde{\boldsymbol{b}} \tag{4.55}$$

gives a nonsingular system of equations, where vector $\tilde{\boldsymbol{x}}$ consists only of displacement unknowns x_{p+1}, x_{p+2}, ..., x_n (in permuted order), and $\tilde{\boldsymbol{b}}$ consists of elements $p-k+1$ to $n-k$ of $\boldsymbol{Q}^{\mathrm{T}}\boldsymbol{b}$. Assuming that this submatrix is not only nonsingular but well-conditioned, the subsystem (4.55) produced by the multi-level QR process can be solved using an efficient conventional algorithm such as LU decomposition or the conjugate

gradient method, depending on the application. In a sense, then, the multi-level QR decomposition proposed here may be viewed as a type of preconditioning process.

4.3.3 Numerical Examples

To demonstrate that the multi-level QR approach is effective in producing a well-conditioned reduced system of equations, the method is applied in this section to the examples described in Section 4.2. The condition numbers for $\boldsymbol{K}$ and the final reduced matrix $\widetilde{\boldsymbol{K}}$ are given in Table 4.5. The von Mises stresses for the block in compression, as calculated using the multilevel QR approach, are given in Table 4.6. The three displacement data sets are the same as those used for testing the modified LU method.

Table 4.5: Condition numbers for numerical examples.

Matrix	Block in Compression	Block in Simple Shear	10 × 10 Cylinder	15 × 15 Cylinder	20 × 20 Cylinder
$\boldsymbol{K}$	6.01×10^{17}	2.79×10^{17}	2.44×10^{15}	9.86×10^{15}	1.26×10^{16}
$\widetilde{\boldsymbol{K}}$	4.82	14.9	16.9	27.5	37.1

It is interesting to note that values of σ_{vM} calculated using the multilevel QR technique (Table 4.6) are identical, within round off error, to those obtained using the modified LU method (Table 4.2). This may be explained by considering the similarities between the two approaches: both involve a reordering of the unknown variables and a reduction of

Table 4.6: Comparison of Theoretical and Finite Element Values for σ_{vM} Calculated Using the Multilevel-QR Method.

Data Set	Theoretical Value (MPa) $\nu = 0.49$	Theoretical Value (MPa) $\nu = 0.4999$	Maximum FEM Value (MPa)	Minimum FEM Value (MPa)
1	86.608	86.602	87.541	85.802
2	86.608	86.602	87.546	86.490
3	86.608	86.602	87.367	85.610

the original system of equations to a smaller subsystem where nodal displacements are the only unknowns. Although the condition numbers in Table 4.5 show a dramatic improvement in numerical stability, the multilevel QR process is clearly inefficient from a computational standpoint as the QR decomposition itself is known to be slow [Woolfe *et al.*, 2008] and in this case must be followed by an additional equation solving step. This raises the question of whether the QR decomposition could be adapted to simultaneously achieve numerical stability and solve for the displacement unknowns in a more efficient manner. In the next chapter, a method for accomplishing this goal is presented.

Chapter 5

A Priori Incorporation of Constraints

5.1 Introduction to the Method

In this chapter, the author proposes an approach for achieving numerical stability with greater efficiency. The method incorporates the constraints before the final system of equations is generated, i.e. early in the formulation, so that unlike the LU and QR methods which must eliminate the pressure field after the u-p equations have been assembled, the system of equations has no pressure unknowns in the first place. This can be better understood by recalling the fundamentals of constrained optimisation in calculus.

Given a function, $\hat{\Pi}$, such that

$$\hat{\Pi}(\boldsymbol{u}) = \hat{U} + \Omega \tag{5.1}$$

to be minimised with respect to $\boldsymbol{u}$ subject to constraints (on $\boldsymbol{u}$) of the form

$$\int e \, \mathrm{d}V = 0 \tag{5.2}$$

where $e = e(\boldsymbol{u})$, the Lagrange multiplier method, described in Chapter 3, may be used so that the new function

$$\Pi(\boldsymbol{u}, p) = \hat{U} + \Omega + p\int e \, \mathrm{d}V \tag{5.3}$$

is minimised where p is the Lagrange multiplier.

However, another fundamental approach from calculus is to substitute the constraints (5.2) into the function (5.1); i.e., each constraint is used to write one of the unknowns in $\boldsymbol{u}$ in terms of the remaining unknowns, thus eliminating that unknown from directly appearing in the function to be minimised and at the same time satisfying the constraints. This has the advantage that Lagrange multipliers (or in the present case, pressure degrees of freedom) are not introduced into the formulation. This approach of *a priori* incorporation of constraints (AIC) forms the basis for the method introduced in this chapter.

5.2 Initial Approach for Incorporating the Constraints

This approach begins by considering the constant volume constraint equations

$$\boldsymbol{G}\boldsymbol{u} = \boldsymbol{0}\,. \tag{5.4}$$

This differs from Chapter 3 as the right hand side of the system (5.4) is zero since no boundary conditions have been applied at this point. From the vector $\boldsymbol{u}$, "some" of the displacement degrees of freedom are "selected" to be eliminated; i.e., to be written in terms of the other unknowns. The words "some" and "selected" are placed in quotes since they identify key issues that arose in developing this initial method for eliminating variables. Originally, it was assumed that one displacement unknown could be eliminated for each constraint equation. As a hypothetical example for the purpose of describing the associated mathematics, consider a set of two constraint equations of the form

$$G_{11}u_1 + G_{12}u_2 + G_{13}u_3 + G_{14}u_4 + G_{15}u_5 = 0 \tag{5.5}$$

$$G_{21}u_1 + G_{22}u_2 + G_{23}u_3 + G_{24}u_4 + G_{25}u_5 = 0\,. \tag{5.6}$$

One might expect that if equations (5.5) and (5.6) were independent, two of the unknowns, for example u_2 and u_5, could be eliminated. Using this naive approach, (5.5) and (5.6) could be rewritten to give

$$G_{12}u_2 + G_{15}u_5 = -G_{11}u_1 - G_{13}u_3 - G_{14}u_4 \tag{5.7}$$

$$G_{22}u_2 + G_{25}u_5 = -G_{21}u_1 - G_{23}u_3 - G_{24}u_4 \tag{5.8}$$

or

$$\boldsymbol{S}_{\text{elim}}\boldsymbol{u}_{\text{elim}} = \boldsymbol{S}_{\text{free}}\boldsymbol{u}_{\text{free}} \tag{5.9}$$

where for this illustrative example

$$\boldsymbol{S}_{\text{elim}} = \begin{bmatrix} G_{12} & G_{15} \\ G_{22} & G_{25} \end{bmatrix}, \tag{5.10}$$

$$\boldsymbol{S}_{\text{free}} = \begin{bmatrix} -G_{11} & -G_{13} & -G_{14} \\ -G_{21} & -G_{23} & -G_{24} \end{bmatrix}, \tag{5.11}$$

$$\boldsymbol{u}_{\text{elim}} = \begin{bmatrix} u_2 \\ u_5 \end{bmatrix} \tag{5.12}$$

and

$$\boldsymbol{u}_{\text{free}} = \begin{bmatrix} u_1 \\ u_3 \\ u_4 \end{bmatrix}. \tag{5.13}$$

IF $\boldsymbol{S}_{\text{elim}}$, which in this approach would always be square, is full rank, then $\boldsymbol{S}_{\text{elim}}^{-1}$ exists,

$$\boldsymbol{u}_{\text{elim}} = \boldsymbol{S}_{\text{elim}}^{-1}\boldsymbol{S}_{\text{free}}\boldsymbol{u}_{\text{free}} \tag{5.14}$$

and (5.14) may be substituted into the function $\hat{\Pi}$ (equation (5.1)) which is then minimised with respect to only $\boldsymbol{u}_{\text{free}}$ variables (a process to be described later in this chapter).

As discovered in the course of this research, this approach has fundamental flaws which frequently lead to a singular $\boldsymbol{S}_{\text{elim}}$ matrix but which can, fortunately, be remedied.

The flaws are twofold. The first flaw is allowing displacements which are boundary conditions to be selected as eliminated displacements. Essential boundary conditions which ensure only admissible configurations so that the model is physically realistic must not be altered. This comes directly from the fundamentals of energy methods and, in particular, the Rayleigh-Ritz method [Cook & Young, 1985] on which the finite element method is based. The second flaw is assuming that the constraint equations are linearly independent. The rank of $\boldsymbol{S}_{\text{elim}}$ does not depend on the rank of $\boldsymbol{G}$ and, in general, is not equal to the number of equations and, in turn, the number of elements.

Chronologically, the development of this method began before producing the methods of Chapter 4, however due to the flaws mentioned above the approach was temporarily abandoned. Refining and correcting the AIC resulted largely from the experience gained in establishing the LU and QR methods. After developing the Multilevel-QR approach, with its considerations of rank and nullspace, the author explored other ways of applying QR decomposition to stabilise the u-p formulation. The result was a QR-Nullspace approach where QR decomposition was used to determine the nullspace vectors of the

constraint submatrix $\boldsymbol{G}$ in (3.35), and the nullspace vectors were then used to eliminate the pressure unknowns in the equilibrium equations $\boldsymbol{A}\boldsymbol{u} + \boldsymbol{G}^{\mathrm{T}}\boldsymbol{p} = \boldsymbol{b}_1$. A subsequent search of the literature revealed an equivalent method by James [1992] in the context of applied mathematics and a similar method by Robey & Schreyer [1988] in the context of a mixed formulation where stresses are the primary unknowns. The nullspace concept was then extended to the AIC philosophy, and the resulting technique is presented in the following section. It is an improvement over the nullspace method of James [1992] in that the u-p equations are not required *a priori*, and therefore a more efficient algorithm is provided.

5.3 Final Approach for Incorporating the Constraints

Recognising that displacement boundary conditions, $\boldsymbol{u}_{\mathrm{BC}}$, cannot be eliminated, the method begins by designating $\boldsymbol{u}_{\mathrm{BC}}$ as degrees of freedom, thus reducing $\boldsymbol{u}$ to $\boldsymbol{u}^*_{\mathrm{elim}}$. Rearranging equation (5.4) then gives

$$\boldsymbol{S}^*_{\mathrm{elim}}\boldsymbol{u}^*_{\mathrm{elim}} = \boldsymbol{S}^*_{\mathrm{free}}\boldsymbol{u}^*_{\mathrm{free}} \tag{5.15}$$

where $\boldsymbol{u}^*_{\mathrm{free}} = \boldsymbol{u}_{\mathrm{BC}}$ and $\boldsymbol{u}^*_{elim}$ consists of all displacement degrees of freedom except $\mathbf{u}_{\mathrm{BC}}$. $\boldsymbol{S}^*_{\mathrm{elim}}$ and $\boldsymbol{S}^*_{\mathrm{free}}$ are the corresponding matrices. To determine what nodal displacements, in addition to $\boldsymbol{u}^*_{\mathrm{free}}$, can be assigned as degrees of freedom in the final function to be minimised, $\boldsymbol{S}^*_{\mathrm{elim}}$ is analysed to determine its rank and a set of free variables within $\boldsymbol{u}^*_{\mathrm{elim}}$. That is, QR decomposition with Householder matrices and column pivoting is applied to $\boldsymbol{S}^*_{\mathrm{elim}}$ to determine its nullspace so that

$$\boldsymbol{QR} = \boldsymbol{S}^{*}_{\text{elim}}\boldsymbol{P} \tag{5.16}$$

where $\boldsymbol{P}$ is the permutation matrix associated with the column pivoting. Now, (5.16) becomes

$$\boldsymbol{S}^{*}_{\text{elim}} = \boldsymbol{QRP}^{-1} \tag{5.17}$$

and from (5.15)

$$\boldsymbol{QRP}^{-1}\boldsymbol{u}^{*}_{\text{elim}} = \boldsymbol{S}^{*}_{\text{free}}\boldsymbol{u}^{*}_{\text{free}} \tag{5.18}$$

or

$$\boldsymbol{Ru}^{*}_{\text{perm}} = \boldsymbol{Q}^{\text{T}}\boldsymbol{S}^{*}_{\text{free}}\boldsymbol{u}^{*}_{\text{free}} \tag{5.19}$$

where

$$\boldsymbol{u}^{*}_{elim} = \boldsymbol{Pu}^{*}_{perm}\,. \tag{5.20}$$

Matrix $\boldsymbol{R}$ will be upper triangular. The number of variables in the final $\boldsymbol{u}^{*}_{\text{elim}}$ will be equal to the number of independent rows. Let n_z be the number of zero rows, and m be the total number of rows (also equal to the number of constraint equations and therefore the number of elements). Then, the number of independent rows is equal to $m-n_z$. If $\boldsymbol{S}^{*}_{\text{elim}}$ is an $m\times n$ matrix, then the corresponding number of additional degrees of freedom required to supplement $\boldsymbol{u}_{BC} = \boldsymbol{u}^{*}_{\text{free}}$ is

$$q = n - (m - n_z), \tag{5.21}$$

where q is also the dimension of the nullspace of $\boldsymbol{S}^{*}_{\text{elim}}$.

Due to the column pivoting, the last q entries in $\boldsymbol{u}^{*}_{\text{perm}}$ will be free variables and the associated terms on the left hand side of (5.19) are taken to the right hand side to give

$$\boldsymbol{S}_{\text{elim}}\boldsymbol{u}_{\text{elim}} = \boldsymbol{S}_{\text{free}}\boldsymbol{u}_{\text{free}} \tag{5.22}$$

where the zero rows are removed and $\boldsymbol{u}_{\text{free}}$ consists of $\boldsymbol{u}_{\text{BC}}$ and q additional free variables. With this process, $\boldsymbol{S}_{\text{elim}}$ will be of size $(m-n_z) \times (n-q)$, but from (5.21) $n-q = m-n_z$. So, $\boldsymbol{S}_{\text{elim}}$ is $(\text{m}-\text{n}_z) \times (\text{m}-\text{n}_z)$, full rank and upper triangular. Therefore, $\boldsymbol{u}_{\text{elim}}$ may now be determined as in equation (5.14) where $\boldsymbol{S}_{\text{elim}}$ is inverted by back substitution.

By an algorithm which sorts and assembles the displacement field, globally, the displacement field may be written as

$$\boldsymbol{u}_{\text{glob}} = \boldsymbol{T}_{\text{glob}}\boldsymbol{u}_{\text{free}} \tag{5.23}$$

where $\boldsymbol{u}_{\text{glob}}$ is the vector of all nodal displacements and $\boldsymbol{T}_{\text{glob}}$ is the matrix relating all of the nodal displacements to the free variables $\boldsymbol{u}_{\text{free}}$. $\boldsymbol{T}_{\text{glob}}$ will contain rows of zeroes with a 'one' in the appropriate position when $\boldsymbol{u}_{\text{free}}$ corresponds to $\boldsymbol{u}_{\text{glob}}$, otherwise it contains the appropriate row of the matrix $\boldsymbol{S}^{-1}_{\text{elim}}\boldsymbol{S}_{\text{free}}$. Similarly, the displacement degrees of freedom for an element can be written in terms of the free variables as

$$\boldsymbol{u} = \boldsymbol{T}\boldsymbol{u}_{\text{free}} \tag{5.24}$$

where $\boldsymbol{u}$ is the vector of all displacement degrees of freedom for an element and $\boldsymbol{T}$ relates those displacements to the free variables. It contains the required rows of $\boldsymbol{T}_{\text{glob}}$.

5.4 Completion of Formulation

By virtue of the approach detailed in Section 5.3, the constraint equations (5.4) take the form of (5.24) for each element. Thus, referring to equation (3.36), the fundamental variational principle for developing the finite element formulation becomes, as follows: minimise

$$\hat{\Pi} = \hat{U} + \Omega \tag{5.25}$$

subject to equation (5.24). Initially, $\hat{\Pi}$ in (5.25) is a function of all element degrees of freedom $\boldsymbol{u}$. To, in effect, "substitute" (5.24) into (5.25), the quantities leading to expressions for $\hat{U}$ and Ω are written in terms of $\boldsymbol{u}_{\text{free}}$. Referring to equation (4.21),

$$\hat{\boldsymbol{\varepsilon}} = \hat{\boldsymbol{B}}\boldsymbol{u} = \hat{\boldsymbol{B}}\boldsymbol{T}\boldsymbol{u}_{\text{free}} \tag{5.26}$$

and from Equation (4.20),

$$\hat{\boldsymbol{\sigma}} = \hat{\boldsymbol{D}}\hat{\boldsymbol{\varepsilon}} = \hat{\boldsymbol{D}}\hat{\boldsymbol{B}}\boldsymbol{T}\boldsymbol{u}_{\text{free}}\,. \tag{5.27}$$

Also,

$$\hat{U} \equiv \frac{1}{12G}\int \hat{\boldsymbol{\sigma}}^{\mathrm{T}}\hat{\boldsymbol{\sigma}}\,\mathrm{d}V = \frac{1}{12G}\int \boldsymbol{u}^{\mathrm{T}}\hat{\boldsymbol{B}}^{\mathrm{T}}\hat{\boldsymbol{D}}^{\mathrm{T}}\hat{\boldsymbol{D}}\hat{\boldsymbol{B}}\boldsymbol{u}\,\mathrm{d}V \tag{5.28}$$

and

$$\Omega = -\boldsymbol{u}^{\mathrm{T}}\boldsymbol{F} = -\boldsymbol{u}_{\text{free}}^{\mathrm{T}}\boldsymbol{T}^{\mathrm{T}}\boldsymbol{F}\,. \tag{5.29}$$

Now, (5.25) becomes

$$\hat{\Pi} = \frac{1}{12G}\int \boldsymbol{u}_{\text{free}}^{\mathrm{T}}\boldsymbol{T}^{\mathrm{T}}\hat{\boldsymbol{B}}^{\mathrm{T}}\hat{\boldsymbol{D}}^{\mathrm{T}}\hat{\boldsymbol{D}}\hat{\boldsymbol{B}}\boldsymbol{T}\boldsymbol{u}_{\text{free}}\,\mathrm{d}V - \boldsymbol{u}_{\text{free}}^{\mathrm{T}}\boldsymbol{T}^{\mathrm{T}}\boldsymbol{F}\,. \tag{5.30}$$

Minimising this with respect to the free variables in $\boldsymbol{u}_{\text{free}}$ gives

$$\boldsymbol{K}_{\text{free}}\boldsymbol{u}_{\text{free}} = \boldsymbol{T}^{\mathrm{T}}\boldsymbol{F} \tag{5.31}$$

where

$$\boldsymbol{K}_{\text{free}} = \frac{1}{6G}\int \left(\hat{\boldsymbol{D}}\hat{\boldsymbol{B}}\boldsymbol{T}\right)^{\mathrm{T}}\left(\hat{\boldsymbol{D}}\hat{\boldsymbol{B}}\boldsymbol{T}\right)\mathrm{d}V\,. \tag{5.32}$$

After $\boldsymbol{u}_{\text{free}}$ is found from solving (5.31), the complete displacement vector is given by Equation (5.23).

After developing the AIC formulation leading to (5.31) and (5.32), the author searched the literature for related methods. Other researchers have considered this idea of *a priori* incorporation of constraints, however their approaches differ from the one in this chapter. Weissman & Taylor [1992 (a)] combine this concept with incompatible modes. Needleman & Shih [1978] used a macroelement; i.e., a quadrilateral element composed of four triangles, and imposed the incompressibility constraints directly. Compared with these other methods, the AIC has some distinct advantages. The macroelement method of Needleman & Shih is less general than AIC and uses triangular elements which are known to be excessively stiff in finite element modelling. Also, the AIC addresses the numerical instability at an earlier stage of the formulation as compared to the Weissman & Taylor approach and therefore has the potential to be more general and efficient. Finally, the AIC technique of applying QR decomposition directly to constraint equations (5.4) has the added benefit of, in a sense, smoothing the noise in measured displacements. Due to the uncertainty in the displacement data, as well the approximation of modelling the material as fully incompressible, the measured boundary values will not conform exactly to the constant volume constraint over the entire domain. This, by itself, would have the potential to create an inconsistency in the system of equations, possibly resulting in failure of an iterative solution process. As part of the AIC, the QR decomposition clearly identifies deviations from constant volume as

degradation of the rows of “zeroes” produced in (5.19) as part of the process. These deviations occur only on the right hand side of (5.19) and can be replaced with zero values, thus providing an additional stabilisation to that achieved by circumventing the use of Lagrange multipliers; i.e., hydrostatic pressures. In addition, the magnitude of the deviations from zero provide information in themselves as they are a measure of the data uncertainty.

Of the algorithms presented in this thesis, the AIC has the potential of being the most efficient method for analysing displacement data in the chiropractic problem. In the next section it is applied to the sample problems that have been used in previous chapters.

5.5 Numerical Examples

In the previous chapters, condition numbers have been given for the final matrix used in calculating the nodal displacements for each of the examples. A major difference with the AIC, however, is that the final system of equations is formed without including the hydrostatic pressures as unknowns, whereas the methods of Chapter 4 have both the nodal displacements and hydrostatic pressures as unknowns originally and then the hydrostatic pressures are removed prior to the solution phase. The AIC, therefore, circumvents assembly of the u-p equations and may be preferable to the LU and QR methods, providing the condition numbers are reasonable. Table 5.1 gives the AIC condition numbers for the rectangular block in compression, the rectangular block in

simple shear, and the thick walled cylinder tests. For comparison, the condition numbers for the LU and QR methods are also given in the table.

Table 5.1: Condition numbers for numerical examples.

Method	**Block in Compression**	**Block in Simple Shear**	**10 × 10 Cylinder**	**15 × 15 Cylinder**	**20 × 20 Cylinder**
Modified LU	6.80	54.6	59.4	171	336
Multilevel QR	4.82	14.9	16.9	27.5	37.1
AIC	10.7	237	207	1130	5590

In assessing the calculated values, it is important to emphasise that all three methods have removed the source of indeterminacy; i.e., the calculation of hydrostatic pressures $\boldsymbol{p}$. Therefore, the condition numbers provide an indication of relative differences in numerical stability between methods which involve nonsingular systems of equations. The multilevel QR appears to be the most robust in terms of dealing with data uncertainty, but this is at the cost of first assembling the u-p equations, determining the stable subsystem, and then applying an appropriate equation solver. In practice, the final choice between methods would depend on the noise level present in the displacement data and the computational expense already associated with iteratively solving geometrically nonlinear equations arising from large deformation in the vertebral artery. It should also be noted that mathematical techniques beyond the scope of finite elements could potentially be applied to the problem addressed in this thesis. For example, the nature of constrained optimisation for incompressible materials is mathematically similar to that arising in both quadratic programming [e.g. Gould, 1991; Li *et al*., 2008]

and the dynamics of multibody systems with holonomic contraints [e.g., Andersen *et al*., 2009]. From another perspective, the indeterminate nature of the coefficient matrix produced in the u-p formulation is amenable to analysis by the theory of generalised inverses [e.g. Wang *et al*., 2009; Toutounian *et al*.]. Existing knowledge in these as well as other disciplines might be adopted and modified for use in the analysis of incompressible materials.

Chapter 6

An Additional Result – the q_o Theorem

6.1 The Theorem

The majority of this thesis has concentrated on establishing a path from the chiropractic problem and leading to the three techniques for stable finite element analysis; i.e., modified LU, multilevel QR, and AIC. In the process of developing the latter two methods for circumventing the hydrostatic pressures, the primary focus was the nullspace $N(\boldsymbol{G})$ of the constraint submatrix $\boldsymbol{G}$. Through this focus, the author discovered a second result related to $N(\boldsymbol{G})$, which pertains to displacement locking under an applied concentrated force on the boundary. Although this result is not directly connected to the chiropractic problem as defined in this thesis, it may find future use in addressing the inverse problem of property determination in the context of other biomechanical applications [Seshaiyer and Humphrey, 2003]. One approach to measuring the elastic modulus of tissue, for example, is to apply a concentrated load with a force transducer and measure the resulting displacements. While a finite element model for incompressible material will not encounter displacement locking if all boundary conditions are specified as displacements, the special case of a single applied load is perhaps the most susceptible to severe locking behaviour. In the result that follows, a method will be outlined to determine when an applied force will have an effect on a

finite element model. In essence, a method based on the nullspace of the constraint matrix, $\boldsymbol{G}$, will determine when displacement locking will or will not occur.

Theorem 6.1: Given a finite element model, let the final system of equations be represented by

$$\boldsymbol{A}\boldsymbol{u} + \boldsymbol{G}^{\mathrm{T}}\boldsymbol{p} = \boldsymbol{b}_1 \tag{6.1}$$

and

$$\boldsymbol{G}\boldsymbol{u} = \boldsymbol{b}_2 \quad , \tag{6.2}$$

where $\boldsymbol{A}$ is an $n \times n$ positive definite matrix, $\boldsymbol{G}$ is an $m \times n$ matrix, $\boldsymbol{u} = \left[u_1\ u_2 \cdots u_n\right]^{\mathrm{T}}$, and $\boldsymbol{p} = \left[p_1\ p_2 \cdots p_m\right]^{\mathrm{T}}$. Let q be the dimension of the nullspace of $\boldsymbol{G}$ for the case where displacements are prescribed on the boundary with the exception of one degree-of-freedom for which a force is specified. Further, let q_{o} be the dimension of the nullspace of $\boldsymbol{G}$ for the case where only displacements are prescribed on the entire boundary. If $q = q_{\mathrm{o}}$, then the solution $\boldsymbol{u}$ will be independent of the prescribed force. If $q > q_{\mathrm{o}}$, then the prescribed force will have an effect.

Proof: For the case with a single force boundary condition, let r be the rank of $\boldsymbol{G}$, $N(\boldsymbol{G})$ be the nullspace of $\boldsymbol{G}$, n be the number of rows of vector $\boldsymbol{u}$, F^* be the specified force, and u_k be the unknown displacement corresponding to F^*. Also, define matrix $\boldsymbol{V} = [\boldsymbol{v}_1\ \boldsymbol{v}_2 \cdots \boldsymbol{v}_q]$, where $\boldsymbol{v}_1, \boldsymbol{v}_2, \cdots, \boldsymbol{v}_q$ form a basis for $N(\boldsymbol{G})$. For the Dirichlet case, let r_0 be the rank of $\boldsymbol{G}$, and n_{o} be the number of rows of $\boldsymbol{u}$. By definition, $n = n_{\mathrm{o}} + 1$. Thus, if $q = q_{\mathrm{o}}$, then $r = r_0 + 1$ and the k^{th} component of $N(\boldsymbol{G})$ is zero. Premultiplying equation (6.1) by $\boldsymbol{V}^{\mathrm{T}}$, we obtain

$$\boldsymbol{V}^{\mathrm{T}}\boldsymbol{A}\boldsymbol{u} = \boldsymbol{V}^{\mathrm{T}}\boldsymbol{b}_1 \tag{6.3}$$

Also, from (6.2),

$$\boldsymbol{u} = \boldsymbol{u}_{\mathrm{p}} + \boldsymbol{V}\boldsymbol{\beta} \tag{6.4}$$

where $\boldsymbol{u}_{\mathrm{p}}$ is a particular solution of (6.2), and $\boldsymbol{\beta}$ is a vector of coefficients in the linear combination of nullspace vectors. From (6.3) and (6.4),

$$\left(\boldsymbol{V}^{\mathrm{T}}\boldsymbol{A}\boldsymbol{V}\right)\boldsymbol{\beta} = \left(\boldsymbol{V}^{\mathrm{T}}\boldsymbol{b}_1 - \boldsymbol{V}^{\mathrm{T}}\boldsymbol{A}\boldsymbol{u}_{\mathrm{p}}\right) \tag{6.5}$$

where, for positive definite $\boldsymbol{A}$, $\boldsymbol{V}^{\mathrm{T}}\boldsymbol{A}\boldsymbol{V}$ is non singular. Together, equations (6.4) and (6.5) give a unique solution for $\boldsymbol{u}$. From the theory of finite elements, F^* is only in the k^{th} component of $\boldsymbol{b}_1$. It is, therefore, annihilated. Conversely, if $q > q_{\mathrm{o}}$, the k^{th} component of $N(\boldsymbol{G})$ will be nonzero, and F^* will not be annihilated. ■

For further explanation as to why $q = q_{\mathrm{o}}$ leads to the annihilation of F*, consider the following simple example. Let the general solution of (6.2), for a given problem, be $\boldsymbol{u} = \boldsymbol{u}_{\mathrm{p}} + \beta_1\boldsymbol{v}_1 + \beta_2\boldsymbol{v}_2$, where $\boldsymbol{u}_{\mathrm{p}}$ is a particular solution, vectors $\boldsymbol{v}_1$ and $\boldsymbol{v}_2$ form a basis for the nullspace of $\boldsymbol{G}$, and β_i are coefficients in the linear combination of nullspace vectors, so that

$$\begin{bmatrix} u_1 \\ u_2 \\ u_3 \end{bmatrix} = \begin{bmatrix} u_{\mathrm{p}1} \\ u_{\mathrm{p}2} \\ u_{\mathrm{p}3} \end{bmatrix} + \beta_1 \begin{bmatrix} 1 \\ 0 \\ 0 \end{bmatrix} + \beta_2 \begin{bmatrix} 0 \\ 1 \\ 0 \end{bmatrix}. \tag{6.6}$$

Referring to nullspace vectors $\boldsymbol{v}_1$ and $\boldsymbol{v}_2$ on the right hand side of (6.6), the nullspace component corresponding to u_3 is zero. Rewriting (6.6) as

$$u_1 = u_{p1} + \beta_1 \tag{6.7}$$

$$u_2 = u_{p2} + \beta_2 \tag{6.8}$$

$$u_3 = u_{p3}, \tag{6.9}$$

it can be seen that u_3 is uniquely determined as having particular value u_{p3}. The order of the forces in $\boldsymbol{b}_1$ matches the order of the unknown displacements. Thus, in the products $\boldsymbol{v}_i^{\mathrm{T}}\boldsymbol{b}_1$ in (6.3), the zero nullspace component in $\boldsymbol{v}_i$ will annihilate the force *F** in $\boldsymbol{b}_1$. That is, *F** is eliminated and has no effect, regardless of its magnitude.

This result will be illustrated by the previously used example, plane strain compression of a rectangular block, and a series of finite element solutions. The specifics of the model will remain the same except at two nodes, labelled "a" and "b" in Figure 6.1, where forces instead of displacements will be applied.

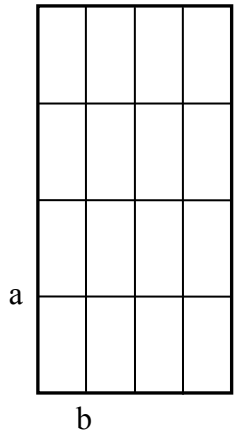

Figure 6.1: Finite element grid (a and b represent nodes for force application).

For case 1, the case of displacements on the entire boundary, the dimension of $N(\boldsymbol{G})$, $q_o = 4$. This was determined using the author's finite element code and MATLAB®.

For case 2, a force of 5 kN is applied to node "a" from Figure 6.1 and $q = 4$. That force value is energy equivalent to the displacement applied in case 1 and therefore no difference in the results is expected. For case 3, the force at "a" is changed to 20 kN and $q = 4$, once again. By the theorem, displacement locking should occur since the dimension of the nullspace did not change and the results shown in Figure 6.2 confirm this. Figure 6.2 compares the results between cases 2 and 3 using ANSYS® plots for the von Mises stress field. The von Mises stress field for case 1 is constant at 86.7 MPa. For case 2, although the colours in the plot suggest a large difference, the numerical values show that the stresses have changed only approximately 0.3% from minimum to maximum. For case 3, the force has increased by four times, however the stresses have only slightly changed. Therefore, displacement locking is confirmed.

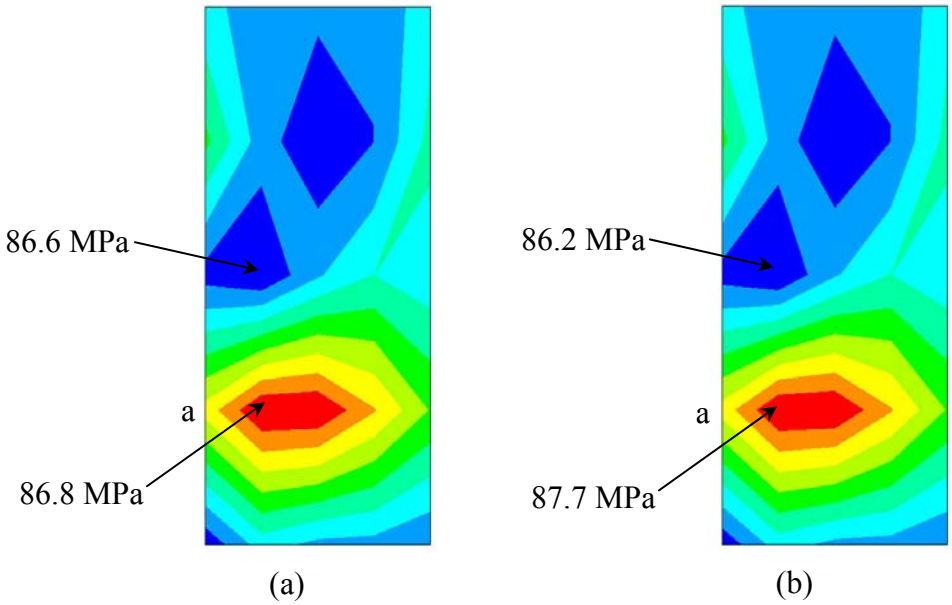

Figure 6.2: ANSYS® plots of the von Mises stress field for (a) case 2 and (b) case 3 showing maximum and minimum von Mises stresses for each case.

For the next set of test cases, the displacement in the *x*-direction on node "b" in Figure 6.1 is changed to a zero force in the *y*-direction. By the model, as described, this is the

correct force for that node. When there is a force specified at node "b" as well as at node "a", $q = 5$ and, by the theorem, the forces should now have an effect on the model. Cases 4 and 5 have the same forces at node "a" as cases 2 and 3, respectively. They also have the zero force as described above on node "b". The results for case 4 are identical to those of case 2. That is to be expected since the force applied at node "a" is the correct force for the model. The results for case 5 (shown in Figure 6.3), however, show a drastic change from case 3. In case 3, the stress field was almost constant; it now goes from a minimum of 40.2 MPa to a maximum of 256 MPa. Clearly, as predicted, the finite element grid is no longer subject to displacement locking.

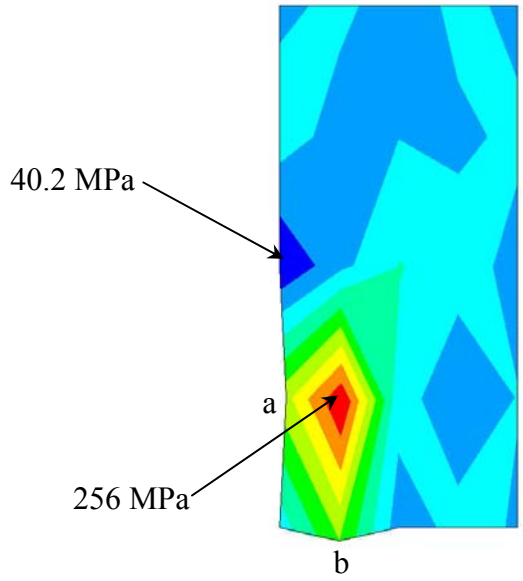

Figure 6.3: ANSYS® plot for case 5: 20 kN *x*-force at node "a" and zero *y*-force at node "b".

This demonstration suggests that the q_o theorem may be used as a basis for identifying models that would be insensitive to a single applied force. Potentially, this could be

useful in designing robust finite element procedures for obtaining tissue properties from measured displacements produced by a load transducer. The accuracy of the specific values presented here may be in dispute as no analytical solution exists for this type of loading. Also, with the amount of displacement that can be seen at nodes "a" and "b", the solution may have gone beyond the linear elasticity range. However, the degree of freedom results for nodes "a" and "b" using both the author's code and ANSYS® are within 2% of each other, suggesting that the solutions may not be totally inaccurate.

Chapter 7

Concluding Remarks

The research described in this thesis began with a single long-term objective: modeling of the vertebral artery during chiropractic manipulation of the cervical spine. Although chiropractic treatment has become prevalent, the possible correlation between neck manipulation and subsequent stroke in patients has been the subject of debate without resolution. In Chapter 2, the review and assessment of pertinent biomedical research confirmed the need for quantitative analysis, and identified the challenges posed by complexity of the anatomy and nonlinearities associated with material properties and geometry of the problem. A major outcome of this review was a perspective towards successful quantitative analysis of the vertebral artery. This perspective depended on reliable stress analysis within a robust method for *in vivo* image data. Numerous research projects would be required to attain this goal. However, a necessary first step would be to establish a finite element algorithm for overcoming the modelling issues inherent in the analysis of soft tissue. It is well known in the finite element community that incompressibility can lead to severe numerical instabilities. These instabilities are exacerbated by the specifics of the chiropractic problem: the nonlinear analysis of measured displacements. In Chapter 3, a mathematical review of finite element procedures revealed that none of the existing methods were suited to this specific

problem. This led to the development of three techniques for stable finite element analysis. To aid in the process, Q4P1 codes were written for testing new concepts.

The process of development followed a path from a simple LU approach to the more robust multilevel QR and then the more fundamental AIC formulation. Each method has its own merits. The LU is fast and easily applied to existing mixed formulations, but may be subject to numerical instabilities during intermediate steps. The multilevel QR may be the most stable, as shown through numerical examples, and might also be the preferred method for augmenting an existing finite element package. In contrast, the AIC reformulates the problem to enforce incompressibility directly, and therefore would be best implemented as a special purpose code. The primary contributions for both the multilevel QR and AIC methods are in the form of mathematical results. For the QR, a theorem establishes the nonsingularity of the final submatrix, and for the AIC which is based on a non-standard formulation, the mathematical representation of the final system of equations is derived in detail.

Successful implementation of the QR and AIC methods relied upon establishing a key concept: the importance of $N(\boldsymbol{G})$, the nullspace of the constraint matrix. This led to a result addressing an important but different issue associated with incompressibility: displacement locking. The q_o theorem may be useful in future studies where material properties are to be determined from solving the inverse problem. It identifies severe displacement locking under the application of a single applied force.

This thesis is meant to provide the impetus for future research. The challenge of combining nonlinear mechanics with high resolution imaging is forthcoming. It will be necessary to implement a stable solution technique such as the multilevel QR or AIC within a finite element code incorporating geometric nonlinearity, viscous effects, high-impact loading, and three-dimensional analysis. This would be followed by a series of experiments to validate the code. The first set of experiments would involve numerical simulations where mixed boundary conditions are used to produce reference displacement fields for a variety of axisymmetric and nonaxisymmetric cases representing deformation of the vertebral artery. The reference displacement fields would then be used to artificially generate displacement boundary conditions with measurement uncertainty to test the code's ability to determine the reference von Mises stress distributions. These simulations would include mesh refinement studies to establish convergence properties.

Once tested by computer simulations, the code would then be further validated by physical experiments with image data. This could begin with ultrasound imaging and then continue with MRI or synchrotron light. A physical model representing the spine and vertebral artery could be constructed within a frame instrumented with load transducers to apply known forces to the physical model. In addition, strain gauges could be used to provide a second measure of deformation to compare with the information acquired through applying the finite element code to the measured displacement data. This stage of the research would necessarily involve a collaborative effort beween experimentalists and theoreticians. A significant component from this point forward would be research in data collection and image processing. Experiments

with physical models would eventually lead to testing on animal subjects, and then finally a methodology for human patients could be developed.

References

Andersen, M.S., Damsgaard, M., and Rasmussen, J. (2009), Kinematic Analysis of Over-Determinate Biomechanical Systems, *Computer Methods in Biomechanics and Biomedical Engineering*, 12: 371-384.

Anton, H. and Busby, R.C., (2003), *Contemporary Linear Algebra*, John Wiley & Sons, Inc., Hoboken, NJ.

Armero, F., (2000), On the Locking and Stability of Finite Elements in Finite Deformation Plane Strain Problems, *Computers and Structures*, 75: 261-290.

Auricchio, F., Beirão da Veiga, L., Lovadina, C. and Reali, A., (2004), Enhanced Strain Methods for Elasticity Problems, *European Congress on Computational Methods in Applied Sciences and Engineering*, July 24-28, 2004, Jyväskylä.

Babuška, I. and Narasimhan, R., (1997), The Babuška-Brezzi Condition and the Patch Test: an Example, *Computer Methods in Applied Mechanics and Engineering*, 140: 183-199.

Bathe, K-J., (2006), *Finite Element Procedures*, Prentice-Hall, Inc., New Jersey.

Bayrak, I.K., Durmus, D., Bayrak, A.O., Diren, B. and Canturk, F., (2009), Effect of Cervical Spondylosis on Vertebral Arterial Flow and its Association with Vertigo, *Clinical Rheumatology*, Volume 28, Number 1, pp.59-64.

Beer, F.P., Johnston, E.R., Jr., and DeWolf, J.T., (2002), *Mechanics of Materials*, 3rd Edition, McGraw-Hill Companies, Inc., Boston.

Belytschko, T. and Bachrach, W.E., (1986), Efficient Implementation of Quadrilaterals with High Coarse-Mesh Accuracy, *Computer Methods in Applied Mechanics and Engineering*, 54: 279-301.

Bonet, J. and Wood, R.D., (1997), *Nonlinear Continuum Mechanics for Finite Element Analysis*, Cambridge University Press, Cambridge.

Boroomand, B. and Khalilian, B., (2004), On Using Linear Elements in Incompressible Plane Strain Problems: A Simple Edge Based Approach for Triangles, *International Journal for Numerical Methods in Engineering*, 61: 1710-1740.

Bozic, K.J., Keyak, J.H., Skinner, H.B., Bueff, H.U. and Bradford, D.S., (1994), Three-dimensional Finite Element Modeling of a Cervical Vertebra: An Investigation of Burst Fracture Mechanism, *Journal of Spinal Disorders*, Volume 7, pp.102-110.

Brolin K. and Halldin P., (2004), Development of a Finite Element Model of the Upper Cervical Spine and a Parameter Study of Ligament Characteristics, *Spine*, Volume 29, Number 4, pp. 376-385.

Budynas, R.G., (1999), *Advanced Strength and Applied Stress Analysis*, 2nd Ed., McGraw-Hill Companies, Inc., Boston.

Canga, M.E. and Becker, E.B., (1999), An Iterative Technique for the Finite Element Analysis of Near-Incompressible Materials, *Computer Methods in Applied Mechanics and Engineering*, 170: 79-101.

Carstensen, M. (2004), Letter to the Editor, *Journal of Manipulative and Physiological Therapeutics*, Volume 27, Number 1, pp.69-70.

Chapelle, D. and Bathe, K-J., (1993), The Inf-Sup Test, *Computers & Structures*, 47: 537-545.

Chen, J.S., Pan, C. and Chang, T.Y.P., (1995), On the Control of Pressure Oscillation in Bilinear-Displacement Constant-Pressure Element, *Computer Methods in Applied Mechanics and Engineering*, 128: 137-152.

Chiumenti, M., Valverde, Q., Agelet de Saracibar, C. and Cervera, M., (2002), A Stabilized Formulation for Incompressible Elasticity Using Linear Displacement and Pressure Interpolations, *Computer Methods in Applied Mechanics and Engineering*, 191: 5253-5264.

Clausen, J.D., Goel, V.K., Traynelis, V.C. and Scifert, J., (1997), Uncinate Processes and Luschka Joints Influence the Biomechanics of the Cervical Spine: Quantification Using a Finite Element Model of the C5-C6 Segment, *Journal of Orthopaedic Research*, Volume 15, pp.342-347.

Coley, L.M., (2000), *A Finite Element Analysis of the Limberg Flap Used in Plastic Surgery*, M.Sc. Thesis, University of Saskatchewan, Saskatoon.

Coley, L.M., Dolovich, A.T., Watson, L.G., and Valnicek, S., (2000), Does the Orientation of a Limberg Flap Matter?, *Proceedings of the 2000 ASME International Mechanical Engineering Congress and Exposition – Advances in Bioengineering*, Nov. 5-10, Orlando, BED-Vol. 48, 193-194.

Cook, R.D. and Young, W.C., (1985), *Advanced Mechanics of Materials*, Macmillan Publishing Company, New York.

Cramer, G.D.and Darby, S.A., (1995), *Basic and Clinical Anatomy of the Spine, Spinal Cord and ANS*, Mosby-Year Book, Inc., Toronto.

Dally, J.W. and Riley, W.F., (1978), *Experimental Stress Analysis*, McGraw-Hill, Inc., New York.

Di Fabio, R.P., (1999), Manipulation of the Cervical Spine: Risks and Benefits, *Physical Therapy*, Volume 79, Number 1, pp. 50-65.

Doherty, B.J. and Heggeness, M.H., (1994), The Quantitative Anatomy of the Atlas, *Spine*, Volume 19, Number 22, pp.2497-2500.

Doherty, B.J. and Heggeness, M.H., (1995), Quantitative Anatomy of the Second Cervical Vertebra, *Spine*, Volume 20, Number 5, pp.513-517.

Dvorkin, E.N., (2001), On the Convergence of Incompressible Finite Element Formulations: The Patch Test and the Inf-Sup Condition, *Engineering Computations*, 18: 539-556.

Ernst, E., (2007), Adverse Effects of Spinal Manipulation: A Systematic Review, Journal of the Royal Society of Medicine, Volume 100, pp.330-338.

Fagan, M.J., Julian, S. and Mohsen, A.M., (2002), Finite Element Analysis in Spine Research, *Proceedings of the Institution of Mechanical Engineers Part H-Journal of Engineering in Medicine*, Volume 216, Number H5, pp.281-298.

Felippa, C.A., (2001), A Historical Outline of Matrix Structural Analysis: A Play in Three Acts, *Computers and Structures*, 79: 1313-1324.

Frisoni, G.B. and Anzola, G.P., (1991), Vertebrobasilar Ischemia after Neck Motion, *Stroke*, Volume 22, pp. 1452-1460.

Fung, Y.C., (1993), *Biomechanics: Mechanical Properties of Living Tissues*, 2nd Edition, Springer-Verlag New York, Inc., New York.

Gatterman, M.I., (1990) *Chiropractic Management of Spine Related Disorders*, Williams and Wilkins, Baltimore, MD.

Gladwell, G.M.L., (1980), *Contact Problems in the Classical Theory of Elasticity*, Sijthoff & Noordhoff International Publishers, The Netherlands.

Good, C., (2003), Letter to the Editor, *Journal of Manipulative and Physiological Therapeutics*, Volume 26, Number 5, pp. 338-339.

Gould, N.I.M., (1991), An Algorithm for Large-Scale Quadratic Programming, *IMA Journal of Numerical Analysis*, 11: 299-324.

Greaves C.Y., Gadala M.S. and Oxland T.R., (2008), A Three-dimensional Finite Element Model of the Cervical Spine with Spinal Cord: An Investigation of Three Injury Mechanisms, *Annals of Biomedical Engineering*, Volume 36, Number 3, pp. 396-405.

Heller, J.G. and Pedlow, Jr., F.X., (1998), Anatomy of the Cervical Spine in *The Cervical Spine*, Third Edition, Lippincott-Raven Publishers, Philadelphia, PA.

Herrmann, L.R., (1965), Elasticity Equations for Incompressible and Nearly Incompressible Materials by a Variational Theorem, *AIAA Journal*, 3: 1896-1900.

Herzog, W., Conway, P.J., Kawchuk, G.N., Zhang, Y. and Hasler, E.M., (1993), Forces Exerted During Spinal Manipulative Therapy, *Spine*, Volume 18, Number 9, pp.1206-1212.

Holzapfel, G.A., Eberlein, R., Wriggers, P. and Weizsäcker, H.W., (1996), Large Strain Analysis of Soft Biological Membranes: Formulation and Finite Element Analysis, *Computer Methods in Applied Mechanics and Engineering*, 132: 45-61.

Huang, M., Yue, Z.Q., Tham, L.G. and Zienkiewicz,. O.C., (2004), On the Stable Finite Element Procedures for Dynamic Problems of Saturated Porous Media, *International Journal for Numerical Methods in Engineering*, 61: 1421-1450.

Hufnagel, A., Hammers, A., Schonle, P-W., Bohm, K-D. and Leonhardt, G., (1999), Stroke Following Chiropractic Manipulation of the Cervical Spine, *Journal of Neurology*, Volume 246, pp. 683-688.

Hughes, T.J.R., (1987), *The Finite Element Method: Linear Static and Dynamic Finite Element Analysis*, Prentice-Hall, Inc., New Jersey.

Hughes, T.J.R., Liu, W.K. and Brooks, A., (1979), Finite Element Analysis of Incompressible Viscous Flows by the Penalty Function Formulation, *Journal of Computational Physics*, 30: 1-60.

Itskov, M. and Aksel, N., (2002), Elastic Constants and Their Admissible Values for Incompressible and Slightly Compressible Anisotropic Materials, *Acta Mechanica*, 157: 81-96.

Jacobs, A., Lanfermann, H., Neveling, M., Szelies, B., Rita Schröder, Heiss, W.-D., (1997), MRI- and MRA-Guided Therapy of Carotid and Vertebral Artery Dissections, *Journal of Neurological Science*, Volume 147, pp. 27-34.

James, D., (1992), Implicit nullspace iterative methods for constrained least squares problems, *SIAM J. Matrix Anal. Appl.* 13, 962-978.

Jankovich, E., Leblanc, F. and Durand, M., (1981), A Finite Element Method for the Analysis of Rubber Parts, Experimental and Analytical Assessment, *Computers and Structures*, 14: 385-391.

Johnson, C.P., How, T., Scraggs, M., West, C.R. and Burns, J., (2000) A Biomechanical Study of the Human Vertebral Artery with Implications for Fatal Arterial Injury, *Forensic Science International*, Volume 109, pp.169-182.

Kansagra, A.P., Wong, E.C., (2008), Mapping of Vertebral Artery Perfusion Territories Using Arterial Spin Labeling MRI, *Journal of Magnetic Resonance Imaging*, Volume 28, pp. 762-766.

Kaps, M., Seidel, G., Bauer, T. and Behrmann, B., (1992), Imaging of the Intracranial Vertebrobasilar System Using Color-Coded Ultrasound, *Stroke*, Volume 23, pp.1577-1582.

Kawchuk, G.N., Jhangri, G.S., Hurwitz, E.L., Wynd, S., Haldeman, S. and Hill, M.D., (2008), The Relation Between the Spatial Distribution of Vertebral Artery Compromise and Exposure to Cervical Manipulation, *Journal of Neurology*, Volume 255, pp.371-377.

Kawchuk, G.N., Wynd, S. and Anderson, T., (2004), Defining the Effect of Cervical Manipulation on Vertebral Artery Integrity: Establishment of an Animal Model, *Journal of Manipulative and Physiologic Therapeutics*, Volume 27, pp.539-546.

Kleinberger, M., (1993), Application of Finite Element Techniques to the Study of Cervical Spine Mechanics, *Proceedings of the 37th Stapp Car Crash Conference, San Antonio,Texas, November 7-8*, pp. 261-272.

Komiyama, M., Morikawa, T., Nakajima, H., Nishikawa, M. and Yasui, T., (2001), High Incidence of Arterial Dissection Associated with Left Vertebral Artery of Aortic Origin, *Neurologia Medico Chirurgica*, Volume 41, Number 1, pp.8-12.

Kouhia, R. and Stenberg, R., (1995), A Linear Nonconforming Finite Element Method for Nearly Incompressible Elasticity and Stokes Flow, *Computer Methods in Applied Mechanics and Engineering*, 124: 195-212.

Krijger, J.K., Heethaar, R.M., Hillen, B., Hoogstraten, H.W. and Ravensbergen, J., (1992), Computation of Three-Dimensional Flow in a Model of the Basilar Artery, *Journal of Biomechanics*, Volume 25, Number 12, pp.1451-1465.

Kumaresan, S., Radhakrishnan and Ganesan, N., (1994), Mixed Models in Finite Element Analysis, *Computers and Structures*, 51: 117-123.

Kumaresan, S., Yoganandan, N. and Pintar, F.A., (1997), Paediatric Neck Modelling using Finite Element Analysis, *IJCrash*, Volume 2, Number 4, pp. 367-376.

Kumaresan, S., Yoganandan, N., Pintar, F.A., (1999), Finite Element Analysis of the Cervical Spine: A Material Property Sensitivity Study, *Clinical Biomechanics*, Volume 14, pp.41-53.

Kumaresan, S., Yoganandan, N., Pintar, F.A., Maiman, D.J., Kuppa, S., (2000), Biomechanical Study of Pediatric Human Cervical Spine, *Journal of Biomechanical Engineering-Transactions of the ASME*, Volume 122, Number 1, pp.60-71.

Kumaresan, S., Yoganandan, N., Pintar, F.A., Voo, L.M., Cusick, J.F., Larson, S.J., (1997), Finite Element Modeling of Cervical Laminectomy with Graded Facetectomy, *Journal of Spinal Disorders*, Volume 10, Number 1, pp. 40-46.

Lee, R.L., Gresho, P.M. and Sani, R.L., (1979), Smoothing Techniques for Certain Primitive Variable Solutions of the Navier-Stokes Equations, *International Journal for Numerical Methods in Engineering*, 14: 1785-1804.

Li, W. and Tian, X., (2008), Numerical Solution Method for General Interval Quadratic Programming, *Applied Mathematics and Computation*, 202: 589-595.

Licht, P.B., Christensen, H.W., Hoilund-Carlsen, P.F., Is There a Role for Premanipulative Testing Before Cervical Manipulation?, *Journal of Manipulative and Physiological Therapeutics*, Volume 23, Number 3, pp.175-179.

Licht, P.B., Christensen, H.W., Hojgaard, P., Marving, J., (1998), Vertebral Artery flow and Spinal Manipulation: A Randomized, Controlled and Observer-Blinded Study, *Journal of Manipulative and Physiological Therapeutics*, Volume 21, Number 3, pp.141-144.

Licht, P.B., Christensen, H.W., Svendensen, P., Hoilund-Carlsen, P.F., (1999), Vertebral Artery Flow and Cervical Manipulation: An Experimental Study, *Journal of Manipulative and Physiological Therapeutics*, Volume 22, Number 7, pp.431-435.

Logan, D.L., (1993), *A First Course in the Finite Element Method*, 2nd Ed., PWS Publishing Company, Boston.

Loredo, A. and Klöcker, H., (1997), Generalized Inverse of the Compliance Tensor, and Behaviour of Incompressible Anisotropic Materials – Application to Damage, *Mechanics Research Communications*, 24: 371-376.

Lovadina, C. and Auricchio, F., (2003), On the Enhanced Strain Technique for Elasticity Problems, *Computers and Structures*, 81: 777-787.

Mader, S.S., (1985), *Biology: Evolution, Diversty, and the Environment*, WM. C. Brown Publishers, Dubuque, IA.

Malkus, D.S. and Hughes, T.J.R., (1978), Mixed Finite Element Methods – Reduced and Selective Integration Techniques: A Unification of Concepts, *Computer Methods in Applied Mechanics and Engineering*, 15: 63-81.

Mallikarjuna Rao, K. and Shrinivasa, U., (2001), A Set of Pathological Tests to Validate New Finite Elements, Sãdhãna-Academy Proceedings in Engineering Sciences, 26: 549-590.

Mascalchi, M., Bianchi, M.C., Mangiafico, S., Ferrito, G., Puglioli, M., Marin, E., Mugnai, S., Canapicchi, R., Quilici, N., Inzitari, D., (1997), MRI and MR Angiography of Vertebral Artery Dissection, *Neuroradiology*, Volume 39, pp. 329-340.

Maurel, N., Lavaste, F., Skalli, W., (1997), A Three-dimensional Parameterized Finite Element Model of the Lower Cervical Spine. Study of the Influence of the Posterior Articular Facets, *Journal of Biomechanics*, Volume 30, Number 9, pp.921-931.

McAfee, M.A., Kaufmann, M.V., Simon, B.R. and Baldwin, A.L., (1994), Experimental/Numerical Approach to the Determination of Material Properties in Large Arteries, *Proceedings of the 1994 ASME International Mechanical Engineering Congress and Exposition – Advances in Bioengineering*, Chicago, BED-Vol. 28, 111-112.

Nagarkal Venkatakrishnaiah, V.K., (2006), *A Numerical Study of Finite Element Calculations for Incompressible Materials under Applied Boundary Displacement*, M.Sc. Thesis, University of Saskatchewan, Saskatoon.

Nagtegaal, J.C., Parks, D.M. and Rice, J.R., (1974), On Numerically Accurate Finite Element Solutions in the Fully Plastic Range, *Computer Methods in Applied Mechanics and Engineering*, 4: 153-177.

Nascimbene, R. and Venini, P., (2002), A New Locking-Free Equilibrium Mixed Element for Plane Elasticity with Continuous Displacement Interpolation, *Computer Methods in Applied Mechanics and Engineering*, 191: 1843-1860.

Needleman, A. and Shih, C.F., (1978), A Finite Element Method for Plane Strain Deformations of Incompressible Solids, *Computer Methods in Applied Mechanics and Engineering*, 15: 223-240.

Norris, J.W., Beletsky, V., Nadareishvili, Z.G., (2000), Sudden Neck Movement and Cervical Artery Dissection, *CMAJ*, Volume 163, Number 1, pp. 38-40.

O'Dell, W.G. and McCulloch, A.D., (1998), *Proceedings of the 1998 ASME International Mechanical Engineering Congress and Exposition – Advances in Bioengineering*, Nov. 15-20, Anaheim, BED-Vol. 39, pp. 391-392.

Oden, J.T. and Key, J.E., (1970), Numerical Analysis of Finite Axisymmetric Deformations of Incompressible Elastic Solids of Revolution, *International Journal of Solids and Structures*, 6: 497-518.

Oh, S-H., Perin, N.I., Cooper, P.R., (1996), Quantitative Three-dimensional Anatomy of the Subaxial Cervical Spine: Implication for Anterior Spinal Surgery, *Neurosurgery*, Volume 38, Number 6, pp.1139-1144.

Oñate, E., Taylor, R.L., Zienkiewicz, O.C. and Rojek, J., (2003), A Residual Correction Method Based on Finite Calculus, *Engineering Computations*, 20: 629-658.

Oñate, E., Rojek, J., Taylor, R.L., and Zienkiewicz, O.C., (2004), Finite Calculus Formulation for Incompressible Solids Using Linear Triangles and Tetrahedra, *International Journal for Numerical Methods in Engineering*, 59: 1473-1500.

Panjabi, M.M., Duranceau, J., Goel, V., Oxland, T., Koichiro, T., (1991), Cervical Human Vertebrae: Quantitative Three-Dimensional Anatomy of the Middle and Lower Regions, *Spine*, Volume 16, Number 8, pp.861-869.

Pantuso, D. and Bathe, K-J., (1995), A Four-Node Quadrilateral Mixed-Interpolated Element for Solids and Fluids, *Mathematical Models and Methods in Applied Sciences*, 5: 1113-1128.

Plaugher, G., (1994), Chiropractic and Cerebrovascular Accidents: Dispelling the Myths, *Dynamic Chiropractic*, Volume 12, Number 15, Online 10 Sept. 2001, http:/www.chiroweb.com/archives/12/15/16.html.

Ravensbergen, J., Krijger, J.K., Hillen, B., Hoogstraten, H.W., (1996), The Influence of the Angle of Confluence on the Flow in a Vertebro-basilar Junction Model, *Journal of Biomechanics*, Volume 29, Number 3, pp.281-299.

Ravensbergen, J., Krijger, J.K.B., Hillen, B., Hoogstraten, H.W., (1997), The Influence of the Blunting of the Apex on the Flow in a Vertebro-Basilar Junction Model, *Journal of Biomechanical Engineering-Transactions of the ASME*, Volume 119, Number 2, pp.195-205.

Reese, S. and Wriggers, P., (2000), A Stabilization Technique to Avoid Hourglassing in Finite Eleasticity, *International Journal for Numerical Methods in Engineering*, 48: 79-109.

Reese, S., Wriggers, P. and Reddy, B.D., (2000), A New Locking-Free Brick Element for Large Deformation Problems in Elasticity, *Computers and Structures*, 75: 291-304.

Refshauge, K.M., (1994), Rotation: A Valid Premanipulative dizziness Test? Does It Predict Safe Manipulation?, *Journal of Manipulative and Physiological Therapeutics*, volume 17, Number 1, pp.15-19.

Reissner, E., (1950), On a Variational Theorem in Elasticity, *Journal of Mathematics and Physics*, 29: 90-95.

Rivett, D.A., Sharples, K.J., Milburn, P.D., (1999), Effect of Premanipulative Tests on Vertebral Artery and Internal Carotid Artery Blood Flow: A Pilot Study, *Journal of Manipulative and Physiological Therapeutics*, Volume 22, Number 6, pp.368-375.

Robey, T.H. and Schreyer, H.L., (1988), The Null Space and Non-Conventional Basis Functions in the Mixed Finite Element Method, *International Journal for Numerical Methods in Engineering*, 26: 843-855.

Rong, T.-Y. and Liu, A.-Q., (2001), Generalized Mixed Variational Principles and Solutions of Ill-Conditioned Problems in Computational Mechanics: Part I. Volumetric Locking, *Computer Methods in Applied Mechanics and Engineering*, 191: 407-422.

Rothwell, D.M., Bondy, S., Williams, I., (2001), Chiropractic Manipulation and Stroke: A Population-Based Study, *Stroke*, Volume 32, pp. 1054-1060.

Sacks, M.S. and Sun, W., (2003), Multiaxial Mechanical Behavior of Biologic Materials, *Annual Review of Biomedical Engineering*, 5: 251-284.

Sadegh, A.M., Tchako, A., (2000), Vertebral Stress of a Cervical Spine Model Under Dynamic Load, *Technology and Health Care*, Volume 8, pp. 143-154.

Saito,T., Yamamuro, T., Shikata, J., Oka, M., Tsutsumi, S. (1991), Analysis and Prevention of Spinal Column Deformity Following Cervical Laminectomy, Pathogenetic Analysis of Post Laminectomy Deformities, *Spine*, Volume 16, pp.494-502.

Sani, R.L., Gresho, P.M., Lee. R.L. and Griffiths, D.F., (1981), The Cause and Cure (?) of the Spurious Pressures Generated by Certain FEM Solutions of the Incompressible Navier-Stokes Equations: Part 1, *International Journal for Numerical Methods in Fluids*, 1: 17-43.

Sani, R.L., Gresho, P.M., Lee. R.L, Griffiths, D.F. and Engelman, M., (1981), The Cause and Cure (!) of the Spurious Pressures Generated by Certain FEM Solutions of the Incompressible Navier-Stokes Equations: Part 2, *International Journal for Numerical Methods in Fluids*, 1: 171-204.

Selecki, B.R., (1969), The Effects of Rotation of the Atlas on the Axis, *Medical Journal of Australia*, Volume 56, pp.1012-1015.

Seshaiyer, P. and Humphrey, J.D., (2003), A Sub-Domain Inverse Finite Element Characterization of Hyperelastic Membranes Including SoftTissues, *Journal of Biomechanical Engineering*, 125: 363-371.

Sheth, T.N., Winslow, J.L., Mikulis, D.J., (2001), Rotational Changes in the Morphology of the Vertebral Artery at a common Site of Artery Dissection, *Canadian Association of Radiologists Journal*, Volume 52, Number 4, pp.236-241.

Simo, J.C. and Armero, F., (1992), Geometrically Non-Linear Enhanced Strain Mixed Methods and the Method of Incompatible Modes, *International Journal for Numerical Methods in Engineering*, 33: 1413-1449.

Simo, J.C., Armero, F. and Taylor, R.L., (1993), Improved Versions of Assumed Enhanced Strain Tri-Linear Elements for 3D Finite Deformation Problems, *Computer Methods in Applied Mechanics and Engineering*, 110: 359-386.

Simo, J.C. and Rifai, M.S., (1990), A Class of Mixed Assumed Strain Methods and the Method of Incompatible Modes, *International Journal of Numerical Methods in Engineering*, 29: 1595-1638.

Simon, B.R., Kaufman, M.V., Liu, J. and Baldwin, A.L., (1998), Porohyperelastic-Transport-Swelling Theory, Material Properties and Finite Element Models for Large Arteries, *International Journal of Solids and Structures*, 35: 5021-5031.

Sloan, S.W. and Randolph, M.F., (1982), Numerical Predictions of Collapse Loads using Finite Element Methods, *International Journal for Numerical and Analytical Methods in Geomechanics*, 6: 47-76.

Smith, R.A., Estridge, M.N., (1962), Neurologic Complications of Head and Neck Manipulations: Report of Two Cases, *JAMA*, Volume 182, pp.528-531.

Stevinson, C., Ernst, E., (2002), Risks Associated with Spinal Manipulation, *American Journal of Medicine*, Volume 112, pp.566-570.

Stoeker, W.F., (1980) *Design of Thermal Systems*, 2nd Ed., McGraw-Hill Book Company, New York.

Strang, G., (1976), *Linear Algebra and its Applications*, Academic Press, Inc., New York.

Strang, G., (2007), Computational Science and Engineering, Wellesley Cambridge Press, Wellesley, MA.

Symons, B.P., Leonard, T., Herzog, W., (2002), Internal Forces Sustained by the Vertebral Artery During Spinal Manipulative Therapy, *Journal of Manipulative and Physiological Therapeutics*, Volume 25, Number 8, pp. 504-510.

Szabó, B.A., Babuška, I. and Chayapathy, B.K., (1989), Stress Computations for Nearly Incompressible Materials by the p-Version of the Finite Element Method, *International Journal for Numerical Methods in Engineering*, 28: 2175-2190.

Taylor, R.L., Simo, J.C., Zienkiewicz, O.C. and Chan, A.C.H., (1986), The Patch Test – A Condition for Assessing FEM Convergence, *International Journal for Numerical Methods in Engineering*, 22: 39-62.

Teo, E.C.. Paul, J.P., Evans, J.H., (1994), Finite Element Stress Analysis of a Cadaver Second Cervical Vertebra, *Med Biol Eng Comput*, Volume 32, pp.236-238.

Thiel, H.W., (1991), *The Effect of Various Head and Neck Positions on Vertebral Artery Blood Flow: A Study Using Doppler Ultrasound*, Thesis, University of Saskatchewan.

Toutounian, F. and Ataei, A., (2009), A New Method for Computing Moore-Penrose Inverse Matrices, *Journal of Computational and Applied Mathematics*, 228: 412-417.

Trattnig, S., Hübsch, P., Schuster, H., Pölzleitner, D., (1990), Color-Coded Doppler Imaging of Normal Vertebral Arteries, *Stroke*, Volume 21, pp.1222-1225.

Trim, D., (2004), Calculus for Engineers, 3rd Ed., Pearson Education Canada, Inc., Toronto.

Tropiano, P., Thollon, L., Arnoux, P.J., Huang, R.C., Kayvantash, K., Poitout, D.G., Brunet, C., (2004), Using a Finite Element Model to Evaluate Human Injuries Application to the HUMOS Model in Whiplash Situation, *Spine*, Volume 29, Number 16, pp. 1709-1716.

Vautravers, P, Maigne, J-Y, (2000), Cervical Spine Manipulation and the Precautionary Principle, *Joint, Bone, Spine*, Volume 67, pp.272-276.

Vito, R.P. and Dixon, S.A., (2003), Blood Vessel Constitutive Models – 1995-2002, *Annual Review of Biomedical Engineering*, 5: 413-439.

Voo, L, Pintar, F.A., Yoganandan, N., Liu, Y.K., (1998), Static and Dynamic Bending Responses of the Human Cervical Spine, *Journal of Biomechanical Engineering*, Volume 120, pp. 693-696.

Wang, S., Zheng, B., Xiong, Z., and Li, Z., (2009), The Condition Numbers for Weighted Moore-Penrose Inverse and Weighted Linear Least Squares Problem, *Applied Mathematics and Computation*, 215: 197-205.

Weinberg, E.J. and Kaazempur-Mofrad, M.R., (2006), A Large-Strain Finite Element Formulation for Biological Tissues with Application to Mitral Valve Leaflet Tissue Mechanics, *Journal of Biomechanics*, 39: 1557-1561.

Weissman, S.L. and Taylor, R.L., (1992) (a), Treatment of Internal Constraints by Mixed Finite Element Methods: Unification of Concepts, *International Journal for Numerical Methods in Engineering*, 33: 131-141.

Weissman, S.L. and Taylor, R.L., (1992) (b), A Unified Approach to Mixed Finite Element Methods: Application to In-Plane Problems, *Computer Methods in Applied Mechanics and Engineering*, 98: 127-151.

Wheeldon, J.A., Stemper, B.D., Yoganandan, N., Pintar, F.A., (2008), Validation of a Finite Element Model of a Young, Normal Lower Cervical Spine, *Annals of Biomedical Engineering*, Volume 36, Number 9, pp. 1458-1469.

Woolfe, F., Liberty, E., Rokhlin, V., Tygert, M., (2008), A Fast Randomized Algorithm for the Approximation of Matrices, *Applied and Computational Harmonic Analysis*, Volume 25, pp. 335-366.

World Chiropractic Alliance, (2001), Chiropractic and the Risk of Stroke, Online 10 Sept. 2001, http://www.worldchiropracticalliance.org/positions/stroke.htm.

Wriggers, P. and Reese, S., (1996), A Note on Enhanced Strain Methods for Large Deformations, *Computer Methods in Applied Mechanics and Engineering*, 135: 201-209.

Wu, C-C., Yuan, L. and Furukawa, T., (1999), Deviatoric Hydrid Model and Multivariable Elimination at Element Level for Incompressible Medium, *International Journal for Numerical Methods in Engineering*, 46: 729-745.

Yoganandan, N., Kumaresan, S., Voo, L, Pintar, F.A., (1996), Spine Update: Finite Element Applications in Human Cervical Spine Modeling, *Spine*, Volume21, Number 15, pp. 1824-1834.

Yoganandan, N., Kumaresan, S., Voo, L, Pintar, F.A., (1997), Finite Element Model of the Human Lower Cervical Spine: Parametric Analysis of the C4-C6 Unit, *Journal of Biomechanical Engineering*, Volume 119, pp. 87-92.

Yoganandan, N., Sances, A. Jr., Pintar, F.A., Maiman, D.J., Reinartz, J., Cusick, J.F., Larson, S.J., (1990), Injury Biomechanics of the Human Cervical Column, *Spine*, Volume 15, Number 10, pp. 1031-1039.

Yu, H.S., (1991), A Rational Displacement Interpolation Function for Axisymmetric Finite Element Analysis of Nearly Incompressible Materials, *Finite Elements in Analysis and Design*, 10: 205-219.

Yu, H.S. and Houlsby, G.T., (1990), A New Finite Element Formulation for One-Dimensional Analysis of Elastic-Plastic Materials, *Computers and Geotechnics*, 9: 241-256.

Yu, H.S. and Netherton, M.D., (2000), Performance of Displacement Finite Elements for Modelling Incompressible Meterials, *International Journal for Numerical and Analytical Methods in Geomechanics*, 24: 627-653.

Zheng, Q.-S., (2002), Constitutive Relations of Linear Elastic Materials Under Various Internal Constraints, *Acta Mechanica*, 158: 97-103.

Zienkiewicz, O.C., Qu, S., Taylor, R.L. and Nakazawa, S., (1986), The Patch Test for Mixed Formulations, *International Journal for Numerical Methods in Engineering*, 23: 1873-1883.

Zienkiewicz, O.C. and Taylor, R.L., (1989), *The Finite Element Method: Volume 1 Basic Formulation and Linear Problems*, 4th Ed., McGraw-Hill Book Company, London.

Zienkiewicz, O.C. and Taylor, R.L., (1997), The Finite Element Patch Test Revisited: A Computer Test for Convergence, Validation and Error Estimates, *Computer Methods in Applied Mechanics and Engineering*, 149: 223-254.

Zienkiewicz, O.C. and Wu, J., (1991), Incompressibility Without Tears – How to Avoid Restrictions of Mixed Formulation, *International Journal for Numerical Methods in Engineering*, 32: 1189-1203.

Appendix A

Linear Algebra Review

In this appendix, some pertinent linear algebra concepts are reviewed [Strang, 1976]. The concepts are presented in the order in which they appear in the thesis.

Orthogonal Matrix

For an orthogonal matrix $\boldsymbol{A}$, its inverse is equal to its transpose; i.e., $\boldsymbol{A}^{-1} = \boldsymbol{A}^{\mathrm{T}}$.

Positive Definite Matrix

A positive definite matrix $\boldsymbol{A}$ has the following characteristics:

- Real and symmetric.
- All eigenvalues of $\boldsymbol{A}$ are positive.
- $\boldsymbol{x}^{\mathrm{T}}\boldsymbol{A}\boldsymbol{x} > 0$ for $\boldsymbol{x} \neq \boldsymbol{0}$.
- Nonsingular and therefore invertible.
- $\boldsymbol{A} = \boldsymbol{Q}\boldsymbol{\Lambda}\boldsymbol{Q}^{\mathrm{T}}$ where $\boldsymbol{Q}$ is the matrix of orthogonal eigenvectors of $\boldsymbol{A}$ and $\boldsymbol{\Lambda}$ is the diagonal matrix of eigenvalues.

Row Space of a Matrix $\boldsymbol{A}$, $R(\boldsymbol{A})$

For $\boldsymbol{A} \in \Re_{m\times n}$, where $\boldsymbol{r}_i$ are the rows of $\boldsymbol{A}$,

$$R(\boldsymbol{A}) = \left\{ \boldsymbol{v} \mid \boldsymbol{v} = a_1 \boldsymbol{r}_1^{\mathrm{T}} + a_2 \boldsymbol{r}_2^{\mathrm{T}} + \cdots + a_m \boldsymbol{r}_m^{\mathrm{T}} \right\}.$$

The row space of a matrix is all vectors which can be written as a linear combination of the rows of $\boldsymbol{A}$.

The dimension of the row space is equal to the number of linearly independent rows of $\boldsymbol{A}$.

Column Space of Matrix $\boldsymbol{A}$, $C(\boldsymbol{A})$

For $\boldsymbol{A} \in \Re_{m \times n}$, where $\boldsymbol{c}_i$ are the columns of $\boldsymbol{A}$,

$$C(\boldsymbol{A}) = \left\{ \boldsymbol{v} \mid \boldsymbol{v} = a_1\boldsymbol{c}_1 + a_2\boldsymbol{c}_2 + \cdots + a_n\boldsymbol{c}_n \right\}.$$

The column space of a matrix is all vectors which can be written as a linear combination of the columns of $\boldsymbol{A}$.

The dimension of the column space is equal to the number of linearly independent columns of $\boldsymbol{A}$ and the dimension of the row space.

Given a consistent system of equations with a unique solution

$$\boldsymbol{A}\boldsymbol{x} = \boldsymbol{b};$$

$\boldsymbol{A}$ is a mapping from the row space to the column space.
$\boldsymbol{x}$ is in the row space of $\boldsymbol{A}$.
$\boldsymbol{b}$ is in the column space of $\boldsymbol{A}$.

Nullspace of a Matrix $\boldsymbol{A}$, $N(\boldsymbol{A})$

For $\boldsymbol{A} \in \Re_{m \times n}$,

$$N(\boldsymbol{A}) = \left\{ \boldsymbol{v} \in \Re_{n \times 1} \mid \boldsymbol{A}\boldsymbol{v} = \boldsymbol{0} \right\}.$$

The row space and the null space are orthogonal complements.

Rank of a matrix $\boldsymbol{A}$, r($\boldsymbol{A}$)

For $\boldsymbol{A} \in \Re_{m \times n}$, the rank of a matrix is equal to the dimension of the row space.

$\dim R(\boldsymbol{A}) + \dim N(\boldsymbol{A}) = n$, where dim = dimension.

Norm of a Vector $\|\boldsymbol{w}\|$

In this thesis, the norm of a vector is $\|\boldsymbol{w}\| = \sqrt{\boldsymbol{w}^{\mathrm{T}}\boldsymbol{w}}$ and therefore $\|\boldsymbol{w}\|^2 = \boldsymbol{w}^{\mathrm{T}}\boldsymbol{w}$.

Norm of a Matrix $\|\boldsymbol{A}\|$

The norm of a matrix is the number $\|\boldsymbol{A}\| = \max_{x \neq 0} \dfrac{\|\boldsymbol{A}\boldsymbol{x}\|}{\|\boldsymbol{x}\|}$.

Condition Number of a Matrix $\boldsymbol{A}$, $CN(\boldsymbol{A})$

For the system of equations $\boldsymbol{A}\boldsymbol{x} = \boldsymbol{b}$,

$$CN(\boldsymbol{A}) = \|\boldsymbol{A}\| \, \|\boldsymbol{A}^{-1}\|.$$

The condition number gives the upper bound of the error magnification from data $\boldsymbol{b}$ to solution $\boldsymbol{x}$.

Singular Value Decomposition:

Applying singular value decomposition to a square matrix $\boldsymbol{K}$ gives

$$\boldsymbol{K} = \boldsymbol{U}\,\boldsymbol{S}\,\boldsymbol{V}^{\mathrm{T}}$$

where $\boldsymbol{U}$ and $\boldsymbol{V}$ are orthogonal matrices and $\boldsymbol{S}$ is a diagonal matrix. The diagonal terms of $\boldsymbol{S}$ are called singular values.

Appendix B

Finite Element Formulation for Q4P1 Code

For this research, a series of finite element codes were written for both compressible and fully incompressible analyses. In all cases, the formulations applied to linear elastic, isotropic material subjected to plane strain conditions, and the geometry and displacements were defined using the standard four-node quadrilateral shown in Figure B.1. The governing equations may be found in any book on the finite element method. In particular, Chapter 9 of Budynas was followed as a guide to creating the codes for compressible materials ($\nu < 0.5$) [Budynas, 1999]. In developing the Q4P1 codes for incompressible materials, the formulation was as follows.

The quadrilateral element chosen uses isoparametric shape functions meaning that the same shape functions are used to map the physical coordinates into natural coordinates as are used to define the displacement field. The physical coordinates may be mapped into the natural coordinates using

$$x = x_1 N_1(\xi,\eta) + \cdots + x_4 N_4(\xi,\eta) \tag{B.1}$$

$$y = y_1 N_1(\xi,\eta) + \cdots + y_4 N_4(\xi,\eta) \tag{B.2}$$

and the displacement field can be expressed as

$$u = u_1 N_1(\xi,\eta) + \cdots + u_4 N_4(\xi,\eta) \tag{B.3}$$

$$v = v_1 N_1(\xi,\eta) + \cdots + v_4 N_4(\xi,\eta) \tag{B.4}$$

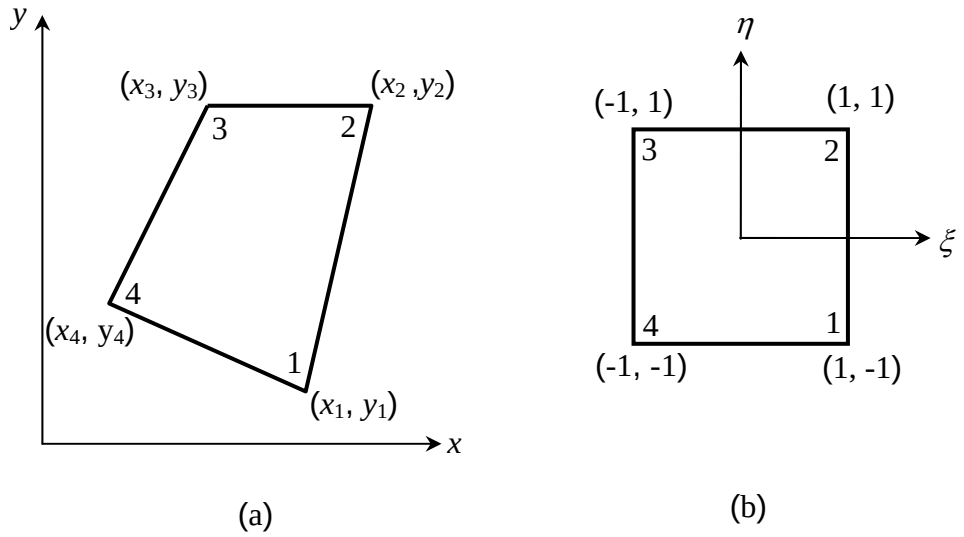

Figure B.1: Quadrilateral element in (a) physical coordinates and (b) mapped in natural coordinates.

where u and v express the displacement in x- and y-directions, ξ and η are the natural coordinates, u_i, v_i are the nodal displacements, and N_i are the isoparametric shape functions for nodes i, defined as

$$N_1 = \frac{1}{4}(1+\xi)(1-\eta) \tag{B.5}$$

$$N_2 = \frac{1}{4}(1+\xi)(1+\eta) \tag{B.6}$$

$$N_3 = \frac{1}{4}(1-\xi)(1+\eta) \tag{B.7}$$

$$N_4 = \frac{1}{4}(1-\xi)(1-\eta). \tag{B.8}$$

The strains are found by taking derivatives of the displacements with respect to x and y and in turn with respect to ξ and η as x and y are functions of ξ and η. In matrix form, the derivatives of u are

$$\begin{Bmatrix} \frac{\partial u}{\partial \xi} \\ \frac{\partial u}{\partial \eta} \end{Bmatrix} = \begin{bmatrix} \frac{\partial x}{\partial \xi} & \frac{\partial y}{\partial \xi} \\ \frac{\partial x}{\partial \eta} & \frac{\partial y}{\partial \eta} \end{bmatrix} \begin{Bmatrix} \frac{\partial u}{\partial x} \\ \frac{\partial u}{\partial y} \end{Bmatrix} \tag{B.9}$$

and similarly for v,

$$\begin{Bmatrix} \frac{\partial v}{\partial \xi} \\ \frac{\partial v}{\partial \eta} \end{Bmatrix} = \begin{bmatrix} \frac{\partial x}{\partial \xi} & \frac{\partial y}{\partial \xi} \\ \frac{\partial x}{\partial \eta} & \frac{\partial y}{\partial \eta} \end{bmatrix} \begin{Bmatrix} \frac{\partial v}{\partial x} \\ \frac{\partial v}{\partial y} \end{Bmatrix}. \tag{B.10}$$

where the 2×2 matrix is the Jacobian matrix, $\boldsymbol{J}$. Its components are determined by finding the derivatives of (B.1) and (B.2). This also involves finding the derivatives of the shape functions, equations (B.5) to (B.8). Therefore,

$$J_{11} = x_1 \frac{\partial N_1}{\partial \xi} + \cdots + x_4 \frac{\partial N_4}{\partial \xi} \tag{B.11}$$

$$J_{12} = y_1 \frac{\partial N_1}{\partial \xi} + \cdots + y_4 \frac{\partial N_4}{\partial \xi} \tag{B.12}$$

$$J_{21} = x_1 \frac{\partial N_1}{\partial \eta} + \cdots + x_4 \frac{\partial N_4}{\partial \eta} \tag{B.13}$$

$$J_{22} = y_1 \frac{\partial N_1}{\partial \eta} + \cdots + y_4 \frac{\partial N_4}{\partial \eta}, \tag{B.14}$$

where

$$\frac{\partial N_1}{\partial \xi} = \frac{1}{4}(1-\eta) \tag{B.15}$$

$$\frac{\partial N_2}{\partial \xi} = \frac{1}{4}(1+\eta) \tag{B.16}$$

$$\frac{\partial N_3}{\partial \xi} = -\frac{1}{4}(1+\eta) \tag{B.17}$$

$$\frac{\partial N_4}{\partial \xi} = -\frac{1}{4}(1-\eta) \tag{B.18}$$

$$\frac{\partial N_1}{\partial \eta} = -\frac{1}{4}(1+\xi) \tag{B.19}$$

$$\frac{\partial N_2}{\partial \eta} = \frac{1}{4}(1+\xi) \tag{B.20}$$

$$\frac{\partial N_3}{\partial \eta} = \frac{1}{4}(1-\xi) \tag{B.21}$$

$$\frac{\partial N_4}{\partial \eta} = -\frac{1}{4}(1-\xi). \tag{B.22}$$

Since the Jacobian matrix transforms derivatives in the physical coordinates into the natural coordinates, the inverse of the Jacobian matrix is required to find the strains. It is given by

$$\boldsymbol{J}^{-1} = \frac{1}{|\boldsymbol{J}|}\begin{bmatrix} J_{22} & -J_{12} \\ -J_{21} & J_{11} \end{bmatrix}. \tag{B.23}$$

So, in matrix form, the strains for a plane strain analysis become

$$\begin{Bmatrix} \varepsilon_x \\ \varepsilon_y \\ \gamma_{xy} \end{Bmatrix} = \frac{1}{|\boldsymbol{J}|}\begin{bmatrix} J_{22} & -J_{12} & 0 & 0 \\ 0 & 0 & -J_{21} & J_{11} \\ -J_{21} & J_{11} & J_{22} & -J_{12} \end{bmatrix}\begin{Bmatrix} \frac{\partial u}{\partial \xi} \\ \frac{\partial u}{\partial \eta} \\ \frac{\partial v}{\partial \xi} \\ \frac{\partial v}{\partial \eta} \end{Bmatrix}, \tag{B.24}$$

or, this may be rewritten as

$$\boldsymbol{\varepsilon} = \hat{\boldsymbol{J}}\boldsymbol{u}' . \tag{B.25}$$

To relate the strains to the displacements, the $\boldsymbol{u}'$ vector is related to $\boldsymbol{u}$, the displacement vector, as

$$\boldsymbol{u}' = \boldsymbol{N}'\boldsymbol{u} , \tag{B.26}$$

where

$$\boldsymbol{N}' = \begin{bmatrix} \frac{\partial N_1}{\partial \xi} & 0 & \frac{\partial N_2}{\partial \xi} & 0 & \frac{\partial N_3}{\partial \xi} & 0 & \frac{\partial N_4}{\partial \xi} & 0 \\ \frac{\partial N_1}{\partial \eta} & 0 & \frac{\partial N_2}{\partial \eta} & 0 & \frac{\partial N_3}{\partial \eta} & 0 & \frac{\partial N_4}{\partial \eta} & 0 \\ 0 & \frac{\partial N_1}{\partial \xi} & 0 & \frac{\partial N_2}{\partial \xi} & 0 & \frac{\partial N_3}{\partial \xi} & 0 & \frac{\partial N_4}{\partial \xi} \\ 0 & \frac{\partial N_1}{\partial \eta} & 0 & \frac{\partial N_2}{\partial \eta} & 0 & \frac{\partial N_3}{\partial \eta} & 0 & \frac{\partial N_4}{\partial \eta} \end{bmatrix} \tag{B.27}$$

and

$$\boldsymbol{u} = \begin{Bmatrix} u_1 & v_1 & u_2 & v_2 & u_3 & v_3 & u_4 & v_4 \end{Bmatrix}^{\mathrm{T}} . \tag{B.28}$$

The strain-displacement relation is now

$$\boldsymbol{\varepsilon} = \hat{\boldsymbol{J}}\boldsymbol{N}'\boldsymbol{u} = \boldsymbol{B}\boldsymbol{u} . \tag{B.29}$$

To this point, the development of this formulation is similar to that found in Budynas [1999]. From here on, the development diverges from the norm to accommodate incompressibility. Generalised Hooke's law can be written in the form

$$\sigma_x = \frac{E}{(1+\nu)(1-2\nu)}\left[(1-\nu)\varepsilon_x + \nu\left(\varepsilon_y + \varepsilon_z\right)\right], \tag{B.30}$$

$$\sigma_y = \frac{E}{(1+\nu)(1-2\nu)}\left[(1-\nu)\varepsilon_y + \nu\left(\varepsilon_z + \varepsilon_x\right)\right], \tag{B.31}$$

$$\sigma_z = \frac{E}{(1+\nu)(1-2\nu)}\left[(1-\nu)\varepsilon_z + \nu(\varepsilon_x + \varepsilon_y)\right]. \tag{B.32}$$

By subtracting (B.31) from (B.30), and (B.32) from (B.31),

$$\sigma_x - \sigma_y = \frac{E}{1+\nu}(\varepsilon_x - \varepsilon_y) \tag{B.33}$$

and

$$\sigma_y - \sigma_z = \frac{E}{1+\nu}(\varepsilon_y - \varepsilon_z), \tag{B.34}$$

respectively. For plane strain analysis, $\varepsilon_z = 0$ and in matrix form, the distortional component of Hooke's law becomes

$$\begin{bmatrix} \sigma_x - \sigma_y \\ \sigma_y - \sigma_z \\ \sigma_z - \sigma_x \\ \sqrt{6}\tau_{xy} \end{bmatrix} = \frac{E}{1+\nu}\begin{bmatrix} 1 & 0 & 0 & 0 \\ 0 & 1 & 0 & 0 \\ 0 & 0 & 1 & 0 \\ 0 & 0 & 0 & 0.5 \end{bmatrix}\begin{bmatrix} \varepsilon_x - \varepsilon_y \\ \varepsilon_y \\ -\varepsilon_x \\ \sqrt{6}\gamma_{xy} \end{bmatrix} \tag{B.35}$$

or

$$\hat{\boldsymbol{\sigma}} = \hat{\boldsymbol{D}}\hat{\boldsymbol{\varepsilon}}, \tag{B.36}$$

where the fourth line of (B.35) expresses the classical linear elastic relationship between shear stress and shear strain.

As a result of the nonstandard stress-strain relation, the strain-displacement relation must also be modified. It must now be written in terms of the deviatoric normal strains and shear strain, as

$$\hat{\boldsymbol{\varepsilon}} = \hat{\boldsymbol{B}}\boldsymbol{u} \tag{B.37}$$

where $\hat{\boldsymbol{B}}$ is given by

$$\hat{\boldsymbol{B}} = \begin{bmatrix} B_{11}-B_{21} & B_{12}-B_{22} & B_{13}-B_{23} & B_{14}-B_{24} & B_{15}-B_{25} & B_{16}-B_{26} & B_{17}-B_{27} & B_{18}-B_{28} \\ B_{21} & B_{22} & B_{23} & B_{24} & B_{25} & B_{26} & B_{27} & B_{28} \\ -B_{11} & -B_{12} & -B_{13} & -B_{14} & -B_{15} & -B_{16} & -B_{17} & -B_{18} \\ \sqrt{6}B_{31} & \sqrt{6}B_{32} & \sqrt{6}B_{33} & \sqrt{6}B_{34} & \sqrt{6}B_{35} & \sqrt{6}B_{36} & \sqrt{6}B_{37} & \sqrt{6}B_{38} \end{bmatrix} \tag{B.38}$$

and B_{ij} are individual components of the standard strain-displacement matrix $\boldsymbol{B}$.

The volumetric constraint is enforced in an average sense over each element. For plane strain, this relation is defined as

$$\int \left(\varepsilon_x + \varepsilon_y\right) \mathrm{d}V = 0 \tag{B.39}$$

over each element where

$$\varepsilon_x + \varepsilon_y = B_{11}u_1 + B_{13}u_2 + B_{15}u_3 + B_{17}u_4 + B_{22}v_1 + B_{24}v_2 + B_{26}v_3 + B_{28}v_4 \tag{B.40}$$

or

$$\varepsilon_x + \varepsilon_y = \boldsymbol{u}^T \tilde{\boldsymbol{B}} \tag{B.41}$$

where

$$\tilde{\boldsymbol{B}} = \begin{bmatrix} B_{11} & B_{22} & B_{13} & B_{24} & B_{15} & B_{26} & B_{17} & B_{28} \end{bmatrix}^{\mathrm{T}}. \tag{B.42}$$

The expression for stationary potential energy is given by

$$\Pi = \hat{U} + \Omega + p\int \left(\varepsilon_x + \varepsilon_y\right) \mathrm{d}V\,, \tag{B.43}$$

and the distortional strain energy, $\hat{U}$, is defined as [Cook and Young, 1985]

$$\hat{U} = \frac{1}{12G}\int \hat{\boldsymbol{\sigma}}^{\mathrm{T}} \hat{\boldsymbol{\sigma}}\, \mathrm{d}V\,, \tag{B.44}$$

where G is the shear modulus. Using (B.36) and (B.37), equation (B.44) becomes

$$\hat{U} = \frac{1}{12G}\int \boldsymbol{u}^{\mathrm{T}}\hat{\boldsymbol{B}}^{\mathrm{T}}\hat{\boldsymbol{D}}^{\mathrm{T}}\hat{\boldsymbol{D}}\hat{\boldsymbol{B}}\boldsymbol{u}\,\mathrm{d}V\,, \tag{B.45}$$

and substituting (B.41) and (B.45) into equation (B.43) gives

$$\Pi = \frac{1}{12G}\int \boldsymbol{u}^{\mathrm{T}}\hat{\boldsymbol{B}}^{\mathrm{T}}\hat{\boldsymbol{D}}^{\mathrm{T}}\hat{\boldsymbol{D}}\hat{\boldsymbol{B}}\boldsymbol{u}\,\mathrm{d}V - \boldsymbol{u}^{\mathrm{T}}\boldsymbol{F} + p\int \boldsymbol{u}^{\mathrm{T}}\tilde{\boldsymbol{B}}\,\mathrm{d}V\,. \tag{B.46}$$

Minimising this with respect to the nodal displacements, u_i, and p gives

$$\left[\frac{1}{6G}\int \hat{\boldsymbol{B}}^{\mathrm{T}}\hat{\boldsymbol{D}}^{2}\hat{\boldsymbol{B}}\,\mathrm{d}V\right]\boldsymbol{u} - \boldsymbol{F} + p\int \tilde{\boldsymbol{B}}\,dV = \boldsymbol{0} \tag{B.47}$$

and

$$\boldsymbol{u}^{\mathrm{T}}\int \tilde{\boldsymbol{B}}\,dV = 0\,. \tag{B.48}$$

The integrals in (B.47) and (B.48) are performed using Gauss-Legendre quadrature where the Gauss points follow a 2×2 quadrature rule for exact integration [Zienkiewicz & Taylor, 1989].

This process is performed for each element in the finite element grid and then the equations are assembled into the global stiffness matrix which takes the form

$$\left[\begin{array}{c|c} \boldsymbol{A} & \boldsymbol{G}^{\mathrm{T}} \\ \hline \boldsymbol{G} & \boldsymbol{0} \end{array}\right]\left[\begin{array}{c} \boldsymbol{u} \\ \hline \boldsymbol{p} \end{array}\right] = \left[\begin{array}{c} \boldsymbol{b}_1 \\ \hline \boldsymbol{b}_2 \end{array}\right], \tag{B.49}$$

Once the equations are assembled, the system may be solved.